Summer 2010

# Molecular simulation of the infrared absorption cross section and thermophysical properties of a polyatomic fluid

Zhi Liang



Department: Mechanical and Aerospace Engineering

# MOLECULAR SIMULATION OF THE INFRARED ABSORPTION CROSS SECTION AND THERMOPHYSICAL PROPERTIES OF A POLYATOMIC FLUID

by

Zhi Liang

A DISSERTATION

Presented to the Faculty of the Graduate School of the

MISSOURI UNIVERSITY OF SCIENCE & TECHNOLOGY

In Partial Fulfillment of the Requirements for the Degree

DOCTOR OF PHILOSOPHY

in

MECHANICAL ENGINEERING

2010

Approved by:

Hai-Lung Tsai, Advisor
Darryl J. Alofs
Frank Liou
John G. Story
Hai Xiao

## PUBLICATION DISSERTATION OPTION

This dissertation has been prepared in the form of five papers for publication. Page 7−36 has been published in Journal of Molecular Spectroscopy. Page 37−69 has been published in Fluid Phase Equilibria. Page 70-101 has been published in Molecular Physics. Page 102-123 has been accepted for publication in Molecular Physics. Page 124-149 has been submitted to Fluid Phase Equilibria. All of them have been prepared in the format for publication in the corresponding journals. The balance of this dissertation follows the standard dissertation format.

## ABSTRACT

The work presented in this dissertation aims at *ab initio* calculations of the infrared absorption cross section, heat capacity, self-diffusion coefficient, shear viscosity and thermal conductivity of a polyatomic fluid with the aid of statistical mechanics. The simulation is firstly focused on calculating single-molecule properties such as molecular structure, vibrational energy eigen values and transition dipole moments using an efficient method based on the density functional theory. Based on these *ab initio* results, the infrared absorption cross sections are determined by the Fermi's Golden rule, and the thermophysical properties are determined from molecular dynamics simulations. Using carbon dioxide as an example, the accuracies of the proposed calculation methods are all examined by comparing the simulated results with the experimental data in a wide range of temperature and pressure. It is found that the thermophysical properties of carbon dioxide at dilute and moderate densities can be accurately calculated without using any experimental data. It is shown that the quantum effects of molecular vibrations can be nicely accounted for by either a Monte Carlo method or an analytical correction term proposed in this work. The simulation results demonstrate the importance of considering the vibrational contribution to the thermal conductivity. It is found vibrations mainly contribute to the thermal conductivity through self-diffusion processes. It is also shown that the present method can be readily extended to calculate the temperature and density dependence of transport properties of other polyatomic fluids such as methane of which the experimental transport property data are of low accuracy or nonexistent.

# ACKNOWLEDGMENTS

I wish to express my sincere gratitude to my academic advisor, Dr. Hai-Lung Tsai, for providing guidance and constant encouragement during my graduate study at Missouri University of Science and Technology. He provided an excellent working atmosphere and supported me in every aspect. It has been a privilege and a pleasure to have worked with him.

I wish to extend my appreciation to Dr. Darryl J. Alofs, Dr. Frank Liou, Dr. John G. Story, and Dr. Hai Xiao for serving as committee members and for their examination of the dissertation.

The dissertation was supported in part by the Office of Naval Research, which is gratefully acknowledged. Thanks are also due to the Department of Mechanical and Aerospace Engineering and the Intelligent Systems Center at Missouri University of Science and Technology for providing me, respectively, a graduate teaching assistantship and a research assistantship.

Lastly, I wish to thank my parents and especially my wife, Yukun Han, for their love, understanding, and support.

# TABLE OF CONTENTS

## LIST OF ILLUSTRATIONS

# LIST OF TABLES

# 1. INTRODUCTION

Fluid properties such as infrared absorption cross section, heat capacity, self-diffusion coefficient, shear viscosity and thermal conductivity are important parameters for device design and modeling of heat and mass transfer in fluids. The accurate experimental data of these properties at conditions close to room temperature and atmospheric pressure are generally available for different fluids. However, fluid properties at high temperatures and/or high pressures are relatively difficult to be measured accurately by experiments. In this case, molecular simulations can serve as an alternate method for obtaining fluid properties data. In principle, as long as the structures of the molecules in the fluid and the intermolecular potentials which describe the interactions between molecules are known, all thermophysical properties of a fluid at any given temperature and pressure can be determined directly from computer simulations. Starting from *ab initio* calculation of single-molecule properties such as molecular structure, the moment of inertia, vibrational energy eigen values *etc.*, it is shown in this dissertation that the thermophysical properties of a polyatomic fluid can be accurately determined without relying on any experimental data. The molecular simulation in this work mainly focuses on the calculation of fluid properties of carbon dioxide because accurate experimental fluid property data of carbon dioxide are available in a wide range of temperature and pressure. The accuracy of the simulation methods can be examined by comparing the calculated carbon dioxide properties with the experimental data. The validated methods are then extended to calculate the thermophysical property of other polyatomic fluids of which the experimental data are of low accuracy or nonexistent.

## 1.1 AB INITIO CALCULATION OF SINGLE-MOLECULE PROPERTIES

The most widely studied molecular fluid is, perhaps, argon because argon is a monatomic molecule and suitable for accurate molecular simulations with a simple isotropic intermolecular potential. In the simulation of a polyatomic fluid, however, the internal modes of motion in addition to the translational motion must be taken into account in order to calculate the fluid property accurately. To include the internal modes of motion, i.e. rotational and vibrational motions into the molecular model, it is necessary to calculate the intramolecular potential energy surface (PES) of a given polyatomic molecule. Once the intramolecular PES is know, it can be used to determine single-molecular properties such as the molecular structure and vibrational energy eigen values. Carbon dioxide molecule is used as an example in the calculation.

The *ab initio* calculation of intramolecular PESs of a triatomic molecule has been implemented in many papers [1-7] by the coupled-cluster singles and doubles excitation with perturbative treatment of triple excitations [CCSD(T)] [8] method and the multi-reference configuration interaction (MRCI) method. Localized basis sets such as augmented correlation-consistent polarized quadruple zeta (aug-cc-pVQZ) functions were used in these calculations. Using these methods and basis sets, the potential energies were normally evaluated at $10^2$ to $10^3$ different nuclear configurations that are close to the molecular equilibrium structures. The data were then fitted by polynomial expansions in displacement coordinates, and used in the calculations of molecular properties. In some calculations [2], the coefficients in polynomial expansions needed to be optimized in order to accurately reproduce the experimental values of fundamental transition energies. Generally, the CCSD(T) and MRCI methods combined with localized basis sets gives

accurate calculated results. But the method is very computationally demanding. In this work, an efficient method based on the density functional theory (DFT) is presented to calculate the intramolecular PES as a function of the nuclear configuration by solving the electronic Schrödinger equation. Once the electronic Schrödinger equation is solved, the electron charge distribution which is used to calculate the molecular dipole moment can be readily obtained. In the calculation, the Projector-Augmented Wave (PAW) exchange-correlation potential functionals [8, 9] and Plane Wave (PW) basis functions are used. The calculation method is much more efficient compared to the CCSD(T) method with localized basis functions. The intramolecular potential energies of carbon dioxide at more than $10^5$ different nuclear configurations are calculated in this work. Using the calculated PES, the equilibrium molecular structure is determined from the conjugate-gradient algorithm [10] and the vibrational energy eigen values are determined by solving the vibrational Schrödinger equation. The calculated vibrational wave functions combined with the calculated dipole moment functions are used to calculate the vibrational transition dipole moment which is an important parameter in the calculation of infrared absorption cross sections. The calculated infrared absorption cross sections are compared with experimental results to examine the accuracy of the calculation method. The calculated equilibrium molecular structure and vibrational energy eigen values are employed in the subsequent molecular dynamics (MD) simulation of thermophysical properties of carbon dioxide.

## 1.2 MD SIMULATIONS OF THERMOPHYSICAL PROPERTIES

The heat capacity, self-diffusion coefficient, shear viscosity and thermal conductivity of carbon dioxide in a wide range of temperature and pressure are

determined from MD simulations. Among these four properties, heat capacity is a static property which can be determined from energy fluctuations of the fluid at a given temperature and pressure. The remaining three are transport properties. Self-diffusion coefficient measures the transport of mass. Shear viscosity measures the transport of momentum. Thermal conductivity measures the transport of energy. In 1950s, Green and Kubo derived exact formulas to calculate the transport properties of fluids as the integrals over the appropriate time correlation functions [11-13]. According to these formulas, the transport properties of a fluid at a given temperature and pressure can be determined directly from computer simulations as long as the structure and the intermolecular potential of molecules in the fluid are known. The time correlation functions associated with the transport properties of interest have been calculated numerically by equilibrium MD simulations since 1970s [14-20]. Although the transport properties calculated based on the Lennard-Jones (LJ) model for fluids over a wide range of fluid states have been fully discussed [21], these results cannot be applied directly to real fluids because a LJ potential is unable to accurately describe the real anisotropic interaction between polyatomic molecules. In this work, the transport properties are all calculated by equilibrium MD simulations from anisotropic pair potentials.

Comparing to other calculation method such as the classical-trajectory (CT) method [22-25], the Rainwater-Friend [26,27] and modified Enskog theories [28,29], and the non-equilibrium MD simulation method [30-33], the equilibrium MD simulation method has the following advantages.

Firstly, the equilibrium MD simulation is applicable at arbitrary densities and temperatures. Secondly, the equilibrium MD simulation is a multi-property method. The

static and transport properties can be all obtained from the output of a single equilibrium run. Thirdly, if an accurate intermolecular PES is available and the simulation length is long enough, the fluid thermophysical properties can be accurately determined from the equilibrium MD simulation without relying on any experimental data. Therefore, the equilibrium MD simulation is applied in this work.

In MD simulation of a polyatomic fluid, a classical treatment of translational and rotational motions is normally valid, which, however, may not be true for vibrational motions. The characteristic vibrational temperature normally varies from a few hundred K's for vibrational modes, such as torsional vibrations, to several thousand K's for vibrational modes, such as stretching vibrations. Generally, two approaches are frequently used to treat different vibrational motions. The first one is to treat the vibrational motion classically [33−39]. This classical approximation is appropriate if the characteristic temperature of the vibrational mode is considerably lower than the simulation temperature. The other approach is to apply constraints to the bond lengths or bond bending angles, and the stretching or bending energy is accordingly neglected [33, 35, 38, 39]. The second approach is normally applied when the characteristic temperature of the vibrational mode is much higher than the simulation temperature. However, there exist many vibrational modes of which the characteristic temperature is not too much higher than the simulation temperature. In these cases, the vibration motion is strongly affected by quantum effects. The classical treatment of vibrational modes is likely to be seriously in error. On the other hand, a simple neglect of vibratoinal energies is also not appropriate, because a non-negligible population of molecules may have been excited at the simulation temperature. As an example, Nieto-Draghi *et al.* [33] have shown that both

the classical treatment and the neglect of vibrational motions of $CO_2$ lead to a significant underestimate of thermal conductivity at the supercritical state. A Monte Carlo (MC) method is proposed in this work to taken into account the quantum effects of molecular vibrations. The MC method is based on the assumption that the exchange of energy between the constrained vibrational motion and all other modes of motion is negligible. The method works well for carbon dioxide at dilute and moderate densities. Based on these results, an analytical correction term is proposed in this work to account for the quantum effects of the vibrational contribution to the thermal conductivity. The proposed correction term is found to be able to nicely account for the transport of the vibrational energy in $CO_2$ fluid at both gaseous and supercritical states. The proposed method is also applied to methane at dilute and intermediate densities. The accuracy of the proposed calculation method is examined by comparing the calculated results with the available experimental data and also with the results from other calculation methods.

In addition, the contribution to the thermophysical properties from intermolecular potential as a function of density is studied in this work. At all simulated state points, the molecules are considered as a rigid rotor and the structure of the molecule is assumed as independent of the vibrational energy state and not affected by the interaction between molecules. In order to obtain calculation results with a low statistical error, a very long simulation length is carried out at each simulated state point. Each long simulation is divided into hundreds of parallel runs which are independently initialized and equilibrated at the given temperature and pressure (or density). A possible extension of the proposed simulation method to more complex molecular fluid system is discussed.

**PAPER**

# 1. Determination of vibrational energy levels and transition dipole moments of $CO_2$ molecules by Density Functional Theory

Zhi Liang and Hai-Lung Tsai*

Department of Mechanical and Aerospace Engineering, Missouri University of Science and Technology (formerly University of Missouri-Rolla), Rolla, MO 65409, USA

## Abstract

An efficient method is presented to calculate the intra-molecular potential energies and electrical dipole moments of $CO_2$ molecules at the electronic ground state by solving the Kohn-Sham (KS) equation for a total of 101,992 nuclear configurations. The Projector-Augmented Wave (PAW) exchange-correlation potential functionals and Plane Wave (PW) basis functions were used in solving the KS equation. The calculated intra-molecular potential function was then included in the pure vibrational Schrödinger equation to determine the vibrational energy eigen values and eigen functions. The vibrational wave functions combined with the calculated dipole moment function were used to determine the transition dipole moments. The calculated results were compared with the experimental data.

* Electronic mail: tsai@mst.edu.

## 1. Introduction

Two important problems in the study of infrared absorption spectrum are to determine vibrational energy levels and molecular transition dipole moments. To obtain these results, it is necessary to calculate the intra-molecular potential energy surface (PES) and molecular dipole moment surface (DMS) by ab initio methods. The ab initio calculations of PESs and DMSs of tri-atomic molecules were implemented in several papers [1-7] by the coupled-cluster singles and doubles excitation with perturbative treatment of triple excitations [CCSD(T)] [8] method and the multi-reference configuration interaction (MRCI) method. Localized basis sets such as augmented correlation-consistent polarized quadruple zeta (aug-cc-pVQZ) functions were used in these calculations. Using these methods and basis sets, the potential energies and dipole moments were usually evaluated at $10^2$ to $10^3$ different nuclear configurations that are close to the molecular equilibrium structures. The data were then fitted by polynomial expansions in displacement coordinates, and used in the calculations of molecular properties. In some calculations[2], the coefficients in polynomial expansions needed to be optimized in order to accurately reproduce the experimental values of fundamental transition energies. Generally, the CCSD(T) and MRCI methods combined with localized basis sets gives accurate calculated results. But the method is very computationally demanding.

In this paper, Density Functional Theory (DFT) was used to determine the electronic ground state potential energy of the $CO_2$ molecule. Using DFT, the many-electron Schrödinger equation could be transformed to an effective one electron Schrödinger equation, i.e., KS equation. There are two critical problems in solving the KS equation;

one is to find appropriate exchange-correlation functionals, and the other is to choose appropriate basis functions. In the calculations, PAW potentials [9,10] and PW basis sets were used. DFT method with PW basis sets has several advantages over CCSD(T) method with localized basis functions. These include:

(i) In DFT, the ground-state electronic energy and dipole moment are uniquely determined by the ground-state charge density which is a function of only three variables. Compared to methods such as CCSD(T), DFT reduces the computational cost so that more configurations of small molecules can be evaluated and rather larger molecules are able to be handled. (ii) The KS equations take on a very simple form if PW basis functions are used. The well-developed numerical schemes for the Fourier transforms can be used to evaluate the Hamiltonian matrix elements so that much computational time is saved. (iii) Compared to localized basis sets, no basis-set corrections to forces are needed for PW basis sets because PW basis sets do not depend on nuclear positions. So the PW basis sets allow for relatively simple calculations of forces in the determinations of molecular equilibrium geometries. (iv) The same PW basis sets can be used for all atomic species [11].

Due to the high efficiency of the calculation method we use, intra-molecular potential energies and molecular dipole moments were evaluated at more than $10^5$ different nuclear configurations so that the PES and MDS could be constructed without interpolations or fitting to polynomial expansions. However, there are some problems we need to consider in the calculations if we want to implement PW basis functions to an aperiodic system

like an isolated molecule [12]. The problems will be discussed Section II. Appropriate parameters should be selected to make a compromise between computational time and accuracy.

By solving the KS equation, both the intra-molecular PES and molecular MDS were obtained. The calculated potential energy function was included in the vibrational Schrödinger equation. To efficiently solving the vibrational Schrödinger equation, we split the four-variable potential energy function into four one-variable potential functions that correspond to the potential functions of four vibrational normal modes of $CO_2$ and one perturbation function. The four one-dimensional Schrödinger equations were then obtained by the separation of variables. The solutions of these Schrödinger equations were used as the $0^{th}$ order results. The perturbation function was then included to obtain the real vibrational energy eigen values and wave functions. These results combined with calculated dipole moment functions were used to calculate the molecular transition dipole moments. The calculated results were compared with the experimental values. The details are shown in Section III.

**2. Potential and dipole moment surfaces**

In the first step, we calculate the intra-molecular potential energy and molecular dipole moment as a function of $CO_2$ nuclear configurations. Using the Density Functional Theory, the Born-Oppenheimer potential energy at each nuclear configuration can be determined by solving an effective one electron Schrödinger equation (i.e., KS equation [13]) as

$$\hat{H}^{KS}\psi_i^{KS}\ 1\ = \varepsilon_i^{KS}\psi_i^{KS}\ 1 \tag{1a}$$

$$\text{where } \hat{H}^{KS} = -\tfrac{1}{2}\nabla_1^2 \underbrace{-\sum_A \frac{Z_A}{\vec{r}_{iA}} + \int \frac{\rho\ \vec{r}_2}{r_{12}} d\vec{r}_2 + v_{xc}\ 1}_{V_{eff}\ \vec{r}} \tag{1b}$$

In Eq. (1), $\psi^{KS}\ 1$ is the one electron wave function and $\rho\ \vec{r}\ = \sum_{i=1}^{n} \left|\psi_i^{KS}\right|^2$ is the electron charge density function. If this equation is solved, the charge density distribution $\rho\ \vec{r}$ is also known. $\rho\ \vec{r}$ can then be used in the calculation of the molecular dipole moment by the following equation

$$\vec{d}\ \vec{r}\ = \int d\vec{r}\,\rho\ \vec{r}\ \cdot\ \vec{r} - \vec{R}_{\text{center}} \tag{2}$$

where $\vec{R}_{\text{center}}$ is the center of the molecule. Note Eq. (1) is written in atomic units.

The first three terms in the Hamiltonian of the KS equation, i.e., the electronic kinetic energy, the electron-nuclear attraction potential, and the electron-electron repulsive potential all have explicit forms. However, the last potential term $v_{xc}$, i.e., the exchange-correlation potential is unknown. Some approximations must be made to obtain an appropriate $v_{xc}$. In our calculations, we used a PAW potential (pseudopotentials were used to represent the core electrons), which is supplied by the Vienna *Ab Initio* Simulation Package (VASP). [14,15]

Now, the problem turns to how to select the basis functions. The basis functions should be chosen so that the wave function $\psi_i^{KS}$ satisfies proper boundary conditions. In our calculations the $CO_2$ molecule was placed in the center of a cubic supercell of side $L$

as shown in Fig. 1. In order to use PW functions as basis functions, Periodic Boundary Conditions (PBC's) were applied. So the one electron wave function can be written as

$$\psi\ \vec{r}\ = \sum_{\vec{K}} \alpha\ \vec{K}\ e^{i\vec{K}\cdot\vec{r}} \tag{3}$$

where $\vec{K}\cdot\vec{l} = 2\pi m$, $m$ is an integer, $\vec{K}$ is a wave vector, and $\vec{l}$ is a lattice vector. The PW functions have a big advantage in solving KS equations because the Hamiltonian matrix elements now become [16] $\hat{H}_{\vec{K}'\vec{K}} = \frac{1}{V_c}\int d\vec{r}_1\ e^{i\vec{K}'\cdot\vec{r}\ *}\hat{H}^{KS}\ 1\ e^{i\vec{K}\cdot\vec{r}}$, where $V_c$ is the volume of the cubic supercell which is used as the normalization factor. In Eq. (1), we know $\hat{H}^{KS} = -\frac{1}{2}\nabla_1^2 + V_{eff}\ \ \vec{r}\ $ . (4a)

Hence, $\hat{H}_{\vec{K}'\vec{K}} = \frac{\vec{K}^2}{2}\delta_{\vec{K}\vec{K}'} + \frac{1}{V_c}\int V_{eff} e^{i\ \vec{K}-\vec{K}'\ \cdot\vec{r}} d\vec{r}$ (4b)

One can see that the second part of Eq. (4b) is the Fourier transform of an effective potential which can be easily evaluated by the well-developed numerical schemes.

In the implementation, the PW basis functions must be truncated at some wave number $\vec{K}$. This wave number should be high enough to account for some fast oscillating components of the electronic wave functions. In the calculation, cut-off energy was used to control the number of basis functions, and the relation is shown Eq. (5).

$$\frac{\hbar^2 K^2}{2m_e} = \frac{\hbar^2\left(\frac{2\pi}{L}\right)^2\ \ N_x^2 + N_y^2 + N_z^2}{2m_e} < E_{cut} \tag{5}$$

where $N_i$ is the number of basis functions in i direction. From Eq. (5) one can see the number of basis functions is determined by both the supercell size $L$ and cut-off energy

$E_{cut}$. A large $L$ or $E_{cut}$ corresponds to a large number of basis functions. A large number of basis functions correspond to a high accuracy and computational cost. Hence, one must pick the appropriate supercell size and cut-off energy to make a compromise between accuracy and computation cost.

*2.1. Choose appropriate supercell size*

Although the PBC's with PW basis functions could save much computational time, this method brings one problem in the calculations of isolated molecules. As shown in Fig. 1, there exist spurious interactions of aperiodic charge density with its images in the neighboring supercells. The potential energy $E\ L$ calculated in a finite cubic supercell with side $L$ differs from the potential energy calculated in the limit $E_0 = E\ L \to \infty$ . To estimate $E_0$ from the calculated $E\ L$ , one needs to know the asymptotic dependence of $E$ on $L$. It was proved [12] that the asymptotic behavior of an isolated neutral molecule without dipole moment in a cubic supercell can be determined by the quadrupole-quadrupole interaction, which has a functional dependence of $L^{-5}$. We calculated the equilibrium C-O separation $r_e$ and the minimal potential energy $U_{\min}$ of the molecule at different supercell sizes. The calculations were performed using the program **VASP**. The cut-off energy was chosen as 1000eV. The results were shown in Fig. 2, where one can see that both $U_{\min}$ and $r_e$ converge very fast with the supercell size. The calculated $r_e$ is 1.162Å which is very close to the experimental value [17] 1.160 Å.

However, a $CO_2$ molecule only has zero dipole moment at symmetric linear configurations. When the molecule deviates from its equilibrium configuration, it could have dipole moment. In this case, the asymptotic dependence of potential energy on supercell size is dominated by a dipole-dependent term $\frac{2\pi}{3V_c}\left|\int_{cell} d^3r\vec{r}\rho\ \vec{r}\ \right|^2$. The absence of this dipolar term could lead to a $O\ L^{-3}$ convergence [12]. Figure 3 shows the potential energy of asymmetric stretching a $CO_2$ molecule by 0.15Å from equilibrium as a function of supercell size. The calculations were performed both with and without the dipolar term, and the results are shown in Fig. 3. One can see the two curves converge to the same value; but the calculation with the dipolar term converges faster than the one without the dipolar term. So, to get a result with the same accuracy, we need to use a relatively larger supercell size if we do not include the dipolar term. However, larger supercell size means more computational time. To save the computational time, we always include the dipolar term in our calculations.

From the above analysis, to make a compromise between computation time and accuracy, we chose a cubic supercell size of 10Å in our calculations. The dipolar potential term is always included.

*2.2. Choose appropriate cut-off energy*

We fix the supercell size at 10Å and change the cut-off energy from 700 to 1300 eV. The minimal potential energy of a $CO_2$ molecule and the dipole moment at the nuclear configuration of asymmetric stretching the molecule by 0.2Å from equilibrium were

calculated. The results were shown in Fig. 4. The molecule has bigger dipole moments and lower potential energies at larger cut-off energies. Note the values only change a little (less than 0.1%) after 1000 eV and hence 1000eV was chosen as the cut-off energy in our calculations.

One can see the PW basis functions only depends on supercell sizes. They do not depend on atomic species in the molecule or nuclear positions. The convergence properties with respect to supercell size and cutoff energy can be easily tested by the above calculations. The computational cost of the test procedure is very small compared to later calculations of PES and MDS. Once the appropriate supercell size and cutoff energy are chosen, one could keep these parameters constant and calculate potential energies and dipole moments at different configurations with a good accuracy and efficiency.

By placing the $CO_2$ molecule at the center of a cubic supercell of side 10Å, choosing the cut-off energy at 1000eV, and including the dipolar potential term, we calculated the intra-molecular potential and molecular dipole moment at 101,992 different nuclear configurations. The details of these configurations are shown in Table 1. The calculated potential energy and dipole moment surfaces will be used in the next section to determine the vibrational energy levels and transition dipole moments.

**3. Vibrational levels and transition dipole moment**

Using the coordinate system as shown in Fig. 5, the pure vibrational Schrödinger equation of a $CO_2$ molecule can be expressed as

$$\hat{H}_v\psi = E\psi \tag{6a}$$

$$\text{where } \hat{H}_v = -\frac{\hbar^2}{2\mu_O}\frac{\partial^2}{\partial r^2} - \frac{\hbar^2}{2\mu_C}\left(\frac{\partial^2}{\partial x^2} + \frac{\partial^2}{\partial y^2} + \frac{\partial^2}{\partial z^2}\right) + U\ \ r, x, y, z \tag{6b}$$

In Eq. (6), $r$ represents the distance between two O atoms; $x$, $y$ and $z$ are the three components of the vector starting from the middle point of the two O atoms and ending at the C atom; U is the potential term; $\mu_O$ and $\mu_C$ are, respectively, the reduced mass of O atom and C atom and they are given by the following equation:

$$\mu_O = \frac{m_O}{2},\ \mu_C = \frac{m_C \cdot 2m_O}{m_C + 2m_O} \tag{7}$$

The potential energy term depends on 4 variables. However, y and z are actually equivalent due to the symmetry of the $CO_2$ molecule. So in the construction of potential and dipole moment surface, to save computational time, we fixed the z to be zero and changed the values of the other three variables. After we get the functions $U\ \ r, x, y, 0$ and $\vec{d}\ \ r, x, y, 0$ , the full surface of the potential and dipole moment, i.e., $U\ \ r, x, y, z$ and $\vec{d}\ \ r, x, y, z$ can be obtained according to the symmetry.

Figures 6(a)–(c) show the iso-surfaces of $U\ \ r, x, y, 0$ , x component of $\vec{d}\ \ r, x, y, 0$ and y component of $\vec{d}\ \ r, x, y, 0$ , respectively. The z component of $\vec{d}\ \ r, x, y, 0$ is not shown because it is always zero. Note in Fig. 6, the unit of U is eV, and the unit of dipole

moment is Debye. The zero potential in Fig. 6(a) corresponds to the minimal potential of a $CO_2$ molecule which is equal to -24.2815 eV.

As Eq. (6) is a four-dimensional Schrödinger equation, in order to solve the equation efficiently, we split $U\ r,x,y,z$ into five parts as follows

$$U\ r,x,y,z = U_r\ r,0,0,0 + U_x\ r_e,x,0,0 + U_y\ r_e,0,y,0 + U_z\ r_e,0,0,z + V\ r,x,y,z \quad (8)$$

where $r_e$ is the equilibrium C-O separation which is a constant. The first four potential functions on the right hand side of Eq. (8) are a function of only one variable which can be directly extracted from the function $U\ r,x,y,z$ . The remaining three variables in each of the four potential functions are fixed at the equilibrium configuration of the molecule. $V\ r,x,y,z$ is the difference between $U\ r,x,y,z$ and the sum of the four one-variable functions. Figures 7(a)-(c) show the four calculated potential functions and the dipole moment functions extracted from $U\ r,x,y,z$ and $\vec{d}\ r,x,y,z$ . Figure 7(a) corresponds to the symmetric stretching vibration mode; Figure 7(b) corresponds to the two degenerate bending vibration modes; and Fig. 7(c) corresponds to the asymmetric stretching vibration mode. We define a new Hamiltonian as follows:

$$\hat{H}_0 = -\frac{\hbar^2}{2\mu_O}\frac{\partial^2}{\partial r^2} - \frac{\hbar^2}{2\mu_C}\left(\frac{\partial^2}{\partial x^2} + \frac{\partial^2}{\partial y^2} + \frac{\partial^2}{\partial z^2}\right) + U_r\ r + U_x\ x + U_y\ y + U_z\ z \quad (9)$$

Hence, $\hat{H}_v = \hat{H}_0 + V$ , where V is a perturbation term.

One can see a Schrödinger equation with the new Hamiltonian can be easily solved by separation of variables. The four separated one-dimensional Schrödinger equations

were solved independently by the Numerov [18] method. The lowest three energy eigen values of each mode were shown in Table 2, and their corresponding normalized wave functions were shown in Fig. 8(a)-(c). The combinations of these energy eigen values and eigen functions form the eigen values $E_n$ and eigen functions $|n\rangle$ of $\hat{H}_0$. The relation is shown as

$$\begin{aligned} |n\rangle &= |n_r n_y n_z n_x\rangle = |n_r\rangle \cdot |n_y\rangle \cdot |n_z\rangle \cdot |n_x\rangle \\ E_n &= E_{n_r} + E_{n_y} + E_{n_z} + E_{nx} \end{aligned} \tag{10}$$

In Eq. (10), each eigen function contain 4 quantum numbers. The first quantum number $n_r$ corresponds to the symmetric stretching quantum number. The second and third quantum numbers $n_y, n_z$ correspond to the two degenerate bending quantum numbers. The last one $n_x$ corresponds to the asymmetric stretching quantum number. These eigen values and eigen functions will be used as the $0^{th}$ order results of vibrational levels. The real vibrational eigen functions can be written as a linear combination of these $0^{th}$ order wave functions as

$$|v\rangle = \sum_n c_{vn} |n\rangle \tag{11}$$

The coefficients $c_{vn}$ and the real vibrational energy eigen values can be obtained by solving the following matrix equation

$$\mathrm{HC_v} = \mathrm{E_v C_v} \tag{12}$$

The matrix elements in the H matrix in Eq. (12) can be determined by

$$H_{mn} = H_{nm} = \langle n | \hat{H}_0 + V | m \rangle = E_n \delta_{mn} + \langle n | V | m \rangle \tag{13}$$

where $\langle n|V|m\rangle$ is actually a four-dimensional integral which can be evaluated by repeatedly using the Simpson Rule.

In the calculation, 50 $0^{th}$ order wave functions corresponding to the 50 lowest $0^{th}$ energy eigen values were chosen as the basis functions. So the matrix H becomes a 50×50 matrix. The matrix Eq. (12) was solved by matrix diagonalization schemes. Table 3 shows nine calculated real vibrational energy eigen values and eigen functions. These vibrational energy levels are related to the transitions shown in Table 4. The eigen functions in Table 3 were expressed as a linear combination of the $0^{th}$ order eigen functions of which the absolute values of the coefficients are greater than 0.01.

After the real energy eigen values and eigen functions were known, the transition dipole moment between different vibrational energy levels can be calculated as

$$\vec{M}_{v_1 v_2} = \langle v_1 | \vec{d} \;\; r, x, y, z \;\; | v_2 \rangle = \sum_{mn} c_{v_1 n} c_{v_2 m} \langle n | \vec{d} | m \rangle \tag{14}$$

The results are shown in Table 4. The calculated vibrational energy levels in Table 3 have generally a good agreement with the experimental data [19]. The biggest inaccuracy is less than 3%. The error is mainly caused by an approximate exchange-correlation ($E_{xc}$) functional used in the calculations. From the wave functions shown in Table 3, one can see (0, 0, 0), (0, $1^1$, 0) and (0, 0, 1) energy levels are dominated by their $0^{th}$ order wave functions. Their real wave functions are only weakly mixed by a few other $0^{th}$ order wave functions of the same species. The remaining six energy levels are originated from the three coupled vibrational levels in resonance (Fermi resonance). The $0^{th}$ order wave

functions of these vibrational levels are strongly mixed with $0^{th}$ order wave functions of the resonant vibrational levels.

In Table 4, the transition dipole moments of nine parallel bands and nine perpendicular bands were calculated. The transition dipole moments of fundamental transition bands like (0, 0, 1) – (0, 0, 0) and (0, 1, 0) – (0, 0, 0) were dominated by only one dipolar integral in Eq. (14) because all other integrals can be neglected due to their small coefficients. For Fermi resonance energy levels, the coefficients of strongly mixed $0^{th}$ order wave functions are related to two constants [19]; one is $\Delta E$ (the unperturbated separation of the energy levels in resonance, $\Delta E = E_n - E_m$) and the other is the interaction matrix elements $\langle n|V|m\rangle$ which is related to the perturbation energy $V$. Hence, the errors in the calculations of $E_n$ and $\langle n|V|m\rangle$ were propagated into the calculations of coefficients $c_{vn}$ and the transition dipole moments $\vec{M}_{v_1 v_2}$ so that bigger errors may be induced. As a result, the transition dipole moments of fundamental transitions in Table 4 have generally better agreements with experimental data [20] than those of Fermi resonance levels. These results will also be improved with improved $E_{xc}$ functionals.

**4. Conclusion**

Using the DFT, intra-molecular PES and DMS were determined by solving the KS equation. Appropriate supercell size and cut-off energy were selected to make a compromise between accuracy and computation speed. DFT combined with PAW

potential functionals and PW basis functions greatly increased the computational speed. The DFT method predicted an excellent $CO_2$ geometry and fairly good vibrational energy eigen values and transition dipole moments. These results are very useful in the calculations of infrared absorption spectra of molecules. However, with the presently available potential functionals, the DFT still cannot match the accuracy that the methods like CCSD(T) and QCISD(T) can achieve [21]. It is believed if better $E_{xc}$ functionals are available, the results would be improved by using the method developed in this paper. The high efficiency of the method developed in this paper makes it applicable to larger and more complicated molecules. However, with the number of atoms in the molecules increases, the computational cost of CCSD(T) method will be prohibitive.

Based on the *ab initio* results of vibrational energy eigen values and transition dipole moments shown in this paper, the infrared absorption cross sections of $CO_2$ at room temperature and 1−10 atm is calculated in a subsequent paper [22]. The good agreement between the calculated results and the available experimental data [23] will further validate the calculation method proposed in this paper.

**Acknowledgements**

This work was supported by Office of Navy Research through the Multidisciplinary University Research Initiative (MURI) program, Award No. N00014-05-1-0432.

**References**

[1] Z. Wang, M. Gong, Y. Zhang, E. Feng, and Z. Cui, Chem. Phys. Lett. **454**, 7 (2008).

[2] C. Leonard, M. Diehr, P. Rosmus, and W.C. Maguire, JQSRT. **109**, 535 (2008).

[3] Z.G. Huang, E. C. Yang, and D.Q. Xie Chin. Chem. Lett., **article in press**, (2008).

[4] T. Stoecklin and A. Voronin, Chem. Phys. **331**, 385 (2007).

[5] K.A. Peterson and G.C. McBane, J. Chem. Phys. **123**, 084314 (2005).

[6] U. Lourderaj, N. Sathyamurthy, Chem. Phys. **308**, 277 (2005).

[7] R. Tarroni, Mol. Phys. **102**, 2167 (2004).

[8] J. Noga and R.J. Bartlett, J. Chem. Phys. **86**, 7041(1987).

[9] P.E. Bl¨ochl, Phys. Rev. B **50**, 17953 (1994).

[10] G. Kresse and J. Joubert, Phys. Rev. B **59**, 1758 (1999).

[11] D. L.G. Cheung, Ph. D thesis, University of Durham, 33 (2002)

[12] G. Makov and M.C. Payne, Phys. Rev. B **51**, 4014 (1995).

[13] W. Kohn, Phys. Rev. **140**, 1133 (1965).

[14] G. Kresse and J. Furthmu¨ller, Phys. Rev. B **54**, 11169 (1996).

[15] G. Kresse and J. Furthmu¨ller, Comput. Mater. Sci. **6**, 15 (1996).

[16] E. Kaxiras, *Atomic and electronic structure of solids*, (2003), p.49.

[17] A.D. Buckingham, *Molecular structure and properties*, (1975), p.23.

[18] T. Pang, *An introduction to computational physics*, (2006), p.105.

[19] G. Herzberg, *Molecular spectra and molecular structure*, **2nd** edition, (1950), p.274.

[20] I. Suzuki, J. Mol. Spec. **80**, 12 (1980).

[21] I.N. Levine, *Quantum Chemistry*, (2000), p.591.

[22] Zhi Liang and Hai-Lung Tsai, 2008 ASME International Mechanical Engineering Congress and Exposition, November 2008: IMECE2008-67776.

[23] Retrieved from HITRAN on April 30, 2008, http://cfa-www.harvard.edu/hitran/

Table 1. Values of r, x, y, z used in the calculations.

| | variation (Å) | increment (Å) | number of points |
|---|---|---|---|
| r | 2.10~2.58 | 0.008 | 61 |
| x | 0~0.172 | 0.004 | 44 |
| y or z | 0~0.37 | 0.01 | 38 |

Table 2. Energy eigen values (unit $cm^{-1}$) where all the values are subtracted by the corresponding ground state energies.

| Eigen energy / Quantum number | $E_{n_r}$ | $E_{n_y}$ or $E_{n_z}$ | $E_{n_x}$ |
|---|---|---|---|
| 0 | 0 | 0 | 0 |
| 1 | 1344 | 662 | 2430 |
| 2 | 2682 | 1332 | 4879 |

Table 3. Energy eigen values and eigen functions of real vibration states. Column 1 shows the notations of the traditional $CO_2$ vibration levels. Columns 2 and 3 show experimental and calculated energy eigen values of $CO_2$ vibrations, respectively. Both of them are in unit $cm^{-1}$. Column 4 shows the real vibrational wave functions expressed as linear combinations of the $0^{th}$ order eigen functions $\left|n_r n_y n_z n_x\right\rangle$.

| $(v_1, v_2^l, v_3)$ | E(exp.) | E(cal.) | wave functions |
|---|---|---|---|
| (0, 0, 0) | 0 | 0 | $0.999\left\|0000\right\rangle - 0.022\left\|1000\right\rangle - 0.015\left\|1200\right\rangle - 0.015\left\|1020\right\rangle$ |
| $(0, 1^1, 0)$ | 667 | 649 | $0.999\left\|0100\right\rangle - 0.015\left\|0300\right\rangle + 0.019\left\|1100\right\rangle - 0.025\left\|1300\right\rangle - 0.015\left\|1021\right\rangle$ |
| $(0, 2^0, 0)$ | 1285 | 1266 | $0.562\left\|0200\right\rangle + 0.562\left\|0020\right\rangle - 0.604\left\|1000\right\rangle + 0.036\left\|1200\right\rangle + 0.036\left\|1020\right\rangle$ |
| (1, 0, 0) | 1388 | 1382 | $-0.427\left\|0200\right\rangle - 0.427\left\|0020\right\rangle) - 0.796\left\|1000\right\rangle - 0.033\left\|2000\right\rangle - 0.024\left\|0000\right\rangle$ |
| $(0, 3^1, 0)$ | 1932 | 1900 | $0.644\left\|0300\right\rangle + 0.370\left\|0120\right\rangle - 0.664\left\|1100\right\rangle + 0.067\left\|1300\right\rangle + 0.037\left\|1012\right\rangle$ |
| $(1, 1^1, 0)$ | 2077 | 2054 | $-0.572\left\|0300\right\rangle - 0.333\left\|0120\right\rangle - 0.747\left\|1100\right\rangle - 0.045\left\|1300\right\rangle - 0.029\left\|1012\right\rangle$ |
| (0, 0, 1) | 2349 | 2372 | $0.989\left\|0001\right\rangle - 0.145\left\|1001\right\rangle$ |
| $(0, 2^0, 1)$ | 3613 | 3617 | $0.594\left\|0201\right\rangle + 0.594\left\|0021\right\rangle - 0.528\left\|1001\right\rangle - 0.100\left\|2100\right\rangle$ |
| (1, 0, 1) | 3716 | 3745 | $-0.380\left\|0201\right\rangle - 0.380\left\|0021\right\rangle - 0.812\left\|1001\right\rangle - 0.176\left\|2100\right\rangle - 0.132\left\|0001\right\rangle$ |

Table 4. Experimental and calculated transition dipole moments $\vec{M}_{v_1 v_2}$ (in Debye) of $CO_2$, where the sign of the transition dipole moment is arbitrary.

| Parallel bands | | | Perpendicular bands | | |
|---|---|---|---|---|---|
| Band | $M_x$(exp.) | $M_x$(cal.) | Band | $M_y$(exp.) | $M_y$(cal.) |
| (0, 0, 1) – (0, 0, 0) | 0.326 | 0.301 | (0, 1, 0) – (0, 0, 0) | 0.131 | 0.120 |
| (0, $2^0$,1) – (0, 0, 0) | 0.027 | 0.020 | (1, 1, 0) – (0, 0, 0) | 0.0011 | 0.0011 |
| (1, 0, 1) – (0, 0, 0) | 0.033 | 0.041 | (0, $3^1$,0) – (0, 0, 0) | 0.0005 | 0.0003 |
| (0, 0, 1) – (0, $2^0$,0) | 0.028 | 0.016 | (1, 0, 0) – (0, 1, 0) | 0.094 | 0.065 |
| (0, 0, 1) – (1, 0, 0) | 0.033 | 0.025 | (0, $2^0$,0) – (0, 1, 0) | 0.090 | 0.099 |
| (0, $2^0$,1) – (0, $2^0$,0) | 0.331 | 0.298 | (1, 1, 0) – (1, 0, 0) | 0.153 | 0.134 |
| (0, $2^0$,1) – (1, 0, 0) | 0.011 | 0.024 | (1, 1, 0) – (0, $2^0$,0) | 0.031 | 0.029 |
| (1, 0, 1) – (0, $2^0$,0) | 0.008 | 0.021 | (0, $3^1$,0) – (1, 0, 0) | 0.024 | 0.015 |
| (1, 0, 1) – (1, 0, 0) | 0.331 | 0.296 | (0, $3^1$,0) – (0, $2^0$,0) | 0.154 | 0.150 |

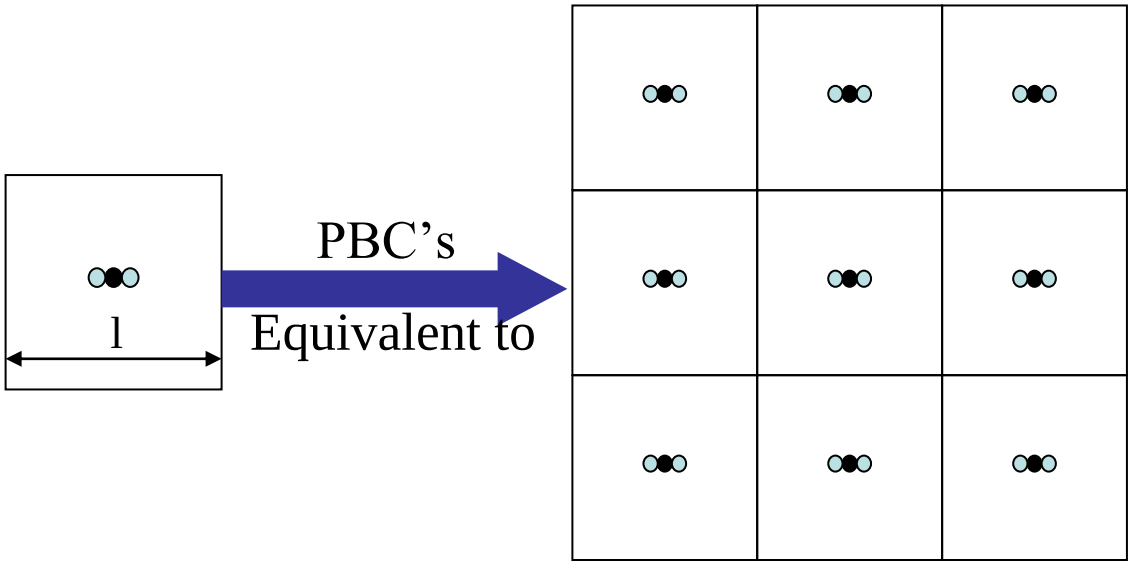


Fig. 1. A $CO_2$ molecule in a cubic supercell with PBC's.

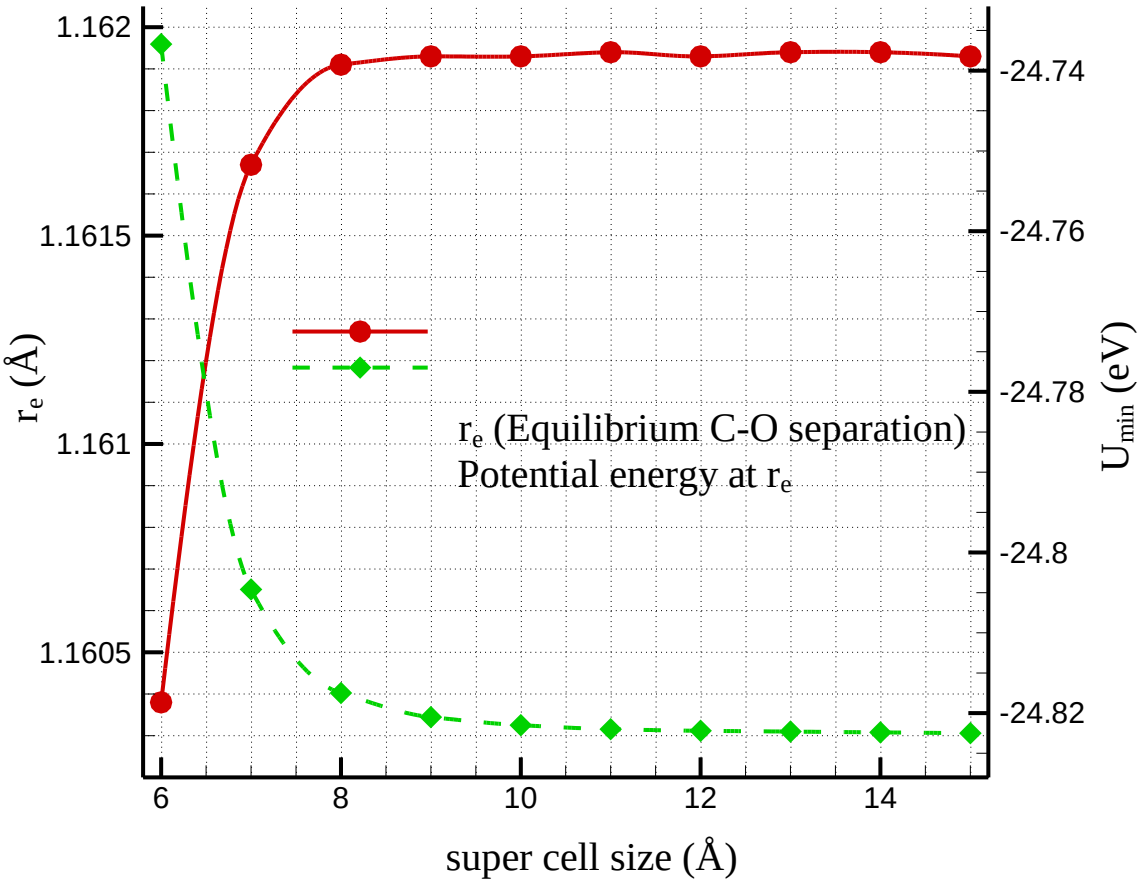


Fig. 2. $r_e$ and $U_{min}$ vs. supercell size.

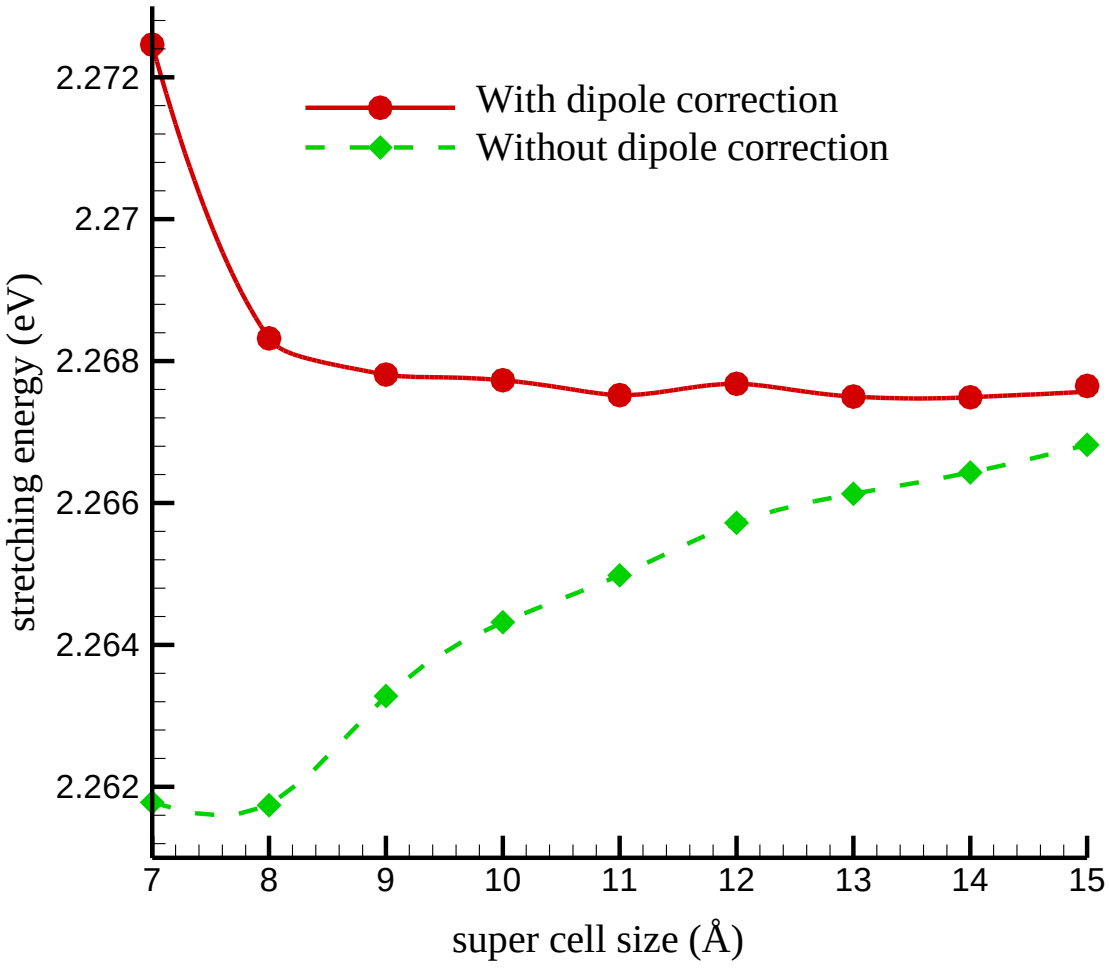


Fig. 3. Potential energy of stretching a $CO_2$ with and without dipole-dependent term.

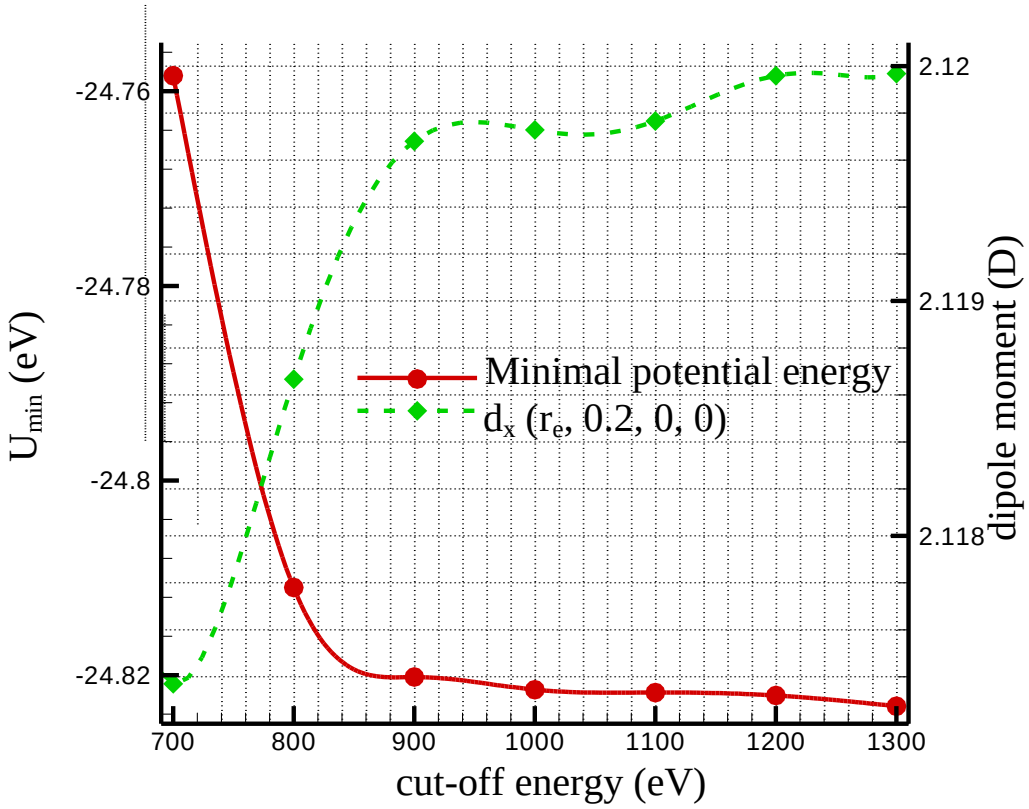


Fig. 4. $U_{\min}$ and dipole moment vs. $E_{cut}$.

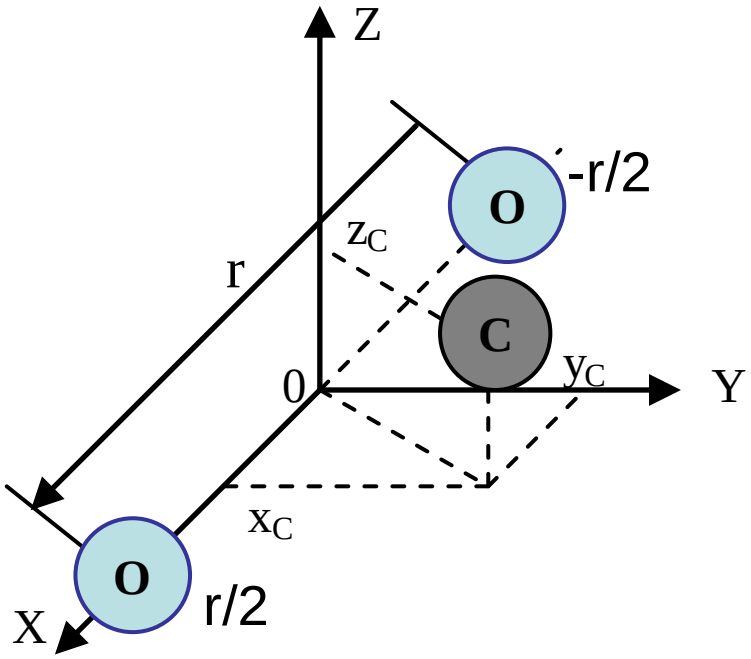


Fig. 5. Coordinates of a $CO_2$ molecule.

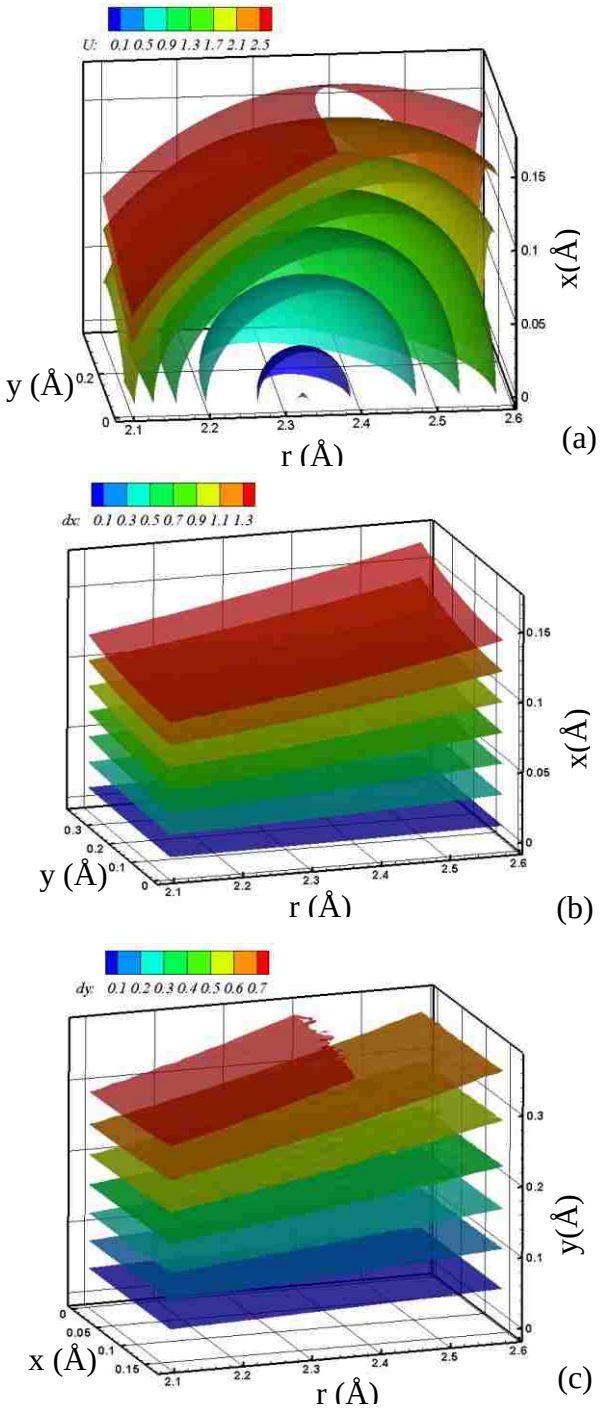


Fig. 6. Iso-value surfaces of (a) intra-molecular potential energy $U\ \ r,x,y,0\ \ $, (b) dipole moment component parallel to the molecular axis $d_x\ \ r,x,y,0\ \ $, (c) dipole moment component perpendicular to the molecular axis $d_y\ \ r,x,y,0\ \ $.

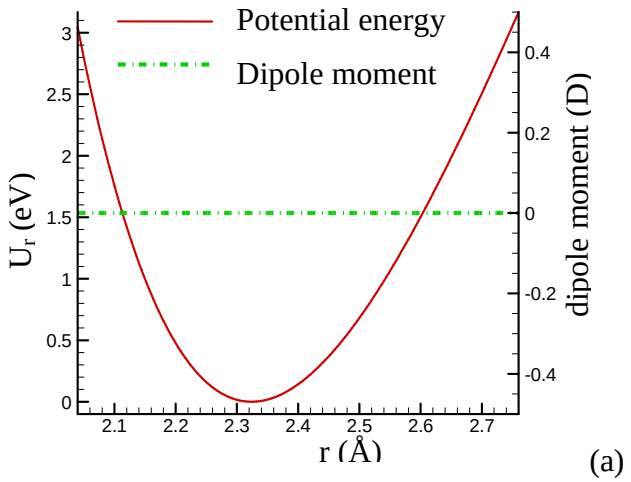


(a)

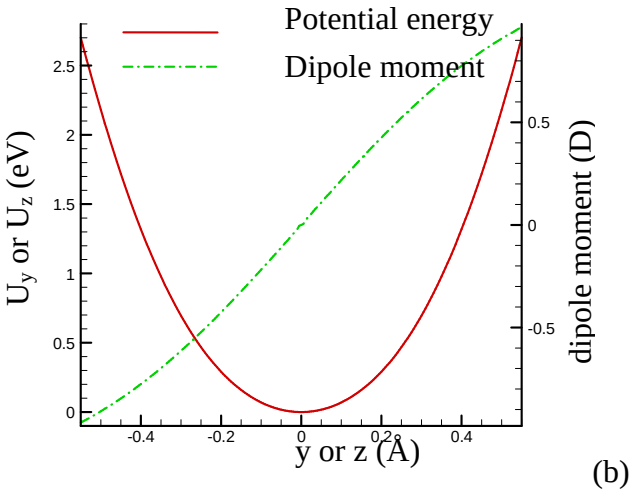


(b)

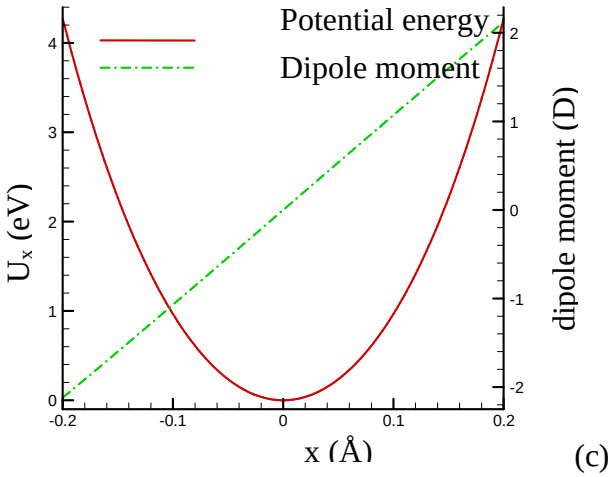


(c)

Fig. 7. Intra-molecular potential energy and dipole moment functions, (a) $U\ r,0,0,0$ and $d_x\ r,0,0,0$ , (b) $U\ r_e,0,y,0$ and $d_y\ r_e,0,y,0$ , (c) $U\ r_e,x,0,0$ and $d_x\ r_e,x,0,0$ .

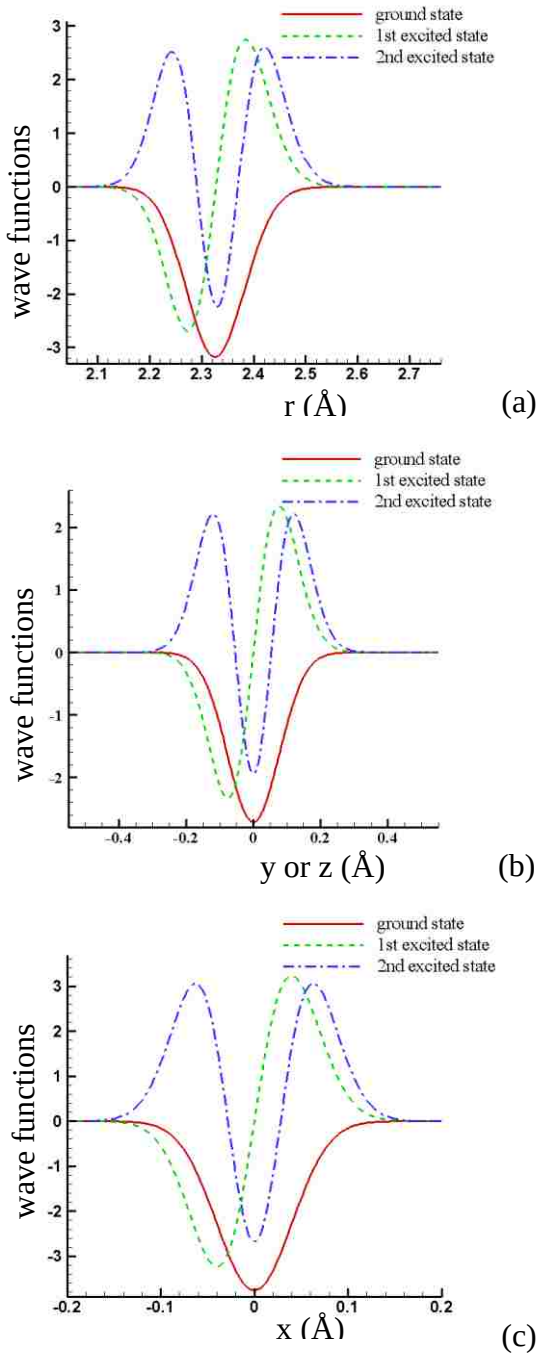


Fig. 8. The $0^{th}$ order normalized vibrational wave functions of lowest three energy states, (a) symmetric stretching mode, (b) doubly degenerate bending mode, (c) asymmetric stretching mode.

## 2. Prediction of the transport properties of a polyatomic gas

Zhi Liang and Hai-Lung Tsai*

Department of Mechanical and Aerospace Engineering, Missouri University of Science and Technology (formerly University of Missouri-Rolla), Rolla, MO 65409, USA

**ABSTRACT**

An *ab initio* molecular potential model is employed in this paper to show its excellent predictability for the transport properties of a polyatomic gas from molecular dynamics simulations. A quantum mechanical treatment of molecular vibrational energies is included in the Green and Kubo integral formulas for the calculation of the thermal conductivity by the Metropolis Monte Carlo method. Using $CO_2$ gas as an example, the fluid transport properties in the temperature range of 300 – 1000 K are calculated without using any experimental data. The accuracy of the calculated transport properties are significantly improved by the present model, especially for the thermal conductivity. The average deviations of the calculated results from the experimental data for self-diffusion coefficient, shear viscosity, thermal conductivity are, respectively, 2.32%, 0.71% and 2.30%.

Keywords: Molecular Modeling; $CO_2$; Transport properties; Ab initio

---

* Corresponding author. Tel: 573 341 4945; fax: 573 341 4607.

*Email address*: tsai@mst.edu.

## 1. Introduction

To successfully predict transport properties of real fluids from molecular simulation, the most critical problem is to develop an accurate interaction potential model. For polyatomic molecules, a widely used potential model is to represent the intermolecular interactions by multi-center Lennard-Jones plus either quadrupole or dipole moments. The parameters in this potential model were normally adjusted or optimized to experimental vapor-liquid equilibria data [1-4]. These potential models usually predict static thermodynamic properties more accurately than transport properties. To get better transport properties predictions, transport properties need to be used directly in the parameterization of the molecular potential [5]. Therefore, the predictions of transport properties by these potential models strongly depend on the existence and accuracy of the experimental data. In the last decades, with the increasing computing power, accurate determinations of intermolecular potential of polyatomic molecules by *ab initio* methods become feasible. As an example, it was found from the *ab initio* calculation [6] that the $CO_2$ molecule is a linear molecule with the C-O bond length $r_0 = 1.162\,\text{Å}$ which agrees with the experimental result [7]. Based on the linear molecular structure, a number of potential surfaces have been proposed for $CO_2$ – $CO_2$ interaction [8-10]. They were all determined by *ab initio* methods and validated by comparing with experimental second virial coefficients. The accurate *ab initio* potentials make it possible to predict a variety of physical properties of fluids without using any experimental data. Once the accurate intermolecular potential is available, appropriate molecular simulation techniques should be employed to calculate the required fluid transport properties. There exist two standard methodologies, i.e. equilibrium molecular dynamics (EMD) which is based on the

Einstein relations or Green-Kubo integral formulas [11-13] and non-equilibrium molecular dynamics (NEMD) in which the transport properties are measured by creating a flow in the fluid under study [14]. A lot of researchers prefer using NEMD because NEMD simulations were considered to be more efficient [15-18]. However, NEMD simulations are normally able to provide only one transport property at once [14], whereas EMD is a multi-property method. The thermodynamic properties and transport properties such as self-diffusion coefficient, viscosity and thermal conductivity can be all obtained from the output of a single equilibrium run. Moreover, when an anisotropic potential is used for the calculations of transport properties of a polyatomic gas, the molecular model is much more complicated than the isotropic Lennar-Jones molecular model. In this case, the overall efficiency of non-equilibrium methods is not necessary to be higher than the equilibrium simulations allowing for the need to extrapolate the non-equilibrium simulation results to thermodynamic equilibrium [19]. Therefore, EMD simulations are used in this work.

Although both *ab initio* potential of $CO_2$ molecules and molecular simulation techniques exist, most of researchers only used the *ab initio* potential to validate phase equilibrium properties of carbon dioxide [9, 20, 21]. The amount of calculations of transport properties such as viscosity and thermal conductivity based on the *ab initio* potential is scarce. On the other hand, there are several calculations of $CO_2$ transport properties based on potential models optimized to experimental data [3, 18, 22]. However, the deviations between the simulated results and experimental data still reached 10% for self-diffusion coefficient [22], 5% for shear viscosity and 10% for thermal conductivity at low temperature and high densities [3]. A deviation of up to 30% was

even found for thermal conductivities at relatively high temperature and low densities [18]. The large deviations are mainly caused by not sufficient accurate potential and inappropriate treatment of molecular vibrations. The purpose of the present work is to use $CO_2$ gas as an example to demonstrate that if quantum effects of molecular vibrations are treated appropriately, the self-diffusion coefficient, shear viscosity and thermal conductivity of a polyatomic gas in a wide range of temperature can all be accurately determined from EMD simulations by employing an *ab initio* potential. The three transport properties of $CO_2$ gas at 1 atm and in the temperature range of 300 – 1000 K are calculated in this work. In this range of temperatures, accurate experimental data are available and can be used to validate the calculation method and the *ab initio* potential employed in the work.

The *ab initio* potential surfaces proposed for carbon dioxide all treated $CO_2$ molecules as linear rigid rotors. Hence, in this work we assume the structure of $CO_2$ is unaffected by the interaction between molecules. The self-diffusion coefficient and shear viscosity measure the transports of mass and momentum in the fluid. The influence of vibrational motions can be neglected in those calculations since the transfer of vibrational energy to rotational and translational degrees of freedom is extremely slow [9] and the vibrational energy can be considered as frozen in the molecule in the simulation. The thermal conductivity, however, measures the transport of energy through the fluid. Hence, the vibrational energy must be considered in the calculation of thermal conductivity.

Based on the above assumptions, the MD simulations are carried out in the microcanonical ensemble. The statistical errors in the calculations of the time correlation

functions are inversely proportional to the square root of the simulation length. To obtain a relative precision of less than 1% in the time correlation function, it is necessary to conduct a run of $10^4$ correlation time [23]. An estimation based on the preliminary results in this work shows the correlation time for a $CO_2$ gas in the temperature range of 300 – 1000 K is in the order of $10^2$ ps. Hence, long simulations up to the order of 10 μs are required to obtain accurate results. To save the total computational cost, the original *ab initio* potential is employed with a small modification so that large time step sizes can be used without causing the energy conservation problem.

This paper is organized as follows. The following section provides the theoretical background of Green-Kubo formula. In Sec. 3, the modified *ab initio* intermolecular potential and force are presented. In Sec. 4, we describe the MC method used for initializing the MD simulations. The results of the MD simulations compared to experimental results are given in Sec. 5. Finally, the conclusions are drawn in Sec. 6.

## 2. Theoretical background

In the time-correlation function theory, the three transport properties considered can be all calculated by either the Green-Kubo integral formulas or the Einstein-Helfand relations in equilibrium simulations. It can be proven [24] that the Einstein-Helfand relations are equivalent to the Green-Kubo formulas. However, due to the periodic boundary conditions (PBC's) used in MD simulations, the original expressions of the Einstein-Helfand relations cannot be applied directly. Also, additional terms must be included allowing for discontinuous particle trajectories in a finite-system simulation with PBC's [25]. Hence, in this work we use the Green-Kubo formulas.

The Green-Kubo formula for self-diffusion coefficient $D$ can be expressed as [14]

$$D = \tfrac{1}{3}\int_0^\infty dt \left\langle \vec{v}_i(t)\cdot\vec{v}_i(0)\right\rangle, \tag{1}$$

where $\vec{v}_i$ is the translational velocity of *i*th molecule, *t* is the time, and $\langle\cdots\rangle$ denotes ensemble average. To improve statistical accuracy, the velocity time correlation function is computed by averaging over 1,000 molecules in the simulation.

The shear viscosity $\eta$ given by the Green-Kubo formula is [14]

$$\eta = \frac{V}{k_B T}\int_0^\infty dt \left\langle \mathrm{P}_{\alpha\beta}(t)\cdot\mathrm{P}_{\alpha\beta}(0)\right\rangle, \tag{2}$$

$$\text{where } \mathrm{P}_{\alpha\beta} = \frac{1}{V}\left(\sum_i m v_{i\alpha} v_{i\beta} + \sum_i \sum_{j>i} r_{ij_\alpha} f_{ij_\beta}\right). \tag{3}$$

In Eqs. (2) and (3), the subscript $\alpha$ and $\beta$ denote the vector component. Due to the PBC's used in the simulation, the minimum-image convention is employed to find all interacting pairs. Since the viscosity is a multi-particle property, no additional averaging over the N particles is possible to improve the statistical accuracy. The viscosity, therefore, requires much longer simulations than the self-diffusion coefficient to get accurate results.

The Green-Kubo formula relates the thermal conductivity $\lambda_T$ to the time autocorrelation function of the energy current via the following relation [14]

$$\lambda_T = \frac{V}{k_B T^2}\int_0^\infty dt \left\langle J_\alpha \;\; t \;\; J_\alpha \;\; 0 \right\rangle. \tag{4}$$

Here, $J_\alpha$ is a component of the energy current, i.e., the time derivative of

$$\delta E = \frac{1}{V}\sum_i r_{i\alpha} \;\; E_i - \left\langle E_i \right\rangle \;\; . \tag{5}$$

It is shown in the Appendix that $J_\alpha$ can be expressed as

$$J_\alpha = \frac{1}{V}\left( \sum_i v_{i\alpha} E_i + \sum_i \sum_{j>i} r_{ij_\alpha} \frac{dE_{ij}}{dt} \right), \tag{6}$$

where $E_i$ is the energy of the molecule *i* which contains the translational, rotational, vibrational and intermolecular potential energies

$$E_i = \tfrac{1}{2} m v_i^2 + \tfrac{1}{2} I u_i^2 + E_{Vi} + \tfrac{1}{2} \sum_{j \neq i} U_{ij} \ , \tag{7}$$

and $\frac{dE_{ij}}{dt}$ represents the time rate of the change of the energy in the molecule *i* due to the interactions between molecule *i* and molecule *j* which can be expressed as

$$\frac{dE_{ij}}{dt} = \tfrac{1}{2} \left( \vec{v}_i + \vec{v}_j \right) \cdot \vec{F}_{ij} + \tfrac{1}{2} \left( \vec{u}_i \cdot \vec{G}_{ij}^{\perp} - \vec{u}_j \cdot \vec{G}_{ji}^{\perp} \right) \ . \tag{8}$$

In Eq. (7), $I$ and $m$ are, respectively, the moment of inertia and mass of the $CO_2$ molecule, $E_{Vi}$ and $U_{ij}$ are, respectively, the vibrational energy of the molecule *i* and the intermolecular potential energy between the molecule *i* and molecule *j*. The vibrational energies in Eq. (7) cannot be neglected especially for polyatomic molecules like $CO_2$ which contain low-lying vibrational states. In Eq. (8), $\vec{u}_i$ is the rotational velocity of the molecule *i* which is defined as $\dot{\vec{e}}_i$ the time derivative of the unit vector along the molecular axis. $\vec{G}_{ij}^{\perp}$ can be determined from the intermolecular forces by Eq. (9).

$$\vec{G}_{ij} = \sum_a d_{ia} \vec{f}_{ija} \ , \tag{9}$$

where $d_{ia}$ is the distance of the site *a* in the molecule *i* relative to the center of mass, $\vec{f}_{ija}$ is the force acting on the site *a* in the molecule *i* due to the interaction between the molecule *i* and molecule *j*. $\vec{G}_{ij}^{\perp}$ is the component of $\vec{G}_{ij}$ perpendicular to $\vec{e}_i$, i.e., the axis of the molecule *i*. Each time autocorrelation function is averaged over the autocorrelation

functions of the energy currents in three directions, i.e., $J_x$, $J_y$, and $J_z$ to reduce the statistical uncertainty of the calculated thermal conductivity.

Due to the interactions among molecules in the system, the translational, rotational and intermolecular potential energies all vary with time. However, the vibrational energies are assumed as frozen in the molecules so that they have no influence on the molecular interactions.

**3. Intermolecular potential**

The intermolecular potential employed in the work was proposed by Bukowski *et al.* (BUK) [8]. The BUK potential was computed using the many-body symmetry-adapted perturbation theory (SAPT) and a large 5*s*3*p*2*d*1*f* basis set. In addition to BUK potential, there are two more *ab initio* potentials proposed for the carbon dioxide dimer which were proved to have good qualities. One is Steinebrunner *et al.* potential based on the MP2 level of theory including corrections for basis set superposition error [9]. Strictly speaking, the Steinebrunner *et al.* potential is not a pure *ab initio* potential because the original *ab initio* potential were scaled by a parameter of 1.16 in order to obtain a good agreement with experimental second virial coefficients. In this work, we would like to predict the transport properties without any experimental data. Hence, the scaled Steinebrunner *et al.* potential is not employed here. The other potential was proposed by Bock *et al.* [10]. The Bock *et al.* potential was calculated with the supermolecular approach on MP2 level of theory including full counterpoise corrections. The shapes of Bock *et al.* potential and the BUK potential are practically the same. They both used a site-site representation of the intermolecular potential, but in different analytical forms.

From our preliminary tests, the application of the Bock *et al.* potential is more time-consuming in the calculations of intermolecular potentials and forces than that of the BUK potential. To save computational time, the BUK potential is employed in this work.

The site-site fit BUK potential reads

$$U_{BUK} = \sum_{a\in A}\sum_{b\in B}\left[ \exp(\alpha_{ab} - \beta_{ab} r_{ab}) + f_1(\delta_1^{ab} r_{ab}) \frac{q_a q_b}{r_{ab}} - f_6(\delta_6^{ab} r_{ab}) \frac{C_6^{ab}}{r_{ab}^6} - f_8(\delta_8^{ab} r_{ab}) \frac{C_8^{ab}}{r_{ab}^8} \right], \quad (10)$$

where $f_n[x] = 1 - e^{-x} \sum_{k=0}^{n} \frac{x^k}{k!}$ . (11)

Here, sites *a* belong to monomer A, sites *b* belong to monomer B and $r_{ab}$ is the distance between *a* and *b*. Each monomer contained five sites, with three corresponding to the centers of the atoms in $CO_2$ and the remaining two on the C-O bonds 0.8456 Å away from the C atom. Parameters $\alpha_{ab}$, $\beta_{ab}$, $\delta_n^{ab}$, $q_a$, and $C_n^{ab}$ are given in Ref. 8.

Figure 1 shows the shapes of the BUK potential for the parallel configuration and the slipped parallel configuration. Although the potential always tends to approach to zero at large intermolecular distances, it could be either a positive or a negative value around zero depending on the relative orientations of two molecules as shown in Fig. 1. Hence, a truncation and shifted procedure is not applicable to the BUK potential no matter the cut-off criterion is based on distance or energy. Hence, the original BUK potential is modified as follows:

$$U_{AB} = \begin{cases} U_{BUK} \cdot \left[ 1 - e^{\frac{(r_{AB} - r_{cut})^2}{-2.0}} \right] & r_{AB} \le r_{cut} \\ 0 & r_{AB} > r_{cut} \end{cases}, \quad (12)$$

where $r_{AB}$ is the intermolecular distance and $r_{cut}$ is the cut-off distance. Both $r_{AB}$ and $r_{cut}$ are in atomic units. In this work, we set $r_{cut} = 12\,\text{Å}$. With such a large cut-off distance, the use of an Ewald sum to treat long range Coulomb interactions is not necessary [9, 21] which is assisted by the fact that $CO_2$ molecules are neither charged nor have a permanent dipole moment. The modified potential makes the intermolecular potential go smoothly to zero at the cut-off distance.

The modified potential also ensures the continuity of the intermolecular forces near the cut-off distance. In addition to the forces acting on five sites of each molecule, there is one more force acting on the center of mass of the molecule as shown below.

$$\vec{F}(\vec{r}_{AB}) = U_{BUK} \cdot \left[ -(r_{AB} - r_{cut}) e^{\frac{(r_{AB} - r_{cut})^2}{-2.0}} \frac{\vec{r}_{AB}}{r_{AB}} \right], \tag{13}$$

In a $CO_2$ molecule, the center of mass happens to be the carbon atom. Hence, this additional force is actually acting on the carbon atom. Using the modified potential, the forces and torques acting on molecules both go smoothly to zero at the cut-off distance. Thus, the problems in energy conservation and numerical instability in the equations of motion are both eliminated by the modified potential. A simple test of the modified potential shows the second virial coefficient calculated from the modified BUK potential at 300 K is only 0.4% higher than that calculated from the original truncated BUK potential. Hence, the macroscopic properties calculated from the modified BUK potential will not significantly deviate from the corresponding properties from the original potential.

## 4. Initialization and equilibration

Before attempting to compute proper simulation averages, the system must be equilibrated to both configuration and velocity distributions appropriate to a gas at the desired temperature and pressure. To save the simulation time for the equilibration process, the configuration of centers of mass and molecular orientations, the translational and rotational velocities should all be initialized at the desired temperature and pressure so that they can relax quickly to the appropriate configuration and velocity distributions.

### *4.1. The initial configuration and initial energies*

The volume of the cubic simulation box is initialized by the ideal gas law

$$V = Nk_B T / P, \tag{14}$$

where $P$ and $T$ are the desired pressure and temperature of the gas, $N = 4096$ is the number of molecules in the system which has the same value in all simulations in this work. The center of mass coordinates $\vec{r}$ are initialized randomly inside the simulation box. The molecular orientations are initialized as random vectors with uniform solid angle.

The initial translational and rotational velocities are given by the Maxwell-Boltzmann distribution at a given temperature. Different from translational and rotational motions, the quantum effects of molecular vibrational motions cannot be neglected. The $CO_2$ molecule has four vibrational modes. The corresponding vibrational energy eigen values can be determined by solving the rovibrational Schrödinger equation of the molecule. To solve the rovibrational Schrödinger equation, it is necessary to calculate the intramolecular potential energy surface (PES) by *ab initio* method. An accurate $CO_2$

intramolecular PES has been calculated by Leonard *et al.* [26] using the coupled-cluster singles and doubles excitation with perturbative treatment of triple excitations method and the multi-reference configuration interaction method. Based on this result, the calculated vibrational energy eigen values corresponding to the 1st excited states of the symmetric stretching mode, the asymmetric stretching mode and the doubly degenerated bending mode are 1387.9 $cm^{-1}$, 2348.8 $cm^{-1}$ and 667 $cm^{-1}$, respectively. Although the energy differences between any two neighboring energy states of each vibratoinal mode are not exactly constant due to the aharmonic component of the intramolecular potential and the Fermi resonance between different vibrational modes, we can still assume the vibrational energies of each mode are equally spaced without causing too much error in the calculations of thermal properties of $CO_2$ gas. Based on the quantum harmonic oscillator assumption, the vibrational energy of each molecule can be calculated by Eq. (15)

$$E_V = \sum_{j=1}^{4} n_j + \tfrac{1}{2} \; E_{vj} \,, \tag{15}$$

where $n_j$ means the vibrational energy level of *j*th vibrational mode, $E_{vj}$ is the fundamental vibrational transition energy of mode *j*.

The average population distribution of vibrational energies fulfills the Boltzmann distribution. At a given temperature, the molecular vibrational energies are initialized by the Metropolis MC method [27]. At the beginning of the initialization, all molecules are on their ground vibrational energy states. Then, the Metropolis scheme is applied to each vibrational mode of each molecule in the system so that the molecules may be excited to higher energy states or decay to lower energy states. After tens of trial transitions, the

average vibrational energy per molecule in the system started to fluctuate around a constant value as shown in Fig. 2. The fluctuating average vibrational energies correspond to different distributions of vibrational energies in the molecules. The average of these distributions is the Boltzmann distribution at the given temperature. Two thousands of these distributions are used to initialize the vibrational energies of the molecules in the system. Hence, each MD simulation actually starts with 2000 different initial vibrational energy distributions but with the same initial configuration and initial translational and rotational velocities. Once the vibrational energies are initialized, they do not change during the simulation. Therefore, 2000 time correlation functions of the energy current corresponding to 2000 different initial vibrational energy distributions are obtained from each MD simulation. These time correlation functions calculated from different initial states are then averaged to determine the final time autocorrelation function at the given temperature.

*4.2. Equilibration*

To equilibrate the system to the desired temperature and pressure, the system is coupled to a constant temperature and pressure bath using the approach proposed by Berendsen *et al* [28]. At each time step, translational velocities are scaled by a factor

$$\lambda = \left[ 1 + \frac{\Delta t}{\tau_T} \left( \frac{T_0}{T} - 1 \right) \right]^{\frac{1}{2}}, \tag{16}$$

where $T_0$ is the desired temperature varying from 300 K to 1000 K, $T$ is the current translational temperature, $\Delta t$ is the time step and $\tau_T$ is a preset time constant. The energy exchanges between the translational motion and rotational motion are fast. Hence, the

scale factor can force both translational and rotational kinetic temperatures to the desired temperature. Simultaneously, the molecular center-of-mass coordinates are scaled by a factor of $\mu$, and the volume of the simulation box is scaled by a factor of $\mu^3$ where

$$\mu = \left[ 1 + \frac{\Delta t}{\tau_p} \beta_T (P - P_0) \right]^{\frac{1}{3}}. \tag{17}$$

Here, $P_0$ is the desired pressure which is equal to 1 atm in this work, $P$ is the instantaneous pressure, $\tau_p$ is a time constant, and $\beta_T$ is the isothermal compressibility. Since $\beta_T \approx \frac{1}{P_0}$ for a gas, Eq. (17) can be rewritten as

$$\mu = \left[ 1 + \frac{\Delta t}{\tau_p} \left( \frac{P}{P_0} - 1 \right) \right]^{\frac{1}{3}}. \tag{18}$$

In the simulations, the time constants $\tau_T$ and $\tau_p$ are set to be 100 ps and 30 ps, respectively. At 1 atm, the long range correction to the pressure of $CO_2$ gas is negligible. Thanks to all these methods we use in the initialization and equilibration, the system is well equilibrated in 500 ps. After the system reaches the thermal equilibrium at the desired temperature and pressure, the coupling to the external bath is turned off and the MD simulation is carried out in a microcanonical ensemble. The translational temperature, the rotational kinetic temperature, and the pressure of the system all fluctuate around the desired values during the simulation as shown in Fig. 3. The energy exchange between the translational and rotational motions is evident. Figure 4(a) and 4(b) depict the distributions of translational energy and rotational energy obtained from simulations and the corresponding Boltzmann energy distributions at the desired

temperature. The good agreement between the calculated results and the theoretical results proves the system is in thermodynamic equilibrium.

## 5. Simulation details and results

We carried out MD simulations in microcanonical ensembles for pure $CO_2$ gas in the temperature range of 300 – 1000 K to calculate the self-diffusion coefficients, shear viscosity and thermal conductivity. The equations of molecular translational motions are integrated by the Verlet leap-frog algorithm. The Singer leap-frog algorithm [29] which constrains the bond length to be a constant is applied to integrate the equations of molecular rotational motions. The modified BUK potential is used for molecular interactions. Compared to the standard LJ potential, the BUK potential has a much more complex form. Therefore, the calculations of forces and potentials are much more time-consuming. To ensure the time step size does not significantly influence the results for the macroscopic properties of the system, the total energy of the system should be kept constant within two parts in $10^5$ [30]. Thanks to the modified BUK potential, a time step of 12.5 fs can be used for low temperatures up to 500 K and a 10-fs time step is appropriate for the gas temperature up to 800 K. For higher temperatures, smaller step size of 8.5 fs should be chosen to assure the energy conservation.

The correlation time $t_c$ for the three properties of interest can be calculated by Eq. (14) [23]

$$t_c = \frac{\int_0^\infty dt \ \langle A(0)A(t)\rangle^2}{\langle A^2(0)\rangle^2}, \tag{19}$$

where $A = \vec{v}_i$ for self-diffusion coefficient, $A = \mathrm{P}_{\alpha\beta}$ for shear viscosity and $A = J_\alpha$ for thermal conductivity. Figure 5 shows the relation between the correlation times and temperature. It can be seen from Fig. 5 that the velocity correlation times are close to the energy current correlation times and are about 50% higher than the correlation time of off-diagonal element of pressure tensor in the temperature range from 300 K to 1000 K. The correlation times of $CO_2$ gas is generally on the order of 100 ps. The total simulation length of order 10 μs, therefore, must be run in order to reduce the statistical errors to less than 1%. If the time step is 10 fs, the total number of steps is about $10^9$. This means a very computational demanding simulation is required. As suggested by Hess and Evans [31], the ensemble average can also be obtained from shorter parallel runs starting from statistically independent initial states. Hence, at each temperature, the long simulation is divided into 100 shorter parallel runs which are independently initialized and equilibrated at the given temperature by the method described in Sec. 4. Depending on the temperature of the system (300 – 1000 K), the length of each parallel run varies between 60 ns and 140 ns to assure low statistical errors. The final time correlation functions are obtained by averaging the time correlation functions calculated from shorter parallel runs.

Figure 6(a), Fig. 7(a) and Fig. 8(a) depict, respectively, the calculated normalized correlation functions of the velocity, the off-diagonal element of pressure tensor and the energy current at 300 K, 600 K and 900 K. The self-diffusion coefficients $D$, shear viscosities $\eta$ and thermal conductivities $\lambda_T$ are determined by the time integrals of the corresponding correlation functions. The results are depicted, respectively, in Fig. 6(b), Fig. 7(b) and Fig. 8(b). After $10\,t_c$, no significant contribution to time integrals of correlation functions is observed and the integrals fluctuate around a constant. We

evaluate the three transport properties by the averages of those fluctuating values between $10\,t_c$ and $30\,t_c$ at each temperature. The statistical errors are obtained from the mean-square deviation of the time correlation functions. Due to the large statistics in the calculations, the statistical error of the self-diffusion coefficient *D* is less than 0.1%, while the shear viscosity $\eta$ and thermal conductivity $\lambda_T$ has a statistical error of about 1%. The magnitude of the statistical errors can be further reduced by longer simulations if larger computational resources are available.

The results of all transport properties between 300 and 1000 K are summarized in Table 1. The experimental data [32, 33] at different temperatures are also included in Table 1 to compare with the calculated results. The uncertainty of the experimental data was estimated to be 5% for self-diffusion coefficients and 0.9% for shear viscosity [32]. The accuracy of the experimental thermal conductivity of carbon dioxide is estimated to be ±1% near room temperature and ±2% at the higher temperatures [33]. From Table 1 we can see the average deviations between the calculated and experimental values for self-diffusion coefficient and shear viscosity are 2.32%, and 0.71%, respectively. The excellent agreement indicates the linear rigid rotor assumption of the $CO_2$ molecule is valid even at 1000 K. As shown in Table 1, the calculated thermal conductivities underestimate the experimental values by 2.30% averagely. The deviation can be further reduced if the aharmonic vibrations of molecules are taken into account. Compared to the calculated $CO_2$ thermal conductivities from other authors who obtained a deviation of 35% without considering the vibrational energies and a deviation of 22% with a classical treatment of the vibrational motions [18], our quantum mechanical treatment of the vibrational energies greatly improves the accuracy of the calculated thermal conductivity.

Overall, excellent agreements are achieved for all the three transport properties of interest.

## 6. Conclusions

The EMD and the time-correlation theory are employed in this work to determine the transport properties of $CO_2$ gas. The calculations demonstrate a procedure of determination of self-diffusion coefficient, shear viscosity and thermal conductivity of a polyatomic gas without using any experimental data. All the parameters used in the calculations such as the C-O bond length, moment of inertia, intermolecular potential and vibrational energy eigen values are determined by *ab initio* method. In order to take into account the quantum effects of molecular vibrations, a MC method is used to initialize the vibrational energies at the given temperature. The good agreement of calculated values with the experimental data validates the rigid-rotor and frozen vibrational energy assumptions we made at the beginning of the calculations. Since the vibrational energies do not vary with time in the simulation after they are initialized, the vibrational contribution to the thermal conductivity might be reduced to a simpler form by separating the terms involving the vibrational energies in the energy current expression from those involving other energies which vary continuously with time. If this simplification can be obtained, a more efficient calculation of the thermal conductivity will be possible.

The present method can be readily extended to the calculations of transport properties of other gases or gas mixtures which contain monatomic, diatomic or polyatomic molecules at different temperatures as long as the accurate intermolecular potentials are available.

*List of symbols*

$d_{ia}$ the distance of the site *a* in the molecule *i* relative to the center of mass

$D$ self-diffusion coefficient

$\vec{e}$ the unit vectors along the molecular axis

$E_p$ total potential energy of the system

$E_i$ the energy of the molecule *i*

$E_{Vi}$ vibrational energy of the molecule *i*

$E_{vj}$ the fundamental vibrational transition energy of mode *j*

$\vec{f}_{ij_\beta}$ a component of the force acting on the molecule *i* due to the molecule *j*

$\vec{F}_{ij}$ intermolecular force due to the interaction between the molecule *i* and the molecule *j*

$\vec{G}$ $\vec{e}\times\vec{G}$ is the torque acting on the molecule

$\vec{G}^{\perp}$ the component of $\vec{G}$ perpendicular to $\vec{e}$

$\hbar$ reduced Planck constant

$I$ moment of inertia

$J_\alpha$ a component of the energy current

$k_B$ Boltzmann constant

$m$ the mass of molecule

$n_j$ the vibrational energy level of *j*th vibrational mode

$N$ number of molecules

$P$ pressure

$P_0$ the desired pressure

$r_{ab}$ distance between nuclei *a* and *b*

$r_0$ C-O bond length

$r_{AB}$ the distance between centers of mass of molecule A and molecule B

$r_{cut}$ cut-off distance

$r_{ij_\alpha}$ a component of the distance vector from the molecule *j* to *i*

$t$ time

$T$ temperature

$T_0$ the desired temperature

$u_i$ rotational velocity of the molecule *i*

$U_{BUK}$ BUK intermolecular potential

$U_{AB}$ modified BUK potential

$v_{i\alpha}$ a component of translational velocity of molecule *i*

$V$ volume

*Greek letters*

| | |
|---|---|
| $\beta_T$ | isothermal compressibility |
| $\eta$ | shear viscosity |
| $\lambda$ | scale factor of velocity |
| $\lambda_T$ | thermal conductivity |
| $\mu$ | scale factor of intermolecular distance |
| $P_{\alpha\beta}$ | off-diagonal element of pressure tensor |
| $\tau_T$ | time constant for temperature relaxation |
| $\tau_p$ | time constant for pressure relaxation |

**Acknowledgments**

This work was supported by Office of Navy Research through the Multidisciplinary University Research Initiative (MURI) program.

**Appendix: Derivation of the expression for the energy current**

$$J_\alpha = \frac{d}{dt}\left[\frac{1}{V}\sum_i r_{i\alpha}\ \ E_i - \langle E_i \rangle\ \right]. \tag{A1}$$

In a constant NVE ensemble, volume $V$ and average energy $\langle E_i \rangle$ are both constant.

$$\begin{aligned} J_\alpha &= \frac{1}{V}\left(\sum_i v_{i\alpha}\ \ E_i - \langle E_i \rangle\ + \sum_i r_{i\alpha}\frac{dE_i}{dt}\right) \\ &= \frac{1}{V}\left(\sum_i v_{i\alpha} E_i + \sum_i r_{i\alpha}\frac{dE_i}{dt}\right) \end{aligned}. \tag{A2}$$

The total momentum of the system is kept constant during the simulation. The initial value of the total momentum is set to zero so that $\sum_i v_{i\alpha} = 0$. Hence, the term $\sum_i v_{i\alpha}\langle E_i \rangle$ vanishes. The time derivative of $E_i$ is

$$\begin{aligned}\frac{dE_i}{dt} &= m\vec{v}_i \cdot \frac{d\vec{v}_i}{dt} + I\vec{u}_i \cdot \frac{d\vec{u}_i}{dt} + \frac{dE_{Vi}}{dt} + \tfrac{1}{2}\sum_{j\neq i}\left[\frac{\partial U_{ij}}{\partial \vec{r}_{ij}} \cdot \frac{\partial \vec{r}_{ij}}{\partial t} + \frac{\partial U_{ij}}{\partial \vec{e}_i} \cdot \frac{\partial \vec{e}_i}{\partial t} + \frac{\partial U_{ij}}{\partial \vec{e}_j} \cdot \frac{\partial \vec{e}_j}{\partial t}\right] \\ &= \vec{v}_i \cdot \sum_{j\neq i}\vec{F}_{ij} + \vec{u}_i \cdot \sum_{j\neq i}\vec{G}_{ij}^{\perp} + \tfrac{1}{2}\sum_{j\neq i}\left[-\vec{F}_{ij}\cdot\ \vec{v}_i - \vec{v}_j\ - \vec{G}_{ij}\cdot\vec{u}_i - \vec{G}_{ji}\cdot\vec{u}_j\right] \\ &= \tfrac{1}{2}\sum_{j\neq i}\left[\vec{F}_{ij}\cdot\ \vec{v}_i + \vec{v}_j\ + \vec{G}_{ij}^{\perp}\cdot\vec{u}_i - \vec{G}_{ji}^{\perp}\cdot\vec{u}_j\right]\end{aligned} \quad , \qquad \text{(A3)}$$

where $\frac{dE_{Vi}}{dt} = 0$ because the vibrational energy is assumed as frozen in the molecule. The intermolecular potential $U_{ij}$ is not only a function of $\vec{r}_{ij}$, the distance between the centers of mass, but also a function of molecular orientations $\vec{e}_i$ and $\vec{e}_j$. Therefore, the chain rule is used to determine the time derivative of $U_{ij}$. Note $\vec{G}_{ij}\cdot\vec{u}_i = \vec{G}_{ij}^{\perp}\cdot\vec{u}_i$ since $\vec{u}_i$ is perpendicular to the molecular axis $\vec{e}_i$, and $\vec{G}_{ij}^{\perp}$ is the component of $\vec{G}_{ij}$ perpendicular to $\vec{e}_i$. Therefore, the second summation in Eq. A(2) is

$$\begin{aligned}\sum_i r_{i\alpha}\frac{dE_i}{dt} &= \sum_i r_{i\alpha}\left(\tfrac{1}{2}\sum_{j\neq i}\left[\vec{F}_{ij}\cdot\ \vec{v}_i + \vec{v}_j\ + \vec{G}_{ij}^{\perp}\cdot\vec{u}_i - \vec{G}_{ji}^{\perp}\cdot\vec{u}_j\right]\right) \\ &= \tfrac{1}{4}\sum_i\sum_{j\neq i} r_{i\alpha}\left[\vec{F}_{ij}\cdot\ \vec{v}_i + \vec{v}_j\ + \vec{G}_{ij}^{\perp}\cdot\vec{u}_i - \vec{G}_{ji}^{\perp}\cdot\vec{u}_j\right] \\ &\quad + \tfrac{1}{4}\sum_j\sum_{i\neq j} r_{j\alpha}\left[\vec{F}_{ji}\cdot\ \vec{v}_i + \vec{v}_j\ + \vec{G}_{ji}^{\perp}\cdot\vec{u}_j - \vec{G}_{ij}^{\perp}\cdot\vec{u}_i\right] \quad , \qquad \text{(A4)} \\ &= \tfrac{1}{4}\sum_i\sum_{j\neq i} r_{ij\alpha}\left[\vec{F}_{ij}\cdot\left(\vec{v}_i + \vec{v}_j\right) + \vec{G}_{ij}^{\perp}\cdot\vec{u}_i - \vec{G}_{ji}^{\perp}\cdot\vec{u}_j\right] \\ &= \tfrac{1}{2}\sum_i\sum_{j>i} r_{ij\alpha}\left[\vec{F}_{ij}\cdot\left(\vec{v}_i + \vec{v}_j\right) + \vec{G}_{ij}^{\perp}\cdot\vec{u}_i - \vec{G}_{ji}^{\perp}\cdot\vec{u}_j\right]\end{aligned}$$

where $\vec{F}_{ij} = -\vec{F}_{ji}$ according to Newton's third law and $r_{ij\alpha} = r_{i\alpha} - r_{j\alpha}$. Note $\vec{G}_{ij}^{\perp} \neq -\vec{G}_{ji}^{\perp}$. Comparing Eq. (A4) to the second term of Eq. (6), one gets

$$\frac{dE_{ij}}{dt} = \tfrac{1}{2}\ \vec{v}_i + \vec{v}_j\ \cdot\vec{F}_{ij} + \tfrac{1}{2}\ \vec{u}_i\cdot\vec{G}_{ij}^{\perp} - \vec{u}_j\cdot\vec{G}_{ji}^{\perp}\ . \qquad \text{(A5)}$$

**References**

[1] B. Eckl, J. Vrabec and H. Hasse, Fluid Phase Equilibr. 274 (2008) 16-26.

[2] X. Li, Li Zhao, T. Cheng, L. Liu and H. Sun, Fluid Phase Equilibr. 274 (2008) 36-43.

[3] G.A. Fernandez, J. Vrabec and H. Hasse, Mol. Simul. 31 (2005) 787-793.

[4] G.A. Fernandez, J. Vrabec and H. Hasse, Fluid Phase Equilibr. 221 (2004) 157-163.

[5] F. Case, A. Chaka, D.G. Friend, D. Frurip, J. Golab, J. Rusel, J. Moore, R.D. Mountain, J. Olson, M. Schiller and J. Store, Fluid Phase Equilibria. 217 (2004) 1-10.

[6] Z. Liang and H.L. Tsai, J. Mol. Spec. 252 (2008) 108-114.

[7] G. Granar, C. Rosseti, and D. Bailly, Mol. Phys. 58 (1986) 627-636.

[8] R. Bukowski, J. Sadlej, B. Jeziorski, P. Jankowski, K. Szalewicz, S.A. Kucharski, H.L. Williams, and B.M. Rice, J. Chem. Phys. 110 (1999) 3785-3803.

[9] G. Steinebrunner, A.J. Dyson, B. Kirchner, and H. Huber, J. Chem. Phys. 109 (1998) 3153-3159.

[10] S. Bock, E. Bich, and E. Vogel, Chem. Phys. 257 (2000) 147 - 156.

[11] M.S. Green, J. Chem. Phys. 19 (1951) 1036-1046.

[12] M.S. Green, Phys. Rev. 119 (1960) 829-830.

[13] R. Kubo, J. Phys. Soc. Jpn. 12 (1957) 570-586.

[14] M.P. Allen and D.J. Tildesley, Computer Simulation of Liquids, Clarendon Press, Oxford, 2000.

[15] D. Evans, Phys. Rev. A 34 (1986) 1449-1458.

[16] D.M. Heyes, Phys. Rev. B 37 (1988) 5677-5696.

[17] F. Müller-Plathe, J. Chem. Phys. 106 (1997) 6082-6085.

[18] C. Nieto-Draghi, T. de Bruin, J. Perez-Pellitero, J. B. Avalos and A.D. Mackie 126 (2007) 064509.

[19] K.P. Travis, D.J. Searles and D.J. Evans, Mol. Phys. 95 (1998) 195-202.

[20] J.G. Harris and K.H. Yung, J. Phys. Chem. 99 (1995) 12021-12024.

[21] C. Bratschi, H. Huber and D.J. Searles, J. Chem. Phys. 126 (2007) 164105.

[22] Z. Zhang and Z Duan, J. Chem. Phys. 122 (2005) 214507.

[23] R. Zwanzig and N.K. Ailawadi, Phys. Rev. 182 (1969) 280-283.

[24] E. Helfand, Phys. Rev. 119 (1960) 1-9.

[25] S. Viscardy, J. Servantie, and P. Gaspard, J. Chem. Phys. 126 (2007) 184513.

[26] C. Leonard, M. Diehr, P. Rosmus, W.C. Maguire, JQSRT 109 (2008) 535-548.

[27] D. Frenkel and B. Smit, Understanding Molecular Simulation, Academic Press, San Diego San Francisco New York Boston London Sydney Tokyo, 2002.

[28] H.J.C. Berendsen, J.P.M. Postma, W.F. Van Gunsteren, A. DiNola, and J.R. Haak, J. Chem. Phys. 81 (1984) 3684-3690.

[29] K. Singer, A. Taylor, and J.V.L. Singer, Mol. Phys. 33 (1977) 1757-1795.

[30] K. Meier, A. Laesecke, and S. Kabelac, J. Chem. Phys. 121 (2004) 3671-3687.

[31] S. Hess and D.J. Evans, Phys. Rev. E 64 (2001) 011207.

[32] A. Boushehri, J. Bzowski, J. Kestin, and E.A. Mason, J. Phys. Chem. Ref. Data. 17 (1988) 255.

[33] V. Vesovic, W.A. Wakeham, G.A. Olchowy, J.V. Sengers, J.T.R. Watson, J. Millat, J. Phys. Chem. Ref. Data 19 (1990) 763-808.

Table 1. The calculated and experimental values [32, 33] of self-diffusion coefficient and shear viscosity of $CO_2$ gas at 1 atm and in the temperature range of 300 – 1000 K. The deviations are determined by |calculated value – experimental value|/experimental value×100%. The experimental self-diffusion coefficients are obtained by linear interpolation of experimental data in Ref. 33. Statistical uncertainty of the simulation results is 0.1% for self-diffusion coefficient and 1% for both shear viscosity and thermal conductivity.

| T (K) | Self-diffusion coefficient $D$ $(cm^2/s)$ | | | Shear viscosity $\eta$ $(\mu Pa \cdot s)$ | | | Thermal conductivity $\lambda_T$ $(W/m \cdot K)$ | | |
|---|---|---|---|---|---|---|---|---|---|
| | Cal. | Exp. | % Dev. | Cal. | Exp. | % Dev. | Cal. | Exp. | % Dev. |
| 300 | 0.1142 | 0.1192 | 4.19 | 15.34 | 15.13 | 1.39 | 0.01646 | 0.01679 | 1.97 |
| 400 | 0.2028 | 0.2063 | 1.70 | 19.79 | 19.70 | 0.46 | 0.02445 | 0.02514 | 2.74 |
| 500 | 0.3116 | 0.3103 | 0.42 | 23.91 | 24.02 | 0.46 | 0.03237 | 0.03350 | 3.37 |
| 600 | 0.4358 | 0.4299 | 1.37 | 28.51 | 28.00 | 1.82 | 0.04041 | 0.04156 | 2.77 |
| 700 | 0.5771 | 0.5640 | 2.32 | 31.90 | 31.68 | 0.69 | 0.04851 | 0.04930 | 1.60 |
| 800 | 0.7310 | 0.7123 | 2.63 | 35.06 | 35.09 | 0.09 | 0.05536 | 0.05671 | 2.38 |
| 900 | 0.8976 | 0.8725 | 2.88 | 38.18 | 38.27 | 0.24 | 0.06185 | 0.06380 | 3.06 |
| 1000 | 1.0770 | 1.0448 | 3.06 | 41.04 | 41.26 | 0.53 | 0.07034 | 0.07057 | 0.57 |

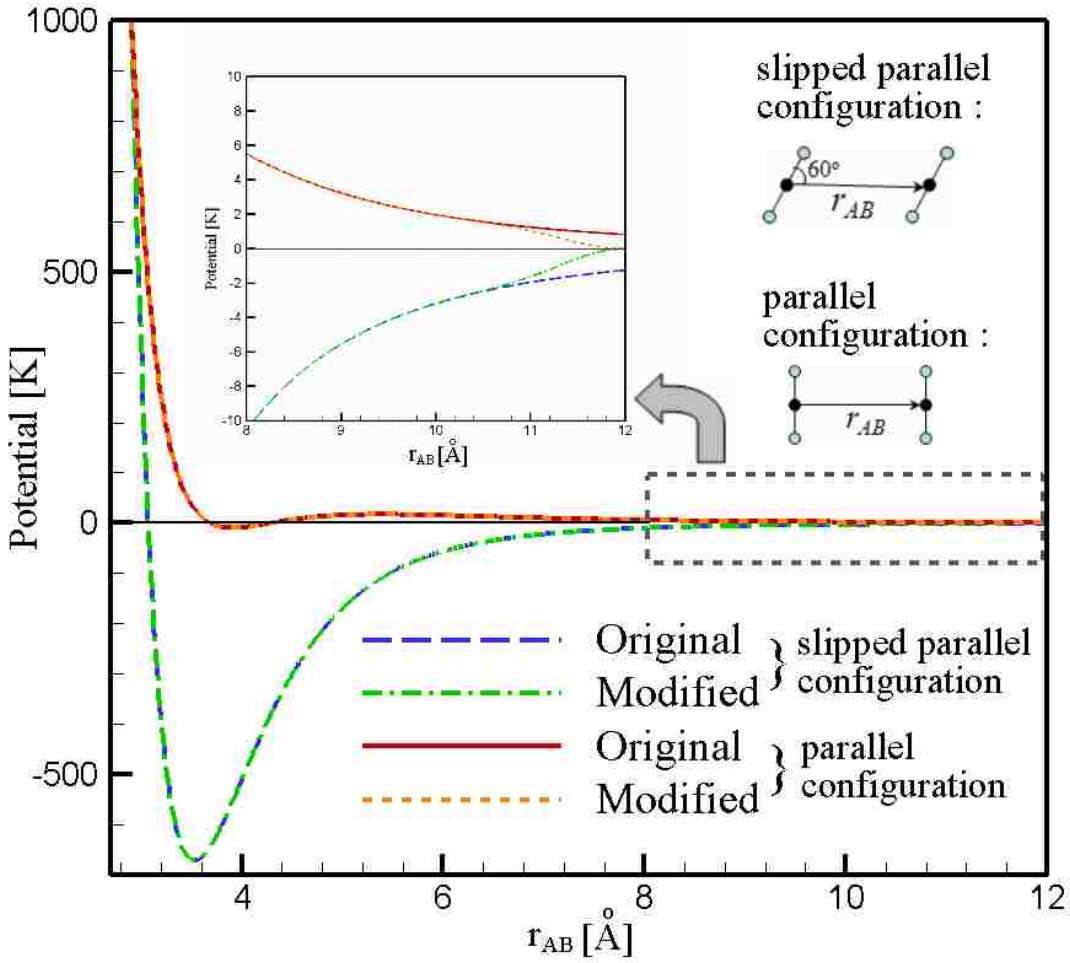


Fig. 1. The shapes of the original and modified BUK intermolecular potential for parallel configuration and slipped parallel configuration.

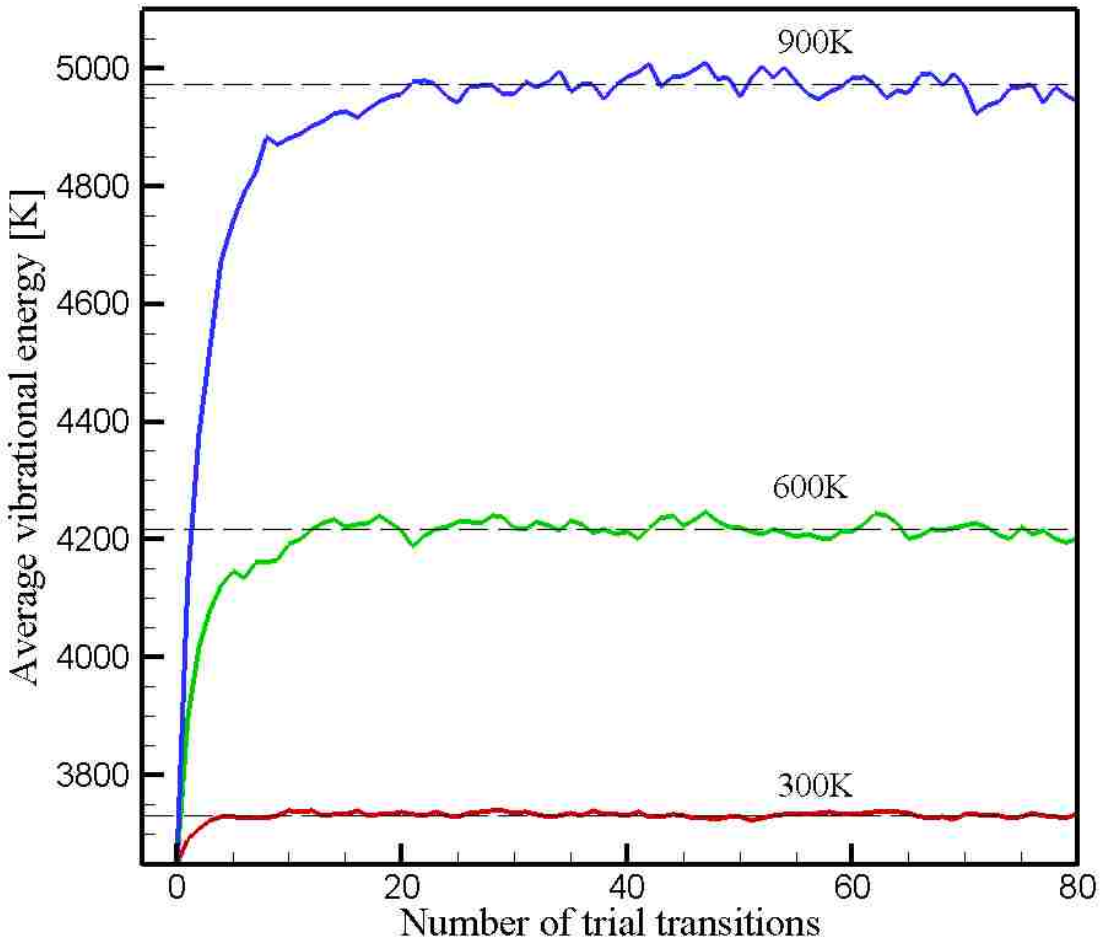


Fig. 2. The average vibrational energy per molecule vs. the number of trail transitions at 300 K, 600 K and 900 K.

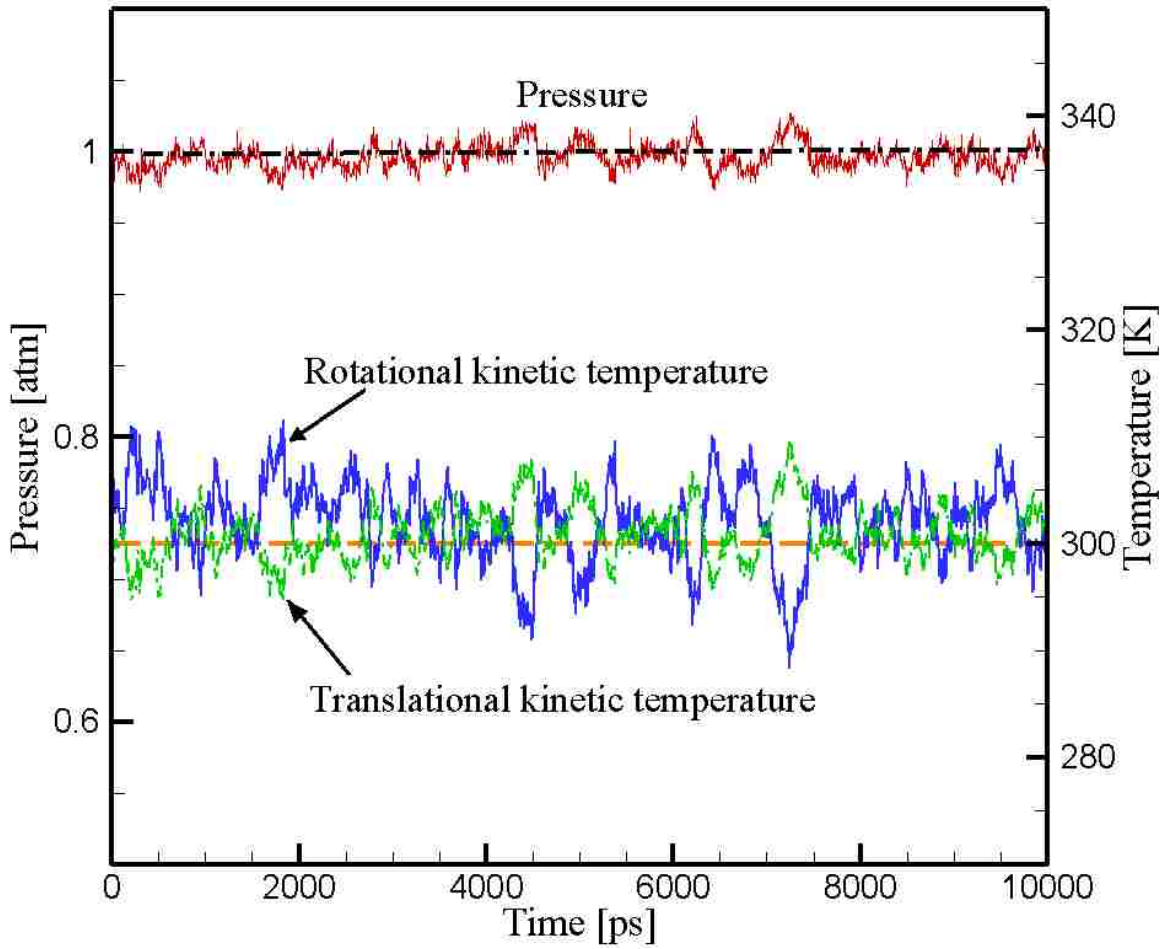


Fig. 3. Translational, rotational kinetic temperatures and pressure vs. time when the equilibrium temperature and pressure are 300 K and 1 atm.

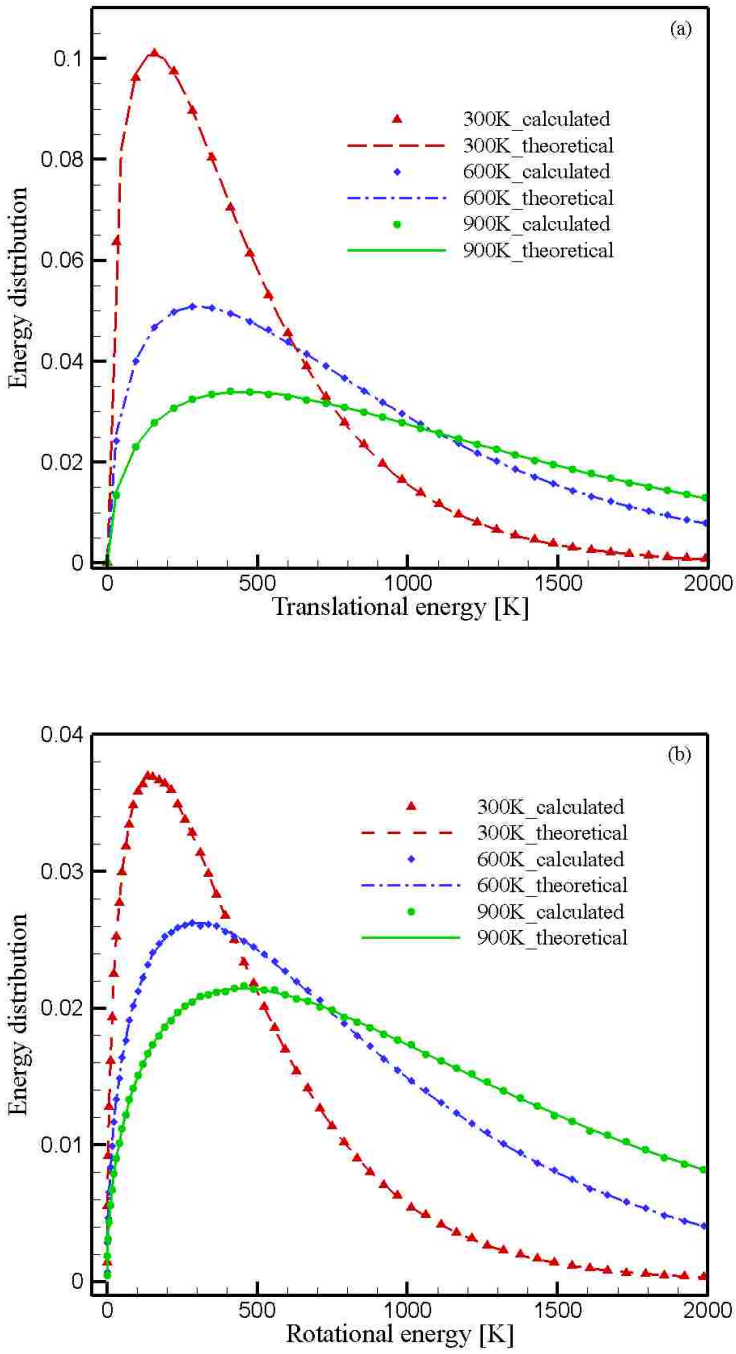


Fig. 4. The calculated and theoretical energy distributions at 300 K, 600 K, and 900 K for (a) translational energies and (b) rotational energies.

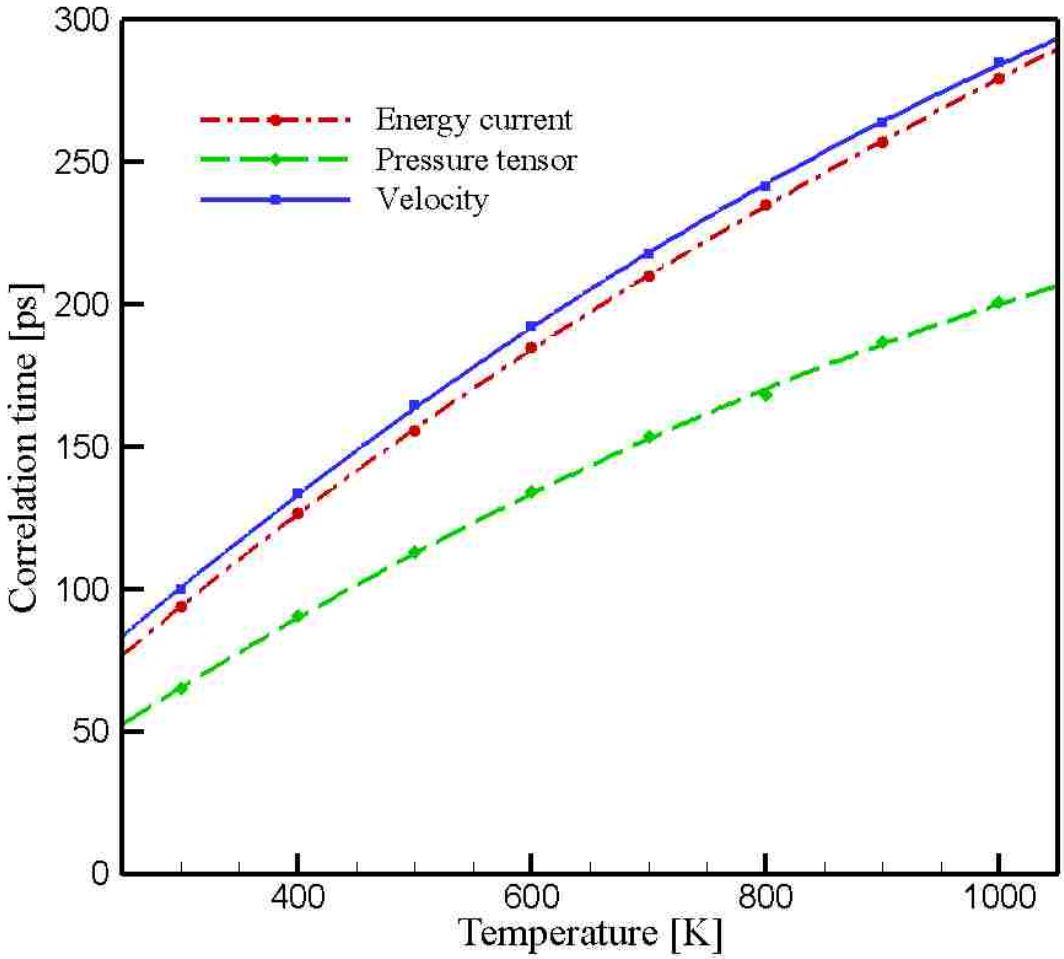


Fig. 5. The correlation times vs. temperature.

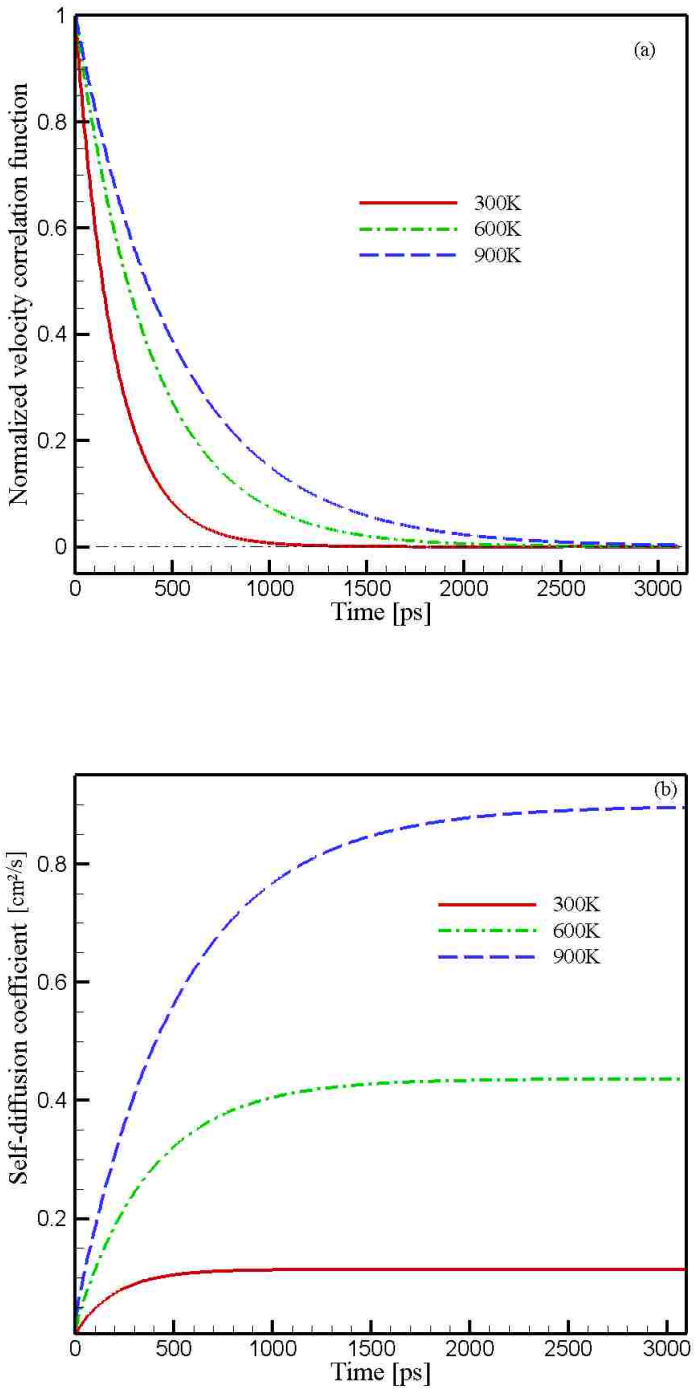


Fig. 6. (a) Normalized velocity correlation functions for selected temperatures, (b) the time integrals of the correlation functions for selected temperatures.

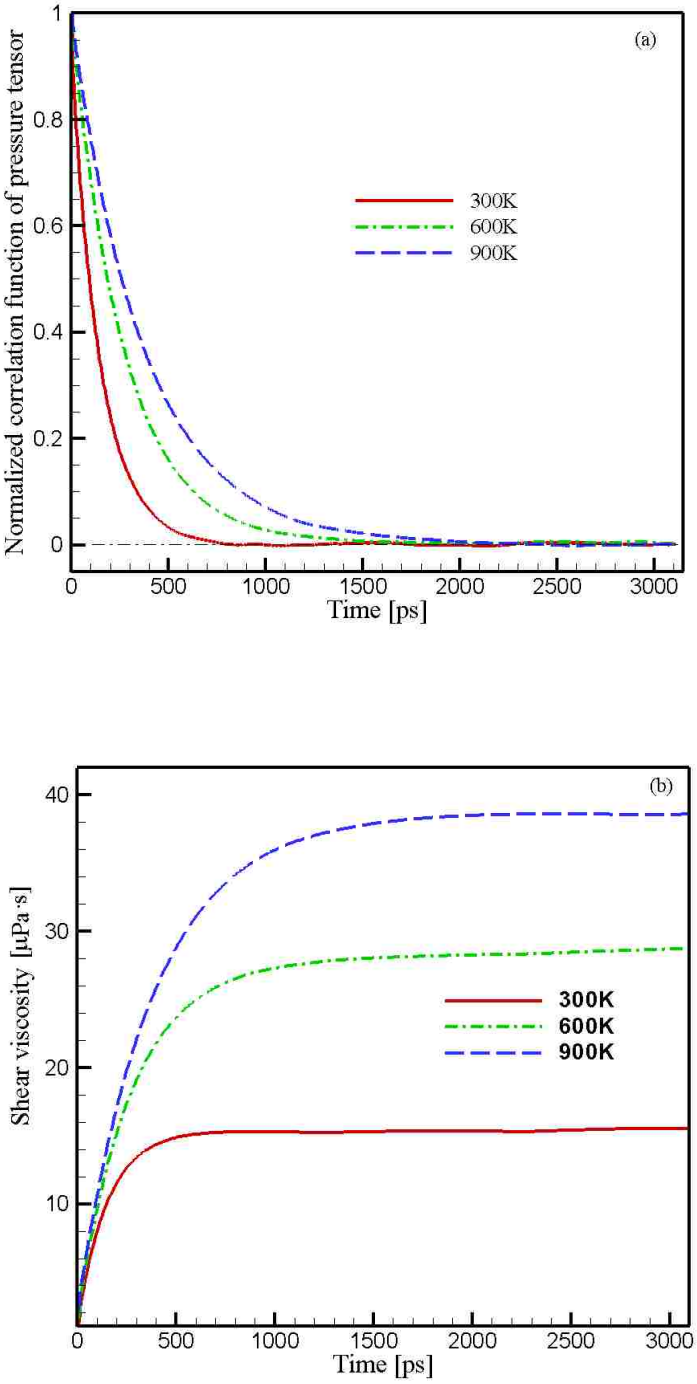


Fig. 7. (a) Normalized correlation functions of off-diagonal elements of pressure tensors for selected temperatures, (b) the time integrals of the correlation functions for selected temperatures.

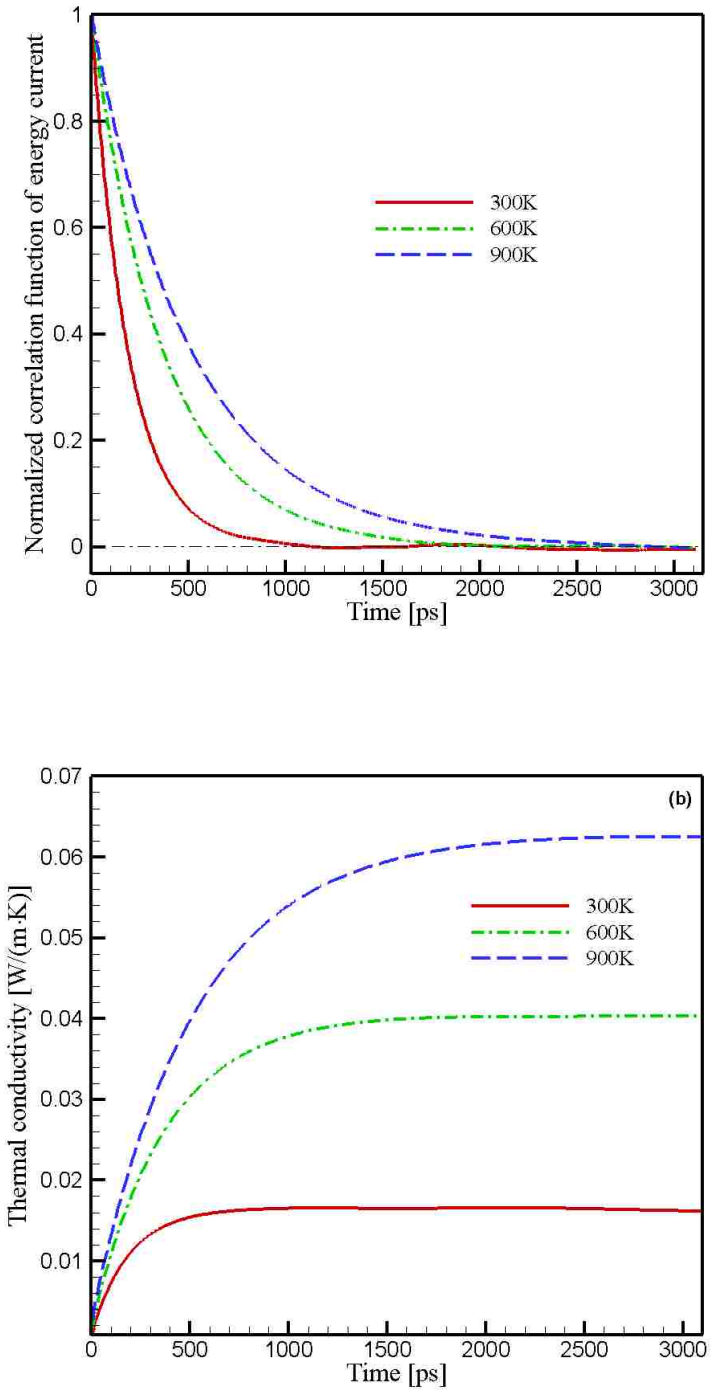


Fig. 8. (a) Normalized correlation functions of energy current at 300 K, 600 K and 900 K. (b) The time integral of the autocorrelation functions for selected temperatures.

# 3. Calculation of density-dependent thermophysical properties for $CO_2$ gas using an ab initio-based potential model

Zhi Liang and Hai-Lung Tsai*

Department of Mechanical and Aerospace Engineering, Missouri University of Science and Technology, 400 W. 13th Street, Rolla, MO 65409, USA

## Abstract

The density, isochoric heat capacity, shear viscosity and thermal conductivity of $CO_2$ gas in the pressure range of 1 – 50 atm and 300 K are calculated based on a five-center potential model obtained from *ab initio* calculations of the intermolecular potential of a $CO_2$ dimer. The quantum effects of the intramolecular motion are included in a model by the Monte Carlo (MC) Method. Without using any experimental data, the present model achieves excellent agreements between the calculated thermophysical properties and experimental data for all simulated $CO_2$ densities except the highest one at 135 kg/m$^3$ (3 mol/l). The contributions of potential to the thermophysical properties of the moderate dense $CO_2$ gas and their dependence on density are investigated in detail.

**Keywords:** Thermophysical properties; Molecular dynamics; Ab initio; $CO_2$ gas

* Corresponding author. Tel.: +1 573 341 4945; fax: +1 573 341 4607.

*E-mail address:* tsai@mst.edu (H.L. Tsai).

## 1. Introduction

In general, as long as the structure of the molecule in a fluid and the intermolecular potentials which describe the interactions between molecules are known, all thermodynamic and transport properties of the fluid at any given temperature and pressure can be calculated by theoretical approaches such as the formal kinetic theory and time-correlation function theory. $CO_2$ is a moderate size molecule and is suitable for very accurate *ab initio* calculations. Based on different molecular potential models, a number of calculations for the $CO_2$ thermophysical properties were carried out in the last decade [1-6]. Bock *et al.* [1-3] calculated accurately the transport properties of $CO_2$ at the zero density limit by evaluating the relevant collision cross sections by means of classical-trajectory calculations directly from *ab initio* potentials. However, their calculation method so far cannot be extended to the calculation of transport properties for dense fluids. The determination of density-dependent thermophysical properties of real fluids based on the formal kinetic theory still strongly relies on experimental data. On the other hand, a lot of calculations [4-6] used molecular dynamics (MD) simulations and the Green and Kubo (GK) formulas [8-10] to calculate the $CO_2$ transport properties because the GK formulas do not depend upon the details of any particular molecular model and are not limited to any density condition [11]. Coelho *et al.* [4] and Ludemann *et al.* [5] used, respectively, a LJ 6-12 potential and a rough hard sphere model to calculate the self-diffusion coefficient of $CO_2$. Both of the molecular models considered the molecule as a structureless spherical particle, and the parameters in the potentials were extracted from experimental data. It is well known that an isotropic potential is inadequate to describe the interactions between polyatomic molecules. Moreover, the parameters used

to calculate the self-diffusion coefficient in these models cannot be used to reliably predict other transport properties such as viscosity and thermal conductivity. Hence, an anisotropic potential is required for quantitative calculations. Fernandez *et al.* [10] used a two-center LJ plus point quadruple pair potential to calculate the shear viscosity and thermal conductivity of low temperature, high density $CO_2$ fluids. In their model, the parameters in the potential were adjusted exclusively to fit the experimental pure substance vapor-liquid equilibrium data. The calculated shear viscosities and thermal conductivities have an average deviation of 5% and 10%, respectively, as compared to experimental data. The deviations are mainly caused by inaccurate intermolecular potential since the experimental data can indicate only a limited region of the potential energy surface [12]. Therefore, one of the difficulties in the calculations of thermophysical properties of real fluids is to obtain the accurate intermolecular potential function. It is impossible to use a single intermolecular potential for the calculations of thermophysical properties at all fluid states. For dilute gases such as the low pressure high temperature $CO_2$ gas, it is possible to obtain an accurate pair potential directly from *ab initio* calculations of the intermolecular potential of a $CO_2$ dimer without adjusting to any experimental data. For instance, Bukowski *et al.* (BUK) [13] accurately computed a four-dimensional intermolecular potential energy surface for the $CO_2$ dimer using the many-body symmetry-adapted perturbation theory and a large 5*s*3*p*2*d*1*f* basis set. With the increase of fluid density, the three-body contribution to the potential becomes important and the potential calculated from the molecular dimer would be inaccurate for dense fluids. However, in moderate dense gases, such as moderate dense $CO_2$ gas, in which the contributions of the potential to thermophysical properties would become

important, it is still possible to use the potential for a $CO_2$ dimer to accurately reproduce the thermophysical properties without considering the three-body effects. In this study, we use MD simulations and a five-center *ab initio* intermolecular potential (BUK potential) to study the dependence of thermophysical properties on density for moderate dense $CO_2$ gas without relying on any experimental data. This study also shows the upper limit of the gas density where the molecular interactions can be well represented by the pair-additive potential obtained from the molecular dimer. Additionally, the potential contributions to thermophysical properties and their dependence on density are studied in details at each simulated state point.

In the present work, the density, isochoric heat capacity, shear viscosity and thermal conductivity of $CO_2$ gas at 300 K and in the pressure range of 1 – 50 atm (which corresponds to the density range of 2 – 140 kg/m$^3$) are calculated by the equilibrium MD simulations using the BUK potential. The simulation conditions are chosen in order to compare against experimental data. Different from a fluid at low temperatures in which the vibrational degrees of freedom can be neglected [6, 14], for a polyatomic gas like $CO_2$ which has low-lying vibrational states, the vibrational energy contributions to the heat capacity and thermal conductivity are important even at room temperature. In this case, it is inappropriate to either neglect the vibrational degrees of freedom or treat the molecular vibration classically. The vibrational heat capacity can be easily calculated independently. However, it is hard to include the variation of vibrational energies directly into the GK formula for the calculation of thermal conductivities because the vibrational energy is not allowed to change continuously. The traditional Eucken formula [15] which accounts for internal degrees of freedom of molecules by Eucken correction factor cannot

reliably predict thermal conductivities over a large range of pressure and temperature. In this work, the quantum effects of molecular vibrational energies are taken into account by the MC method [16]. Using this method, thermal conductivities can be obtained much more accurately than those obtained from a classical treatment of vibrational motions or by the neglect of vibrational energies [17]. The present molecular model can accurately reproduce the thermophysical properties of moderate dense $CO_2$ gas totally based on *ab initio* calculation results.

**2. The molecular structure and inter-molecular potential**

In order to include the rotational and vibrational motions of molecules in the MD model, the moment of inertia and the vibrational energy eigen values are both calculated from the intramolecular potential. Two *ab initio* intramolecular potential surfaces have recently been proposed for the $CO_2$ molecule; one is based on the Coupled-Cluster Singles and the Doubles excitation with perturbative treatment of the Triple excitations [CCSD(T)] method [18] and the other is the Density Functional Theory (DFT) method [19]. The CCSD(T) method is generally more accurate than the DFT method, but is computationally more expensive. Both the intramolecular potentials predicted the linear symmetric equilibrium structure of $CO_2$. Our previous *ab initio* results [19] show the C-O bond length $r_0 = 1.162\,\text{Å}$ which is consistent with the experimental data [20]. In this work, we assume the $CO_2$ molecules to be linear rigid rotors. Hence, the moment of inertia, *I*, of $CO_2$ is a constant in the simulation and can be computed via $I = 2m_O r_0^2$, where $m_O$ is the mass of the oxygen atom. Using the *ab initio* intramolecular potential,

the vibrational energy eigen values are obtained by solving the vibrational Schrödinger equation. The energy eigen values calculated from the intramolecular potential obtained by the CCSD(T) method normally gives more accurate results. Therefore, the corresponding results of $CO_2$ vibrational states are used in this work. The $CO_2$ molecule has four vibrational modes. The vibrational energy eigen values of the 1st excited states of the symmetric stretching mode, the asymmetric stretching mode, and the doubly degenerated bending modes are, respectively, 1387.9 $cm^{-1}$, 2348.8 $cm^{-1}$ and 667 $cm^{-1}$ [18]. In the calculation, we assume the energy differences between any two neighboring energy states of each vibratoinal mode are constant. Due to the strong quantum effects, the classical MD simulation of molecular vibrational motions is inappropriate. We use the MC calculations to take into account the quantum effects in the work.

The most important issue in a MD simulation is to use an appropriate intermolecular potential. The BUK potential employed in this work used a site-site representation of the intermolecular potential and was validated by comparing to the experimental second virial coefficients. The site-site fit BUK potential reads

$$U_{BUK} = \sum_{a\in A}\sum_{b\in B}\left[ \exp(\alpha_{ab} - \beta_{ab} r_{ab}) + f_1(\delta_1^{ab} r_{ab}) \frac{q_a q_b}{r_{ab}} - f_6(\delta_6^{ab} r_{ab}) \frac{C_6^{ab}}{r_{ab}^6} - f_8(\delta_8^{ab} r_{ab}) \frac{C_8^{ab}}{r_{ab}^8} \right], \qquad (1)$$

where $f_n[x] = 1 - e^{-x} \sum_{k=0}^{n} \frac{x^k}{k!}$ . (2)

In Eq. (1), the parameters $\alpha_{ab}$, $\beta_{ab}$, $\delta_n^{ab}$, $q_a$, and $C_n^{ab}$ are given in Ref. 13.

Figure 1 shows the radial dependence of the intermolecular potential for different $CO_2$ dimer configurations. To ensure the continuity of the potential and force near the

cut-off radius, the original BUK potential $U_{BUK}$ is employed with a small modification as follows

$$U_{\mathrm{mod}} = \begin{cases} U_{BUK} \cdot \left[ 1 - e^{\frac{r_{AB} - r_{cut}^{\ 2}}{-2.0}} \right] & r_{AB} \le r_{cut} \\ 0 & r_{AB} > r_{cut} \end{cases} \tag{3}$$

where $r_{cut}$ is the cut-off radius and $r_{AB}$ is the distance between the center of mass for each of the two $CO_2$ monomers. Both the $r_{AB}$ and $r_{cut}$ are in atomic units. The modification only takes effects in the weak interaction region which is close to the cut-off radius. In this work, we set $r_{cut} = 14\,\mathrm{\AA}$. Tests showed that with such a large cut-off radius, the use of an Ewald sum to treat long range Coulomb interactions was not necessary [21]. The modified potential makes the intermolecular potential, the intermolecular force, and the torque acting on the molecule all go smoothly to zero at the cutoff radius so that possible problems associated with the energy conservation and numerical instability in the equations of motion are eliminated.

## 3. Theoretical background

The computations of thermophysical properties are all carried out by the equilibrium MD simulations in a microcanonical ensemble. The time-correlation function theory is employed for the calculations of shear viscosity and thermal conductivity. The heat capacity can be simply obtained from the energy fluctuations. The density is determined directly from the equilibration process described next.

### *3.1. Shear viscosity*

The GK formula for shear viscosity $\eta$ can be expressed as [22]

$$\eta = \frac{V}{k_B T}\int_0^\infty dt \left\langle \mathrm{P}_{\alpha\beta}\ \ t\ \cdot \mathrm{P}_{\alpha\beta}\ \ 0\ \right\rangle \tag{4}$$

$$\text{where } \mathrm{P}_{\alpha\beta} = \underbrace{\frac{1}{V}\sum_i m v_{i\alpha} v_{i\beta}}_{\mathrm{P}_{\alpha\beta,k}} + \underbrace{\frac{1}{V}\sum_i \sum_{j>i} r_{ij_\alpha} f_{ij_\beta}}_{\mathrm{P}_{\alpha\beta,p}} \tag{5}$$

In Eqs. (4) and (5), $\mathrm{P}_{\alpha\beta}$ are the off-diagonal ($\alpha \neq \beta$) elements of the pressure tensor, $\langle \cdots \rangle$ denotes the ensemble average which can be determined from MD simulations. The variations of translational velocities, $v_i$, intermolecular distances, $r_{ij}$, and forces, $f_{ij}$, in Eq. (5) are all caused by the interactions between molecules and are assumed to be not affected by molecular vibrational motions. To study the potential contribution to the shear viscosity as a function of gas density, Eq. (5) is separated into two parts as suggested by Meier *et al.*[23]; one is the kinetic contribution $\mathrm{P}_{\alpha\beta,k}$ and the other is the potential contribution $\mathrm{P}_{\alpha\beta,p}$. When this separation is inserted into Eq. (4), the viscosity is divided into three different contributions, i.e., the kinetic-kinetic contribution $\eta_{kk}$, kinetic-potential contribution $\eta_{kp}$ and potential-potential contribution $\eta_{pp}$. The three contributions as a function of gas density are all calculated in this work.

### *3.2. Thermal conductivity*

The GK formula relates the thermal conductivity $\lambda_T$ to the time autocorrelation function of the energy current [11].

$$\lambda_T = \frac{V}{k_B T^2} \int_0^\infty dt \left\langle J_\alpha \;\; t \;\; J_\alpha \;\; 0 \right\rangle \tag{6}$$

Here, $J_\alpha$ is a component of the energy current. For a linear molecule like $CO_2$, $J_\alpha$ can be expressed as Eq. (7) based on the frozen vibrational energy assumption [16]

$$\begin{aligned} J_\alpha = & \frac{1}{V} \sum_i v_{i\alpha} \left( \tfrac{1}{2} m v_i^2 + \tfrac{1}{2} I u_i^2 + E_{Vi} + \tfrac{1}{2} \sum_{j \neq i} U_{ij} \right) \\ & + \frac{1}{V} \sum_i \sum_{j>i} r_{ij_\alpha} \;\; \tfrac{1}{2} \;\; \vec{v}_i + \vec{v}_j \;\; \cdot \vec{F}_{ij} + \tfrac{1}{2} \;\; \vec{u}_i \cdot \vec{G}_{ij} - \vec{u}_j \cdot \vec{G}_{ji} \end{aligned} \tag{7}$$

where $\vec{u}_i$ is the rotational velocity of molecule *i* which is defined as $\dot{\vec{e}}_i$, the time derivative of the unit vector along the molecular axis, and $U_{ij}$ represents the intermolecular potential. In Eq. (7), $\vec{G}_{ij}$ can be determined from the intermolecular forces by

$$\vec{G}_{ij} = \sum_a d_{ia} \vec{f}_{ija} \tag{8}$$

where $d_{ia}$ is the distance of the site *a* in molecule *i* relative to the center of mass, $\vec{f}_{ija}$ is the force acting on the site *a* in molecule *i* due to the interaction between molecule *i* and molecule *j*.

Most of the papers which calculated the thermal conductivity of the molecular fluids from the GK formula either removed the vibrational energy $E_{Vi}$ [6, 14, 17, 24] or treated the vibrational motions classically [17, 25, 26]. However, neither of the methods is appropriate for polyatomic gases. In this work, the quantized vibrational energy of each molecule is initialized by MC method at the desired temperature. Due to the interactions among molecules in the system, the translational, rotational, and intermolecular potential

energies all vary with time. However, the vibrational energies are assumed to be frozen in the molecules so that they have no influence on the molecular interactions.

To study the potential contribution to the thermal conductivity as a function of the gas density, the energy current expression is also separated into the kinetic contribution $J_{\alpha,k}$ and the potential contribution $J_{\alpha,p}$ as follows:

$$J_\alpha = \underbrace{\frac{1}{V}\sum_i v_{i\alpha}\ \tfrac{1}{2}mv_i^2 + \tfrac{1}{2}Iu_i^2 + E_{Vi}}_{J_{\alpha,k}} + \underbrace{\frac{1}{V}\left[\sum_i v_{i\alpha}\left(\tfrac{1}{2}\sum_{j\neq i}U_{ij}\right) + \sum_i\sum_{j>i} r_{ij_\alpha}\ \tfrac{1}{2}\ \vec{v}_i + \vec{v}_j\ \cdot\vec{F}_{ij} + \tfrac{1}{2}\ \vec{u}_i\cdot\vec{G}_{ij}^{\perp} - \vec{u}_j\cdot\vec{G}_{ji}^{\perp}\right]}_{J_{\alpha,p}} \quad (9)$$

Similarly, the thermal conductivity is divided into three different contributions, i.e., kinetic-kinetic contribution $\lambda_{T,kk}$, kinetic-potential contribution $\lambda_{T,kp}$ and potential-potential contribution $\lambda_{T,pp}$. The density dependence of the three contributions is studied in details in this work.

### *3.3. Heat capacity*

The calculation of isochoric heat capacity is much easier than the transport properties such as shear viscosity and thermal conductivity. In a constant NVE ensemble, the heat capacity can be calculated by [27]

$$\left\langle E_P^2\right\rangle - \left\langle E_P\right\rangle^2 = \frac{d}{2}Nk_B^2T^2\left(1-\frac{dNk_B}{2C_V}\right) \quad (10)$$

where $E_P$ is the total potential energy of the system, $C_V$ is the isochoric heat capacity excluding the vibrational contributions, and $d$ is the degree of freedom. Since the

vibrational energies are assumed frozen in the molecules during the simulation, the $C_V$ in Eq. (10) does not include the contribution from the vibrational degree of freedom. Hence, $d = 5$ for $CO_2$ molecules which include 3 degrees of freedom of translational motion and 2 degrees of freedom of rotational motion. The vibrational heat capacity is calculated independently at the desired temperature. Since we assume the vibrational energies of each mode are equally spaced, the vibrational heat capacity can be calculated as the sum of four independent harmonic oscillators.

$$C_{V,vib} = Nk_B \sum_{j=1}^{4} \left[ \left( \frac{E_{vj}}{k_B T} \right)^2 \frac{e^{-E_{vj}/k_B T}}{1 - e^{-E_{vj}/k_B T}{}^2} \right] \tag{11}$$

where $E_{vj}$ means the fundamental vibrational transition energy of mode *j* whose value is given in Sec. 2.1. The sum of the calculated $C_V$ from Eq. (10) and the vibrational heat capacity from Eq. (11) is the isochoric heat capacity of $CO_2$ gas. The potential contribution $C_{V.p}$ to the isochoric heat capacity is obtained directly from the difference between the heat capacity of a real gas and the heat capacity of the ideal polyatomic gas at the corresponding temperature.

**4. Initialization and equilibration**

The MD simulations in this work are all carried out in a constant NVE ensemble with $N = 1024$. This number was chosen since no systematic dependence on the system size was found for the calculated thermophysical property when the number of molecules is greater than 1024. The pressure and temperature of the system each fluctuates around a desired value during the simulations. In order to be able to compare the calculated results

with experimental data at the given temperature and pressure, the corresponding volume and energy of the constant NVE ensemble must be evaluated at the desired temperature and pressure. The two values are obtained by an equilibration process described in this section. To save the simulation time for the equilibration process, the configuration of molecules and the distribution of energies should all be initialized at the desired temperature and pressure so that they can relax quickly to the appropriate distributions.

### *4.1. Initialization*

The coordinates of the molecular center of mass are initialized randomly inside the cubic simulation box and its volume can be initialized by the ideal gas law. The minimum distance between any two molecules is controlled to be greater than 6 Å to avoid unrealistic large potentials and forces. The molecular orientations are initialized as random vectors uniform in solid angle.

The distributions of translational, rotational and vibrational energies all fulfill the Boltzmann distribution at the given temperature. The translational velocities are initialized directly by the Maxwell-Boltzmann distribution. Theoretically, the rotational and vibrational energies are both quantized. The rotational energy levels of a $CO_2$ molecule which is modeled as a rigid rotor are determined by the following equation,

$$E_{rot}\ J\ = J\ \ J+1\ \frac{\hbar^2}{2I}\ \text{with}\ J = 0,1,2,\cdots,\infty \tag{12}$$

where the degeneracy of level $J$ equals $2J+1$. The rotational energy level of each molecule in the system can be initialized by the Metropolis MC method [27]. Initially, we set all molecules on the ground rotational energy state, i.e., *J = 0*. Then, a trial transition

from the current energy level *o* to the new level *n* is carried out. The probability of accepting such a trial transition is $acc\ \ o \to n$ which can be determined by

$$acc\ \ o \to n\ \ = 0.5 \cdot \min\left(1, \frac{g\ \ n}{g\ \ o} \exp\left\{-\frac{E_{rot}\ \ n\ \ - E_{rot}\ \ o}{k_B T}\right\}\right) \tag{13}$$

where $n = o \pm 1$ and $n \geq 0$. In Eq. (13), $g\ \ n$ and $g\ \ o$ are, respectively, the degeneracy of level *n* and level *o*, and $E_{rot}\ \ n$ and $E_{rot}\ \ o$ are, respectively, the rotational energy on level *n* and level *o*. After several thousand trial transitions, the average rotational energy per molecule starts to fluctuate around a constant value. The fluctuating rotational energies correspond to different distributions of rotational energies in the molecule. Any one of these distributions can be used to initialize the rotational energy distribution at the given temperature. After the rotational energy is initialized, the energy is allowed to change continuously in the simulation since the rotational quantum effects can be neglected. Hence, the rotational velocity is also allowed to change continuously. The magnitude of rotational velocity, $\vec{u}$, is determined by

$$E_{rot} = \tfrac{1}{2} I \vec{u}^{\,2} \tag{14}$$

where the directions of $\vec{u}$ are chosen randomly in the plane perpendicular to the molecular axis.

The vibrational energy levels of a $CO_2$ molecule which is modeled as a combination of four independent harmonic oscillators are determined by

$$E_{vib} = \sum_{j=1}^{4} n_j + \tfrac{1}{2}\ \ E_{vj} \tag{15}$$

where $n_j$ is the vibrational energy level of the *j*th vibrational mode. A similar Metropolis MC method as described above can be employed to initialize vibrational energy of each

molecule at the given temperature. Since the vibrational quantum effects cannot be neglected, it is not appropriate to initialize the vibrational velocities of the molecules. In practice, the vibrational energies do not change during the simulation once they are initialized.

### *4.2. Equilibration*

In the equilibration process, the volume and total energy of the system should be relaxed to values that correspond to the desired temperature and pressure. Once these two values are found, they are used as preset values in the constant NVE ensemble. Therefore, the equilibration procedure is needed before starting the calculations of thermophysical properties.

To equilibrate the system to the desired temperature and pressure, the system is coupled to a constant temperature and pressure bath using the approach proposed by Berendsen et al. [28]. At each time step, the translational velocities are scaled by a factor

$$\lambda = \left[1 + \frac{\Delta t}{\tau_T}\left(\frac{T_0}{T} - 1\right)\right]^{\frac{1}{2}} \tag{16}$$

where $T_0$ is the desired temperature, $T$ is the current translational temperature, $\Delta t$ is the time step and $\tau_T$ is a preset time constant. The scale factor can force both the translational and rotational kinetic temperatures to the desired temperature since the energy exchanges between the translational and rotational motions are fast. Meanwhile, the molecular center-of-mass coordinates are scaled by a factor of $\mu$, and the volume of the simulation box is scaled by a factor of $\mu^3$, where

$$\mu = \left[ 1 + \frac{\Delta t}{\tau_p} \left( \frac{P}{P_0} - 1 \right) \right]^{\frac{1}{3}} \tag{17}$$

where $P_0$ is the desired pressure, $P$ is the instantaneous pressure, and $\tau_p$ is a time constant. The long range correction to the pressure [22] is calculated by orientational averaging of the virial beyond the cut-off radius. It is found in the simulation that $\tau_T \approx 25 ps$ and $\tau_p \approx 10 ps$ are appropriate for $CO_2$ gas studied in this work. Thanks to all these methods we used in the initialization and equilibration, the system can be well equilibrated within 500 ps. An example of the equilibration process of $CO_2$ gas at 300 K and 30 atm is shown in Fig. 2(a) and Fig. 2(b). From Fig. 2 we can see after the temperature and pressure are relaxed to the desired values, the total internal energy *E* and the volume *V* of the system both fluctuate around a constant value. After the system reaches the equilibrium, the equilibrium process runs for 2 more ns to determine the desired energy and volume from the average of those fluctuating values. The desired *V* can be used to calculate the density of the gas at the corresponding temperature and pressure.

The calculated densities together with experimental data and the gas densities predicted by using the second virial coefficient of $CO_2$ are shown in Fig. 3. The deviations of the calculated densities from experimental values are negligibly small except at the highest pressure of our calculation. The maximum deviation, 4.4%, is found at 300 K, 50 atm and density of about 135 kg/m$^3$ (3 mol/l). From Fig. 3 we can see the second virial coefficient becomes inadequate to accurately predict gas density when the $CO_2$ density is higher than 70 kg/m$^3$. In the moderate high density region, the third virial coefficient contribution becomes non-negligible. The pair-additive potential employed in

this work can partially account for the third virial coefficient because the third virial coefficient depends on both the pair interactions and non-additive three-body interactions. Therefore, our MD simulation based on the BUK potential predicts much better results than those predicted by using the second virial coefficient, but the deviation still exists due to the neglect of the three-body contributions to the intermolecular potential. At higher densities, the deviations are supposed to be even greater and the results will be unacceptable. This is a systematic error of applying the BUK potential to high density $CO_2$ fluids and hence cannot be improved by simulation techniques. Therefore, 135 kg/m$^3$ or 3 mol/l is about the upper limit of the $CO_2$ density above which the thermophysical properties cannot be reliably predicted from the potential for the $CO_2$ dimer.

**5. Simulation details and the results**

The shear viscosity, thermal conductivity, and heat capacity of $CO_2$ gas at different pressures are all produced from the equilibrium MD simulations. The equations of molecular translational motions are integrated by the Verlet leap-frog algorithm. For linear molecules like $CO_2$, the Singer leap-frog algorithm [29] can be applied to integrate the equations of molecular rotational motions. Compared to the standard implicit quaternion algorithm [22], the Singer algorithm preserves the linear rigid molecular structure and improves the energy conservation so that a considerably large step size can be employed in the simulations to save total computational cost.

Since the molecular vibrational energies are frozen in each MD simulation, the variations of molecular vibrational energies are considered separately. Using the MC

method described in the last section, 2000 distributions of vibrational energies are used to initialize the vibrational energies of the molecules in the system. Hence, each MD simulation actually started with 2000 different initial vibrational energy distributions but with the same initial configuration and initial translational and rotational velocities. In the calculation of thermal conductivities, the corresponding time autocorrelation functions of the energy current calculated from different initial states are averaged to determine the final time autocorrelation function at the given temperature and pressure. The time step size used in the simulation are chosen so that the total energy of the system is always kept constant within 1 part in $10^4$. Thanks to the modified BUK intermolecular potential and the Singer leap-frog algorithm which improve the numerical stability, a step size up to 12.5 fs can be used for the $CO_2$ gas at 1 atm and 300 K. The step sizes for higher pressures in this work are all set as 8.5 fs to ensure the energy conservation.

The shear viscosity and thermal conductivity are both transport properties which have long correlation times in the gas phase. Accurate determinations of the ensemble averages in Eqs. (4) and (6) require extremely long simulations whose length would be more than $10^4$ times of the correlation time [31]. The calculated time correlation functions of the off-diagonal elements of the pressure tensor and energy current are shown in Fig. 4(a) and Fig. 4(b) for pressures at 10 atm, 20 atm and 50 atm. It is seen from these figures that the correlation time of the energy current are a little larger than that of the pressure tensors and both correlation times decrease with pressure. Hence, the total simulation lengths required for the calculations of shear viscosity and thermal conductivity decrease with pressure from 7 μs at 1 atm to 200 ns at 50 atm. The computational cost for such long simulation lengths is very high because of the complex

expression of the BUK potential used in this model. Hence, at each pressure, the long simulations are divided into 100 shorter parallel runs which are independently initialized and equilibrated at the given temperature and pressure. The final results are obtained by averaging the results calculated from shorter parallel runs. The statistical errors are obtained from the mean-square deviation of the correlation functions. The time integrals of the calculated autocorrelation functions are the shear viscosities and thermal conductivities at the corresponding temperature and pressures. Compared to the above two transport properties, the heat capacity is a static property and hence easier to be calculated. The heat capacities at different pressures are obtained directly from the fluctuations of potential energies as shown in Eq. (10). The calculated isochoric heat capacities, shear viscosities, and thermal conductivities, together with the experimental data [32, 33] are shown in Fig. 5 through Fig. 7.

Similar to the calculated densities, the deviations between the calculated heat capacity and experimental data are negligible (within 1%) except at the highest pressure as shown in Fig. 5(a). The largest deviation of about 4.7% is found at 50 atm. Since the BUK potential does not take into account the three-body contribution, the deviation will be even larger at higher pressures if we still employ the same potential in the calculation. In order to improve the accuracy of the calculated heat capacities at higher densities, the parameters in the original *ab initio* potential need to be adjusted to include the average three-body effects. So far, a very accurate *ab initio* calculation of an intermolecular potential which includes the three-body effects is unavailable. Hence, the potential model must be optimized to the available experimental data to get better calculation results of thermophysical properties of dense fluids. From Fig. 5(b) we can see the increase of the

heat capacity at constant temperature is purely attributed to the increase of the potential contribution to the heat capacity. Although the highest density in our calculation is still far less than the critical density of the $CO_2$, the weight of the potential contribution $C_{V,p}$ in the heat capacity has reached 25% which shows a significant contribution.

The dependence of the calculated shear viscosity on the pressure shown in Fig. 6(a) seems a little irregular. This is because the statistical uncertainty of the calculated viscosity is about 1.6%, whereas the maximal increment of the calculated viscosity between any two adjacent pressures in the calculation is only 3.7%. Hence, we can only see the viscosity generally increases with pressure, but the clear dependence is blurred by the statistical uncertainty. Nevertheless, the calculated viscosities have generally a very good agreement with the experimental data. The deviations are within 1.8% except at 50 atm. At the highest pressure, the deviation is about 4.5% which is mainly caused by the neglect of three-body contribution to the potential. Compare to heat capacity, the shear viscosity as well as thermal conductivity cannot be divided into pure kinetic and potential contributions. There also exist kinetic-potential cross contributions to these two properties as discussed in Sec. 3. Figure 6(b) depicts the density dependence of the three viscosity contributions. In the density range of our calculation, the kinetic-kinetic contribution $\eta_{kk}$ decreases with density, while the kinetic-potential contribution $\eta_{kp}$ and potential-potential contribution $\eta_{kp}$ both increase with density. The kinetic-potential contribution is generally a little larger than the potential-potential contribution. The above observation agrees with the density dependence of the viscosity contributions of a LJ model fluid at the subcritical gaseous states calculated by Meier *et al.*[23]. The viscosity calculated in this work is dominated by the kinetic-kinetic viscosity contribution. The

kinetic-potential contribution and the potential-potential contribution only account for, respectively, 10% and 5% at the highest density of the calculation.

As shown by Fig. 7(a), the calculated thermal conductivity agrees very well with the experimental data. Similar to the other three thermophysical properties, the maximal deviation of 2% is found at the highest pressure. The density dependence of the three thermal conductivity contributions depicted in Fig. 7(b) is similar to that of the three viscosity contributions. The difference is the kinetic-potential $\lambda_{T,kp}$ and the potential-potential $\lambda_{T,pp}$ contributions to the thermal conductivity are more significant. At the highest density, $\lambda_{T,kp}$ and $\lambda_{T,pp}$ account for, respectively, 23% and 19% of the thermal conductivity. The statistical uncertainty of the calculated thermal conductivity is estimated to be within 1.2%. The contribution of the vibrational energy term to the total thermal conductivity can be easily examined by calculating the difference between the thermal conductivity which includes the vibrational energy term and the one which sets the vibrational energy to zero. The weights of the vibrational energy contribution in the total thermal conductivity at 1 atm, 10 atm, 20 atm, 30 atm, 40 atm and 50 atm were calculated, and they are, respectively, 22.6%, 21.6%, 20.6%, 19.5%, 17.8% and 15.0%. Hence, there is a significant contribution from the vibrational energy term to the thermal conductivity for dense $CO_2$ gas even around room temperature.

## 6. Conclusions

In this work, the density, isochoric heat capacity, shear viscosity, and thermal conductivity of $CO_2$ gas in the pressure range of 1 – 50 atm and 300 K are calculated directly from computer simulations without using any experimental data. The potential

contributions to the thermophysical properties are studied at every simulated state point, and their characteristic dependence on density is described. The MC method is employed in the model to include the quantum effects of the vibrational motions. For the intramolecular dynamics of $CO_2$ molecules, the assumptions of rigid-rotor for rotational motion and of quantum harmonic oscillator for vibrational motion are both validated by good agreements between the calculated thermophysical properties and experimental data. For the intermolecular interactions, accurate thermophysical properties can be predicted by a pair-additive potential which is obtained from an *ab initio* calculation of the intermolecular potential of a $CO_2$ dimer if the $CO_2$ density is less than 135 kg/m$^3$ or 3 mol/l. For the calculations of thermophysical properties at higher densities, the *ab initio* intermolecular potential of a $CO_2$ dimer becomes inaccurate and the three-body contribution to the intermolecular potential must be taken into account. So far, the three-body contribution cannot be accurately obtained without experimental data. Therefore, 135 kg/m$^3$ is the upper limit of the $CO_2$ density in which the thermophysical properties can be accurately calculated from molecular simulation without using any experimental data.

$CO_2$ is a small molecule. The frozen vibrational energy assumption for $CO_2$ molecule is valid at temperatures up to 1000 K [16] since all the vibrational modes of $CO_2$ have a high energy gap between two neighboring vibrational energy levels. For larger molecules, however, there might exist torsional motions which are typically at lower frequencies than bond vibrations. In this case, it might be necessary to treat some vibrational modes in a classical way and the rest of them by a quantum mechanical way as described in this work. In all cases, a quantum mechanical treatment of some

vibrational modes must be performed; otherwise a significant underestimate of the thermal conductivity of a polyatomic fluid would be found in the calculation. As the vibrational energy for a given molecule is independent of time during the simulation when a quantum treatment of vibrational energy is carried out, its contribution to the thermal conductivity might be reducible to a simpler, perhaps analytic form.

**Acknowledgement**

This work was supported by Office of Naval Research through the Multidisciplinary University Research Initiative (MURI) program, Award No. N00014-05-1-0432.

**References**

[1] S. Bock, E. Bich, E. Vogel, A.S. Dickinson and V. Vesovic, J. Chem. Phys. **117**, 2151 (2002).

[2] S. Bock, E. Bich, E. Vogel, A.S. Dickinson and V. Vesovic, J. Chem. Phys. **120**, 7987 (2004).

[3] S. Bock, E. Bich, E. Vogel, A.S. Dickinson and V. Vesovic, J. Chem. Phys. **121**, 4117 (2004).

[4] L.A.F. Coelho, J.V. de Oliveira, F.W. Tavares, M.A. Matthews, Fluid Phase Equilib. **194-197**, 1131 (2002).

[5] H.D. Ludemann and L.P. Chen, J. Phys. Condens. Matter **14**, 44 (2002).

[6] G.A. Fernandez, J. Vrabec and H. Hasse, Mol. Simul. **31**, 787 (2005).

[7] J. Millat, V. Vesovic, and W.A. Wakeham, *Transport Properties of Fluids* (Cambridge University Press, Cambridge, 1996), Chap. 5.

[8] M.S. Green, J. Chem. Phys. **19,** 1036 (1951).

[9] M.S. Green, Phys. Review **119**, 829 (1960).

[10] R. Kubo, J. Phys. Soci. Japan **12**, 570 (1957).

[11] D.A. McQuarrie, *Statistical Mechanics* (University Science Books, Sausalito, 2000).

[12] S. Bock, E. Bich, and E. Vogel, Chem. Phys. **257**, 147 (2000).

[13] R. Bukowski, J. Sadlej, B. Jeziorski, P. Jankowski, K. szalewicz, S.A. Kucharski, H.L. Williams, and B.M. Rice, J. Chem. Phys. **110**, 3785 (1999).

[14] P. Ungerer, C. Nieto-Draghi, B. Rousseau, G. Ahunbay and V. Lachet, J. Mol. Liq. **134**, 71 (2007).

[15] J.O. Hirschfelder, C.F. Curtiss, R.B. Bird, *Molecular Theory of Gases and Liquids* (John Wiley & Sons., New York, 1967).

[16] Z. Liang and H.L. Tsai, Fluid Phase Equilib. (submitted).

[17] C. Nieto-Draghi, T. de Bruin, J. Perez-Pellitero, J.B. Avalos, and A.D. Mackie, J. Chem. Phys. **126**, 064509 (2007).

[18] C. Leonard, M. Diehr, P. Rosmus, W.C. Maguire, JQSRT **109**, 535 (2008).

[19] Z. Liang and H.L. Tsai, J. Mol. Spect. **252**, 108 (2008).

[20] G. Granar, C. Rosseti, and D. Bailly, Mol. Phys. **58**, 627 (1986).

[21] G. Steinebrunner, A.J. Dyson, B. Kirchner, and H. Huber, J. Chem. Phys. **109**, 3153 (1998).

[22] M.P. Allen and D.J. Tildesley, *Computer Simulation of Liquids* (Clarendon, Oxford, 2000).

[23] K. Meier, A. Laesecke and S. Kabelac, J. Chem. Phys. **121**, 3671 (2004).

[24] B. Eckl, J. Vrabec, H. Hasse, Fluid Phase Equilib. **274**, 16 (2008).

[25] D.K. Dysthe, A.H. Fuchs, and B. Rousseau, J. Chem. Phys. **110**, 4047 (1999).

[26] D.K. Dysthe, A.H. Fuchs, B. Rousseau and M. Durandeau, J. Chem. Phys. **110**, 4060 (1999).

[27] D. Frenkel and B. Smit, *Understanding Molecular Simulation* (Academic Press, San Diego, 2002).

[28] H.J.C. Berendsen, J.P.M. Postma, W.F. Van Gunsteren, A. DiNola, and J.R. Haak, J. Chem. Phys. **81**, 3684 (1984).

[29] K. Singer, A. Taylor, and J.V.L. Singer, Mol. Phys. **33**, 1757 (1977).

[30] K. Meier, A. Laesecke, and S. Kabelac, J. Chem. Phys. **121**, 3671 (2004).

[31] E.B. Smith and B.H. Wells, Mol. Phys. **52**, 701 (1984).

[32] Eds. P.J. Linstrom and W.G. Mallard, National Institute of Standards and Technology, Gaithersburg MD, 20899, http://webbook.nist.gov (retrieved June 13, 2009).

[33] V. Vesovic, W.A. Wakeham, G.A. Olchowy, J.V. Sengers, J.T.R. Watson, J. Millat, J. Phys. Chem. Ref. Data **19**, 763 (1990).

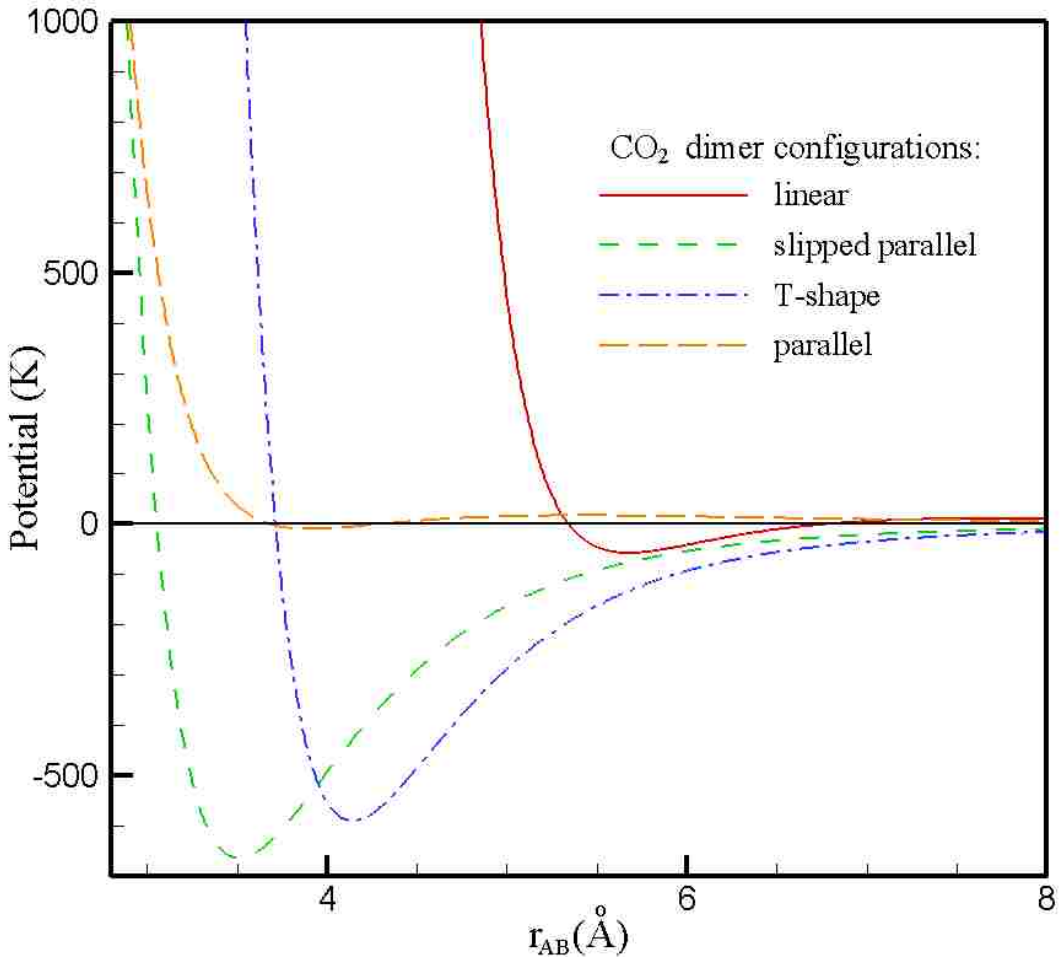


Fig. 1. The radial dependence of BUK intermolecular potential for different $CO_2$ dimer configurations.

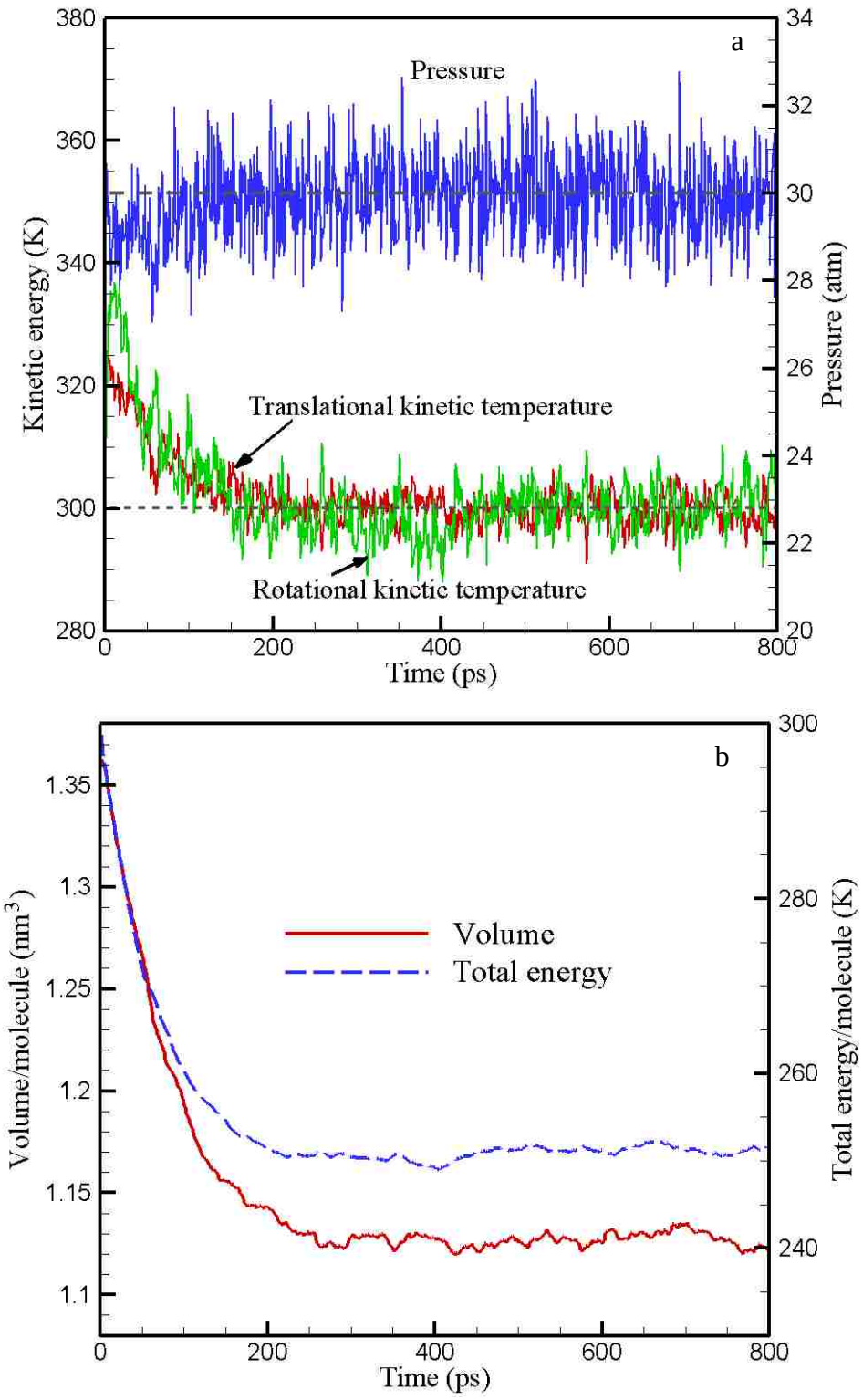


Fig. 2. The equilibration process of $CO_2$ gas at 300 K and 30 atm: (a) temperature and pressure vs. time and (b) volume and total energy vs. time.

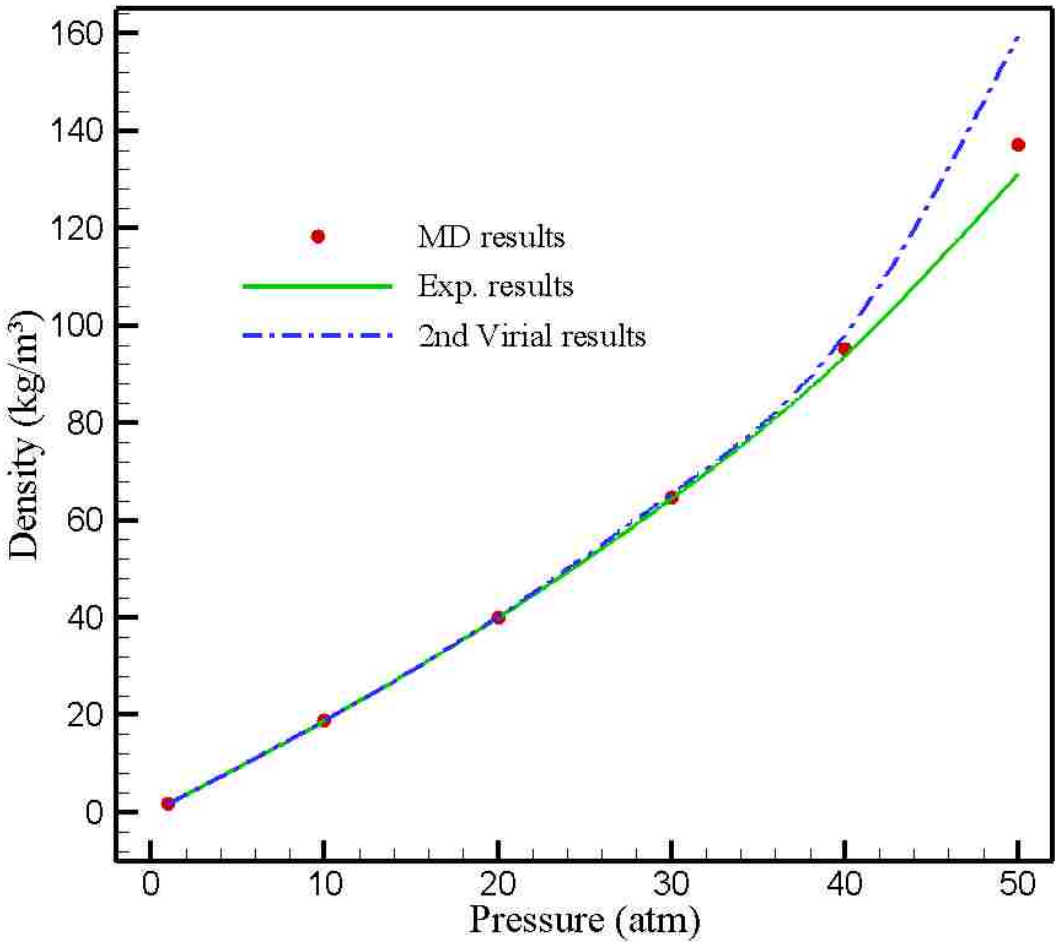


Fig. 3. $CO_2$ gas density vs. pressure at 300 K. The BUK potential predicts the 2nd virial coefficient to be –121.3 $cm^3$/mol at 300 K. The value is used to calculate the density from the 2nd virial correction.

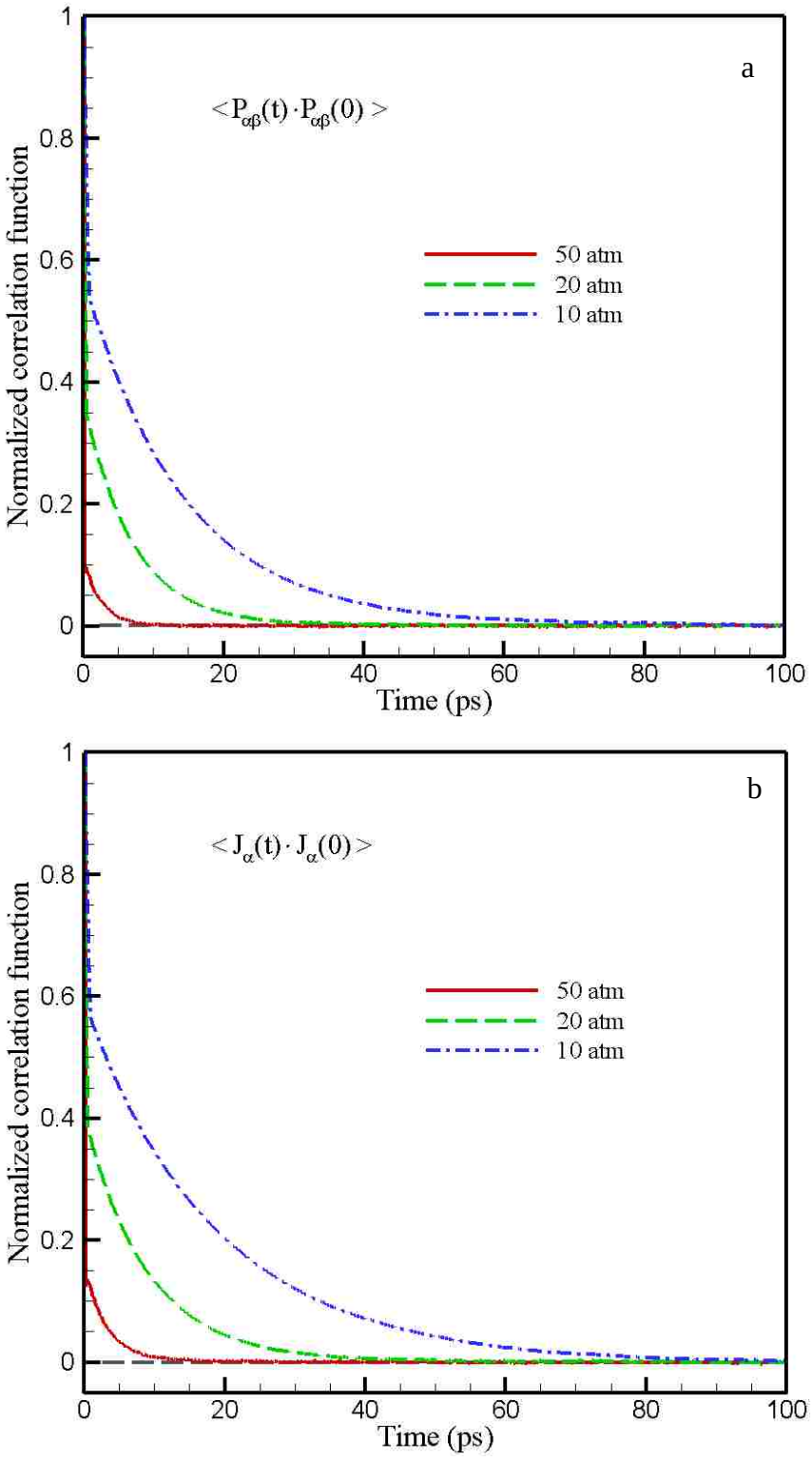


Fig. 4. Normalized autocorrelation functions of (a) off-diagonal elements of pressure tensors and (b) energy current at 10 atm, 20 atm and 50 atm and 300 K.

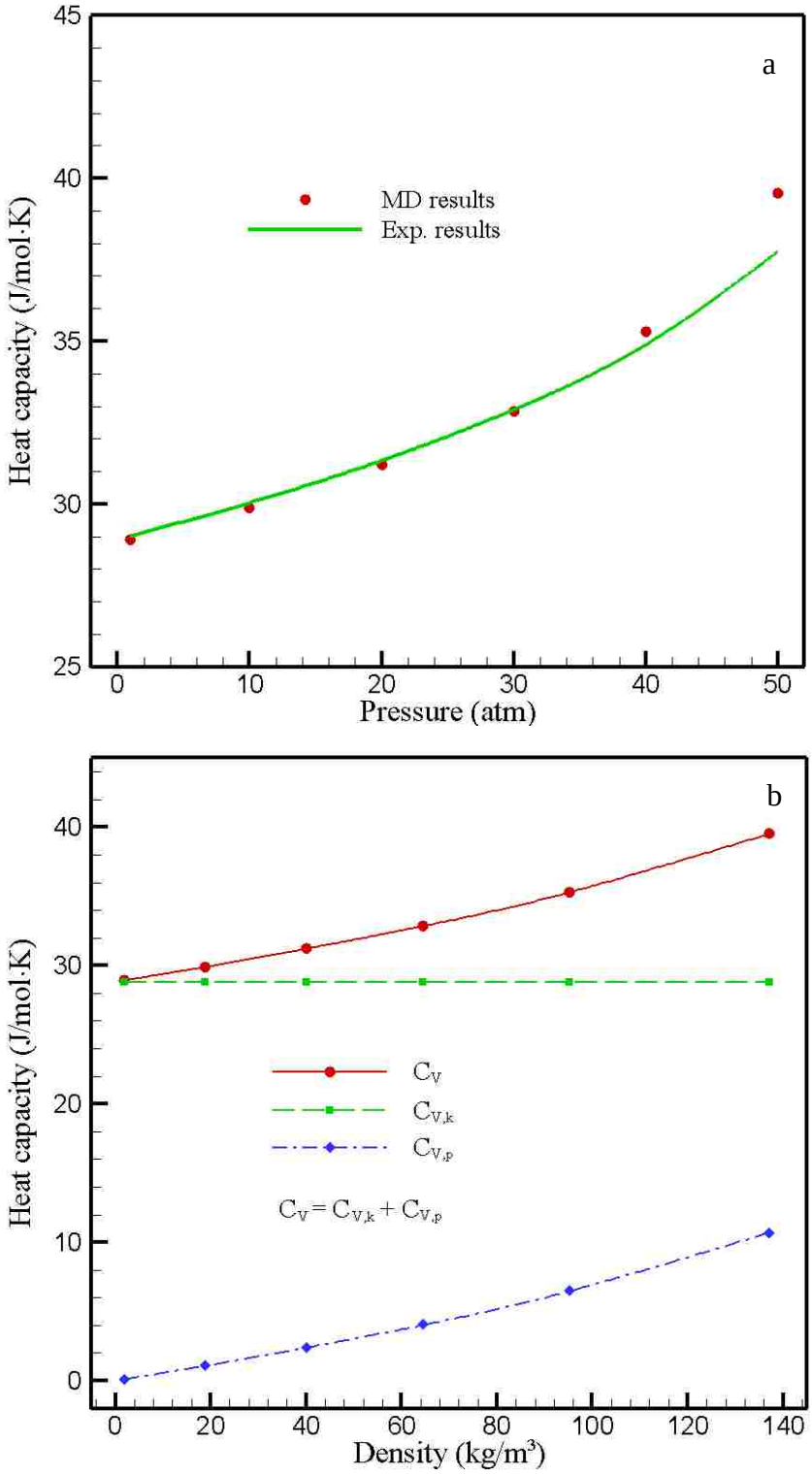


Fig. 5. (a) Isochoric heat capacity vs. pressure at 300 K. (b) The kinetic and potential contributions to the heat capacity as a function of density.

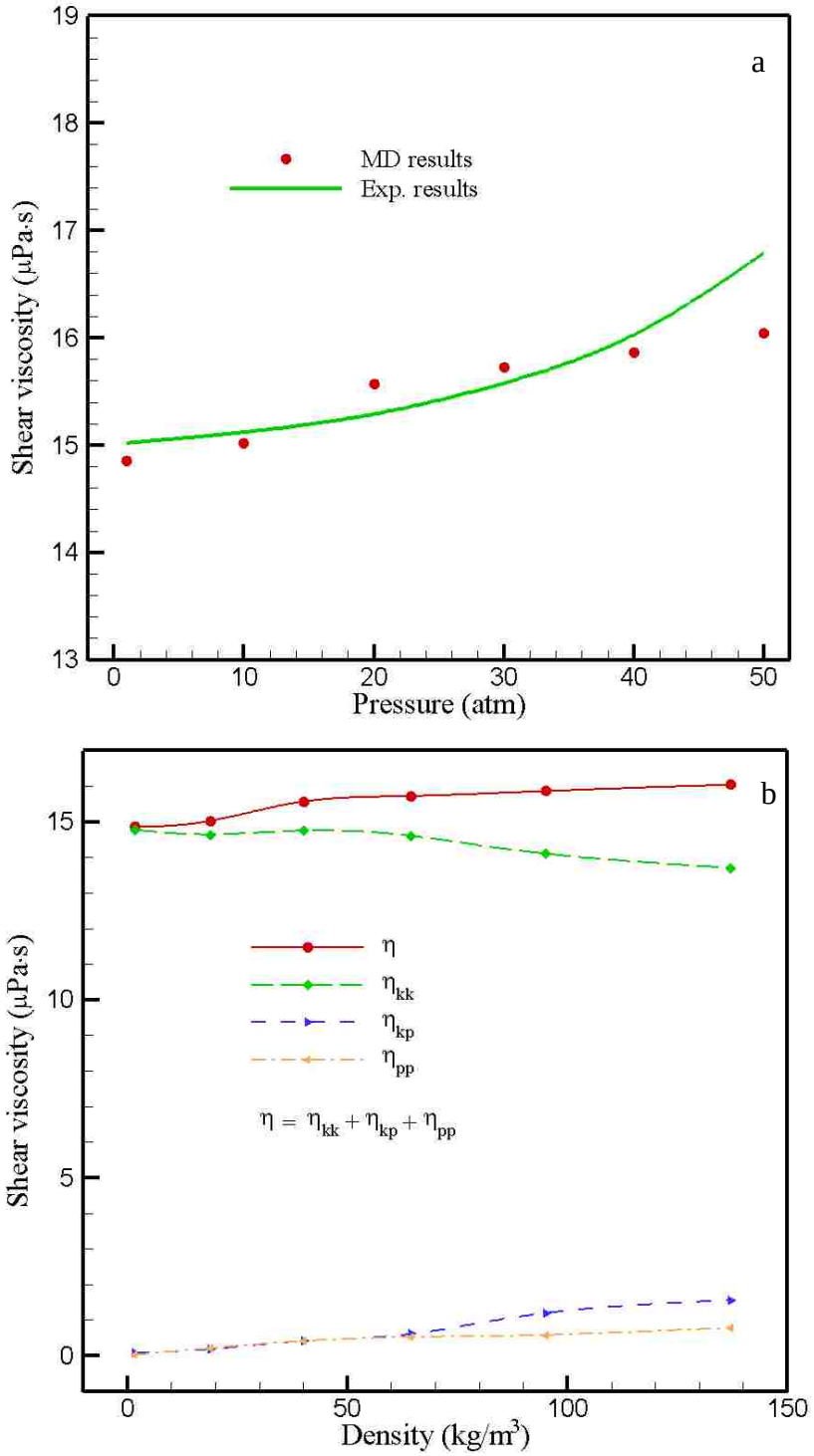


Fig. 6. (a) Shear viscosity vs. pressure at 300 K. (b) The viscosity contributions $\eta_{kk}$, $\eta_{kp}$ and $\eta_{pp}$ as a function of the gas density. The statistical error is within 1.6%. The uncertainty of the experimental data is 0.9%.

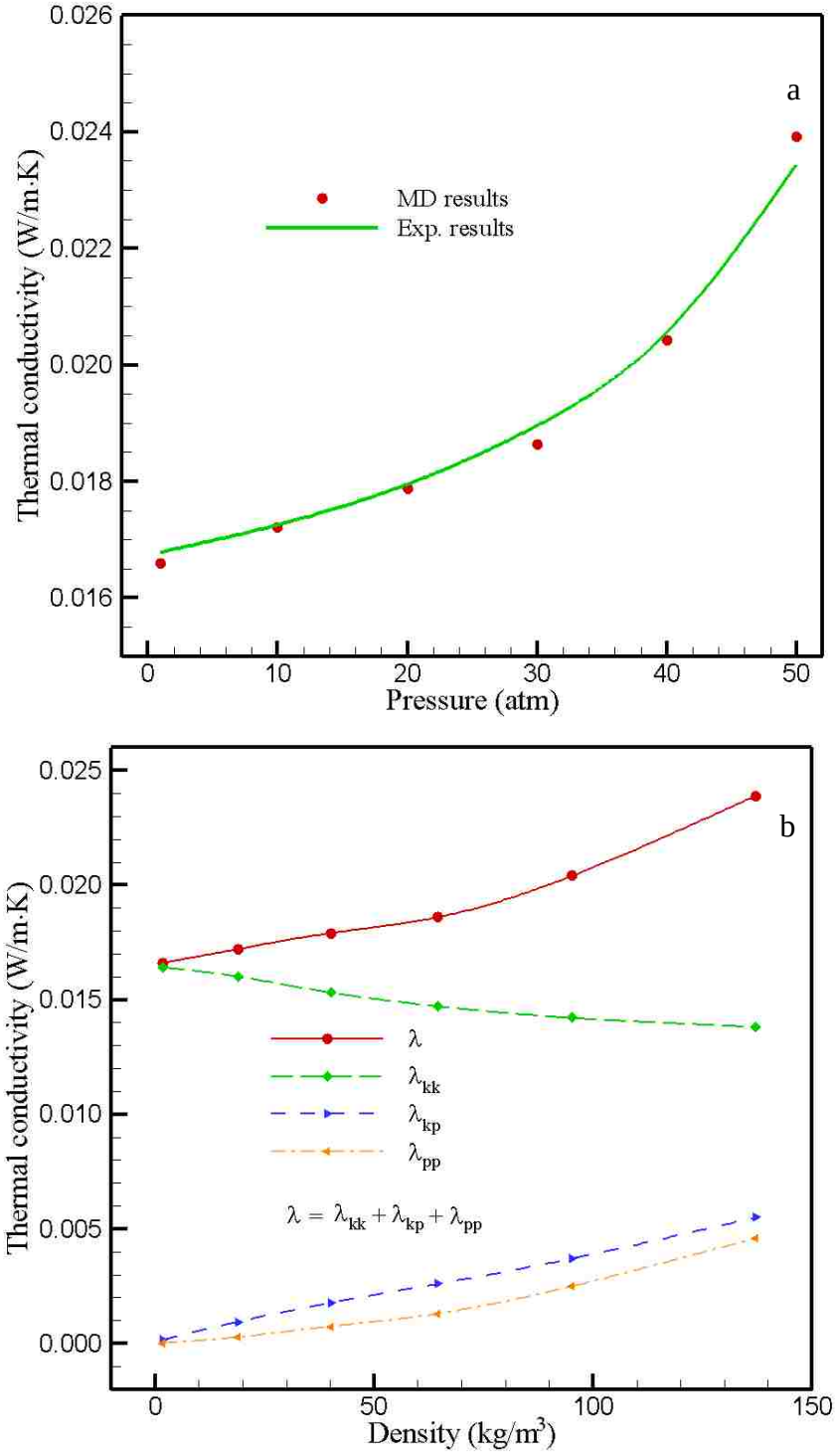


Fig. 7. (a) Thermal conductivity vs. pressure at 300 K. (b) The thermal conductivity contributions $\lambda_{T,kk}$, $\lambda_{T,kp}$ and $\lambda_{T,pp}$ as a function of the gas density. The statistical error is within 1.2%. The uncertainty of the experimental data is 2%.

## 4. The vibrational contribution to the thermal conductivity of a polyatomic fluid

Zhi Liang and Hai-Lung Tsai*

Department of Mechanical and Aerospace Engineering, Missouri University of Science and Technology, 400 W. 13th Street, Rolla, MO 65409, USA

**Abstract**

A simple analytic expression is proposed in this article to calculate the vibrational contribution to the thermal conductivity of a polyatomic fluid. The analytic expression was obtained based on the assumption that the self-diffusion process is the major mechanism in the transport of vibrational energy. The proposed expression is validated by comparing the thermal conductivity of $CO_2$ calculated by molecular dynamics (MD) simulations to experimental data over a wide range of temperature and pressure. It is also demonstrated that the proposed analytic expression greatly increases the accuracy of calculated thermal conductivity for $CO_2$ at the supercritical state.

**Keywords:** Thermal conductivity; Vibrational contribution; Molecular dynamics

* Corresponding author. Tel.: +1 573 341 4945; fax: +1 573 341 4607.

*E-mail address:* tsai@mst.edu (H.L. Tsai).

## 1. Introduction

The thermal conductivities of polyatomic fluids have been calculated using equilibrium or nonequilibrium MD simulations for decades [1-7]. Since thermal conductivity measures the transport of energy through the fluid, the inclusion of vibrational energy of the molecule into the calculation is important. No matter which MD simulation is used, however, there always exists a problem of how to treat molecular vibrations properly. As the number of atom in a molecule increases, more vibrational modes need to be considered in the calculation. The characteristic vibrational temperature normally varies from a few hundred K's for vibrational modes, such as torsional vibrations, to several thousand K's for vibrational modes, such as stretching vibrations. Generally, two approaches are frequently used to treat different vibrational motions. The first one is to treat the vibrational motion classically with a potential in which the parameters are often determined from infrared spectroscopy data or quantum chemistry results [1, 2, 4, 6, 7]. This classical approximation is appropriate if the characteristic temperature of the vibrational mode is considerably lower than the simulation temperature. The other approach is to apply constraints to the bond lengths or bond bending angles, and the stretching or bending energy is accordingly neglected [1, 3, 4, 5]. The second approach is normally used when the characteristic temperature of the vibrational mode is much higher than the simulation temperature. However, there exist many vibrational modes of which the characteristic temperature is higher but not too much higher than the simulation temperature. In these cases, the vibration motion is strongly affected by quantum effects. The classical treatment of vibrational modes may lead to wrong vibrational energies and hence wrong vibrational contributions to the

thermal conductivity. On the other hand, a simple neglect of vibratoinal energies is also not appropriate, because a nonnegligible population of molecules may have been excited to the corresponding vibrational modes at the simulation temperature. As an example, Nieto-Draghi *et al.* [1] have shown that both the classical treatment and the neglect of vibrational motions of $CO_2$ lead to a significant underestimate of thermal conductivity at the supercritical state. This problem was resolved recently by using a Monte Carlo (MC) method to treat the quantum effects of the vibrational motion [8, 9]. The proposed MC method is based on the assumption that the exchange of energy between the constrained vibrational motion, which is strongly affected by quantum effects, and all other modes of motion is negligible. In implementation, the vibrational energies of constrained vibrational modes are considered to be constant during the simulation after they are initialized by the Metropolis algorithm [10] at the simulation temperature. Meanwhile, the molecule (in the case when all vibrational modes are constrained) or a part of the molecule (in the case when a part of the molecule is constrained) is considered rigid in the simulation, and the structure of the constrained part of the molecule is considered unaffected by the initial vibrational energies. This MC method used for quantum treatments of constrained vibrational motion has been applied to accurately determine the thermal conductivity of $CO_2$ gas in a wide range of temperature and pressure [8, 9]. It was found [9] that the vibrational contribution to the thermal conductivity of $CO_2$ gas has reached about 20% of the total thermal conductivity at 300 K. This temperature is much lower than all characteristic vibrational temperatures of $CO_2$, but a significant vibrational contribution has been observed.

In the aforementioned studies [8, 9], it was found that the vibrational energies of all constrained modes can be considered constant and, hence, independent of time during the simulation. Hence, it may be possible to find an analytic expression that can be used to calculate the vibrational contribution to the thermal conductivity. This work aims to develop such an analytic expression for a polyatomic fluid. In order to test the validity of the proposed analytic expression, it is necessary to ensure that an accurate intermolecular potential is used in the simulation and all other parameters in the MD simulation such as cut-off radius, simulation time step, and total simulation length do not significantly influence the calculation results of thermal conductivity. It has been shown that an *ab initio* intermolecular potential for $CO_2$ dimer proposed by Bukowski *et al.* (BUK) [11] can be used to accurately reproduce the thermophysical property of $CO_2$ gas in a wide range of temperature and pressure [8, 9, 12, 13]. Therefore, in this study the MD calculation of the thermal conductivity of $CO_2$ gas based on BUK potential is used to test the validity of the proposed analytic expression in the temperature range of 300−1000 K and pressure range of 1−40 atm. In addition to $CO_2$ gas, the analytic expression is applied to the calculation of thermal conductivity of supercritical $CO_2$ [1].

## 2. Theoretical background

In this work, the computations of thermal conductivity are carried out by the equilibrium MD simulation in a microcanonical ensemble. To study the vibrational contribution to the thermal conductivity, we start with the well-known Green-Kubo (GK) formula for the calculation of thermal conductivity $\lambda$ [14, 15].

$$\lambda = \frac{V}{3k_B T^2} \int_0^\infty dt \left\langle \vec{J}\ t\ \cdot \vec{J}\ 0\ \right\rangle \tag{1}$$

where $\vec{J}$ represents the energy current, *t* is the time, $\langle \cdots \rangle$ denotes the ensemble average, $k_B$ is the Boltzmann constant, $V$ is the volume of the system and $T$ is the average temperature of the system. The general expression for the energy current $\vec{J}$ in pure fluids which contain flexible, multicenter molecules can be expressed as Equation (2) [6, 16, 17].

$$\vec{J} = \frac{1}{V} \sum_i \left[ E_i \vec{v}_i + \frac{1}{2} \sum_{a \in i} \sum_{i \neq j} \sum_{b \in j} \vec{r}_{ij} \cdot \vec{f}_{ab} \cdot \vec{v}_a \right] \tag{2}$$

where *i* and *j* are molecular indices, and *a* and *b* are atomic indices. $\vec{v}$ is the velocity vector (all velocities are barycentric), $\vec{r}_{ij} = \vec{r}_i - \vec{r}_j$ is the center-center intermolecular distance vector and $\vec{f}_{ab}$ is the intermolecular force. The internal energy $E_i$ of molecule *i* in Equation (2) includes the translational, rotational, intermolecular potential energies and energies of vibrational modes that can be treated classically in the MD simulation. All these energies vary continuously with time in the simulation. For the constrained vibrational motion of which quantum effects cannot be neglected, however, the energies do not vary continuously with time and hence were normally not considered in the MD simulation. This is a defect in most MD simulations of thermal conductivity of polyatomic fluids in the past.

Our previous work [8, 9] has shown that the quantum effects of the constrained vibrational motion can be included in MD simulation by a MC method. Our simulation results indicate that the exchange of energy between the constrained vibrational motion and all other modes of motion is negligible for a dilute and moderate dense polyatomic fluid. This conclusion is similar to the assumption made by Chapman and Cowling [18] when they derived the modified Eucken formula for a dilute polyatomic gas. Based on the assumption that there is no exchange of energy between translational and internal

modes (rotational and vibrational) of motion, Chapman and Cowling argued that the transport of internal energy would take place by the diffusion of molecules. Hence, Chapman and Cowling divided the thermal conductivity $\lambda_{all}$ which includes all modes of motions into two parts in the following Equation (3) [18].

$$\lambda_{all} = \lambda_{tr} + \rho D C_{V,\text{int}} \tag{3}$$

where $\lambda_{tr}$ represents the thermal conductivity due to the transport of translational energy, $\rho$ is the density of the system, $D$ is the self-diffusion coefficient and $C_{V,\text{int}}$ is the contribution to the isochoric heat capacity from internal modes of motion. $\rho D C_{V,\text{int}}$ represents the thermal conductivity due to the transport of internal energy.

However, neglecting the exchange of energy between the translational and internal modes of motion (especially the rotational motion) is generally a crude approximation. Instead, it is more appropriate to use the approximation made in our previous work which only neglects the exchange of energy between the constrained vibrational motion and all other modes of motion. In this study, we propose the thermal conductivity $\lambda_{all}$ can be divided into two parts as the following equation.

$$\lambda_{all} = \lambda + \rho D C_{V,vib} \tag{4}$$

where $\lambda$ is the thermal conductivity due to the transport of intermolecular potential energy and energies of all modes of motion which can be treated classically. Here, $\lambda$ is identical to the thermal conductivity in Equation (1) and, hence, can be obtained from MD simulations. $\rho D C_{V,vib}$ represents the thermal conductivity due to the energy transport of constrained vibrational modes through the self-diffusion process. In Equation (4), $\rho D C_{V,vib}$ can be considered as the "correction" term to the original thermal

conductivity $\lambda$. The quantum effects of constrained vibrational motions are taken into account by the isochoric vibrational heat capacity $C_{V,vib}$ which can be calculated by the harmonic assumption via Eq. (5) [19].

$$C_{V,vib} = k_B \sum_{j=1}^{n} \left[ \left( \frac{E_{vj}}{k_B T} \right)^2 \frac{e^{-E_{vj}/k_B T}}{1 - e^{-E_{vj}/k_B T}^{\ 2}} \right] \tag{5}$$

where $E_{vj}$ is the fundamental vibrational transition energy of $j^{th}$ constrained vibrational mode of the molecule and $n$ is the total number of constrained vibrational modes. The self-diffusion coefficient $D$ in Equation (4) can be readily obtained from the MD simulation by Equation (6) [20].

$$D = \tfrac{1}{3} \int_0^\infty dt \left\langle \vec{v}_i(t) \cdot \vec{v}_i(0) \right\rangle \tag{6}$$

The validity of Equation (4) is to be tested in this work by calculating the thermal conductivity of $CO_2$ fluid. The $CO_2$ molecule has four vibrational modes, among which the bending mode has the lowest characteristic temperature of about 960 K. Hence, quantum effects of all vibrational modes of the $CO_2$ molecule cannot be neglected unless the simulation temperature is higher than 1000 K. All MD simulations in this work are carried out at a temperature lower than 1000 K. According to the assumption made in this work, therefore, all vibrational modes are constrained in the simulation so that the $CO_2$ molecule is modeled as a linear rigid rotor. For a linear rigid molecule, the energy current $\vec{J}$ which does not include the contribution from the vibrational energy can be simplified to Equation (7) [8].

$$\vec{J} = \frac{1}{V} \sum_i \left[ \tfrac{1}{2} \vec{v}_i \left( m\vec{v}_i^{\,2} + I\vec{u}_i^{\,2} + \sum_{j \neq i} U_{ij} \right) + \tfrac{1}{2} \sum_{j>i} \vec{r}_{ij} \cdot \left( \vec{v}_i + \vec{v}_j \right) \cdot \vec{F}_{ij} + \left( \vec{u}_i \cdot \vec{G}_{ij} - \vec{u}_j \cdot \vec{G}_{ji} \right) \right] \tag{7}$$

where $m$ and $I$ represent, respectively, the mass and the moment of inertia of the $CO_2$ molecule, $\vec{u}_i$ is the rotational velocity of molecule $i$ which is defined as the time derivative of the unit vector along the molecular axis, $\vec{F}_{ij}$ is the intermolecular force acting on molecule $i$ due to the interaction between the molecule $i$ and the molecule $j$, and $U_{ij}$ represents the intermolecular potential. In Equation (7), $\vec{G}_{ij}$ can be determined from the intermolecular forces by

$$\vec{G}_{ij} = \sum_a d_{ia} \vec{f}_{ija} \tag{8}$$

where $d_{ia}$ is the distance of the site $a$ in molecule $i$ relative to the center of mass and $\vec{f}_{ija}$ is the force acting on the site $a$ in molecule $i$ due to the interaction between molecule $i$ and molecule $j$.

**3. Simulation details**

The BUK potential employed in this work use a site-site representation of the intermolecular potential for $CO_2$ dimer as shown in the following equation.

$$U_{BUK} = \sum_{a\in i}\sum_{b\in j}\left[ \exp(\alpha_{ab} - \beta_{ab} r_{ab}) + f_1(\delta_1^{ab} r_{ab}) \frac{q_a q_b}{r_{ab}} - f_6(\delta_6^{ab} r_{ab}) \frac{C_6^{ab}}{r_{ab}^6} - f_8(\delta_8^{ab} r_{ab}) \frac{C_8^{ab}}{r_{ab}^8} \right], \tag{9}$$

where $f_n[x] = 1 - e^{-x} \sum_{k=0}^{n} \frac{x^k}{k!}$ . (10)

Here, sites $a$ belong to molecule $i$, sites $b$ belong to molecule $j$ and $r_{ab}$ is the distance between $a$ and $b$. Each molecule contains five sites, with three corresponding to the centers of the atoms in $CO_2$ and the remaining two on the C-O bonds 0.8456 Å away from the C atom. The C-O distance is fixed at 1.16047 Å. Parameters $\alpha_{ab}$, $\beta_{ab}$, $\delta_n^{ab}$, $q_a$,

and $C_n^{ab}$ are given in [11]. Since the $CO_2$ molecule is modeled as a linear rigid rotor in this work, the dipole moment of the $CO_2$ molecule is zero at every time step of the simulation. Hence, it is not necessary to use the reaction field method [21] to account for the long-range electrostatic interactions. In the application of BUK potential, the cut-off radius, within which all pair interactions are calculated, is chosen to be 14 Å. The long range correction to the pressure is calculated by orientational averaging of the virial beyond the cut-off radius.

The equilibrium MD simulations are all carried out in a constant NVE ensemble with $N = 4096$ for dilute $CO_2$ gas at 1 atm and 300−1000 K, and $N = 1024$ for moderate dense $CO_2$ gas at 300 K and 10−40 atm. The volume $V$ (or density $\rho$) and the total energy $E$ of the constant NVE ensemble corresponding to each simulation temperature and pressure are obtained by the method described in [9]. The coordinates of the molecular center of mass and the molecular orientations are all initialized randomly in a cubic box. The translational and rotational velocities are both initialized by the Maxwell-Boltzmann relation at the simulation temperature. The equations of molecular translational motions and molecular rotational motions are integrated by, respectively, the Verlet leap-frog algorithm and the Singer leap-frog algorithm [22]. The molecules in the system are equilibrated for 500 ps using the Berendsen's velocity scaling method [23] with a time constant of 100 ps for dilute gases and 25 ps for moderate dense gases before the calculation of the time-correlation function starts. The time step size, total simulation length of each simulation and the calculated density of the fluid at each simulated state point are given in Table 1. The time step size is chosen so that the total energy of the system remains constant within a relative accuracy of $10^{-4}$. As shown in Table 1, a very

long total simulation length is used at each simulated state point to ensure the statistical error of the calculated thermal conductivity is lower than or around 1%. The statistical error is calculated by Fincham's block averaging method [23]. Each long simulation shown in Table 1 is divided into 100 shorter parallel runs which are independently initialized and equilibrated at the given temperature and pressure.

The self-diffusion coefficient and vibrational heat capacity at a given temperature and pressure must be accurately determined before the calculation of vibrational contribution to the thermal conductivity is carried out. The velocity autocorrelation function used for the calculation of self-diffusion coefficient is averaged over the autocorrelation functions of all molecules in the system so that the statistical error of the calculated self-diffusion coefficient is less than 0.1%. In order to study the validity of Equation (4), the values of all variables used in the calculation should be as accurate as possible. Since very accurate experimental data of the heat capacity of $CO_2$ at zero density are available [25] at every simulation temperature, the vibrational heat capacity used in the calculation is obtained by Equation (10) which is more accurate than Equation (5).

$$C_{V,vib} = C_{V,\rho=0} - 2.5R \tag{10}$$

where $C_{V,\rho=0}$ represents the experimental data of isochoric heat capacity of $CO_2$ at zero density, $R$ is the gas constant.

## 4. Results and discussion

The first set of calculation is carried out at 1 atm and 300−1000 K. The calculated results are shown in Table 2. The uncertainty of the experimental data of the self-

diffusion coefficient at 1 atm was estimated to be ±5% [26]. It can be seen from Table 2 that the deviations between the calculated and experimental self-diffusion coefficients are within the experimental uncertainty. The error caused by decoupling the vibrations from other degrees of freedom is assumed negligible and Equation (10) is applied to calculate the vibrational heat capacity. The uncertainty of the experimental data of the heat capacity was estimated to be ±0.15% [25]. In Table 2, $\lambda_{MD}$ the thermal conductivity which does not include the vibrational contribution is obtained directly from the MD simulation with the statistical error of less than 1.0%. It is evident that $\lambda_{MD}$ significantly underestimates $\lambda_{all,\exp.}$ the experimental thermal conductivity at all simulation temperatures. The uncertainty of $\lambda_{all,\exp.}$ was estimated to be ±1% near room temperature and ±2% at the higher temperatures. As shown in Table 2, the density-diffusion product, $\rho D$ and vibrational heat capacity both increase with temperature. As a result, the magnitude of $\rho D C_{V,vib}$, i.e., the vibrational contribution to the thermal conductivity also increases with temperature. When the vibrational contribution is included, the corrected thermal conductivity $\lambda_{all,MD}$ has a good agreement with the experimental data as shown in Table 2. The significance of the vibrational contribution to the thermal conductivity for $CO_2$ gas at 1 atm is calculated by $\rho D C_{V,vib} / \lambda_{all,MD} \times 100\%$. The results are shown in Figure 1. The vibrational contribution increases with temperature from 24% at 300 K to 46% at 1000 K.

If the simulation temperature is higher than 1000 K, it may not be appropriate to assume the $CO_2$ molecule is a linear rigid rotor because the quantum effects of bending motions becomes negligible. In this case, it is more appropriate to treat the bend mode of

$CO_2$ classically and an intramolecular potential for bending motions should be included in the MD model. On the other hand, the other two vibrational modes of the $CO_2$ molecule should still be constrained because their characteristic temperatures are much higher than 1000 K. In these high temperature cases, the vibrational heat capacity $C_{V,vib}$ in Equation (4) only includes the contribution from the two constrained vibrational modes. The intermolecular potential employed in this work is based on a rigid geometry. Hence, it might not be appropriate to use it for the interaction between flexible $CO_2$ molecules at high temperatures.

The second set of calculation is performed at 300 K and 10−40 atm. Similar to the 1 atm case, the calculated self-diffusion coefficient is firstly compared with the experimental data. Stiel *et al.* [28] established a relationship between the self-diffusion coefficients and temperature for gases at moderate pressures. The relationship as shown in Equation (11) was found to reproduce the experimental data of the self-diffusion coefficient of $CO_2$ gas with an average deviation of 1.99%.

$$\rho D = \frac{0.464}{\xi}\left[1.391\frac{T}{T_c} - 0.381\right]^{2/3} \tag{11}$$

where $T_c = 304.2K$ is the critical temperature of $CO_2$, $\xi = 0.0224$ is constant for $CO_2$. According to Equation (11) at $T = 300K$, $\rho D = 20.58\ mg/m \cdot s$ is constant for $CO_2$ gas at moderate pressures. The calculated self-diffusion coefficient compared to the experimental value obtained from Equation (11) is shown in Table 3. It can be seen the calculated results generally agree well with the experimental data. However, a slightly decrease of the calculated $\rho D$ with density (or pressure) is observed. The decreasing trend agrees with the density dependence of $\rho D$ for a fluid at the subcritical gaseous

states calculated by Meier *et al.* [29] using the Lennard-Jones potential model. Liang and Tsai [9] have shown that the decoupling between vibrations and other degrees of freedom is appropriate for moderate dense $CO_2$ gas. Hence, the vibrational heat capacity used in this set of calculation is the same as that of dilute $CO_2$ at 300 K in Table 2. When the vibrational contribution is not included, the calculated thermal conductivity $\lambda_{MD}$ significantly underestimates the experimental thermal conductivity $\lambda_{all,\exp.}$ [27] at all simulation pressures as shown in Table 3. After the vibrational contribution $\rho DC_{V,vib}$ is included, very good agreement is achieved.

The statistical error of $\lambda_{MD}$ is about 1.2%. The uncertainty of the experimental data was estimated to be ±2% [27]. Since the vibrational heat capacity is constant and the density-diffusion product decreases with density, the magnitude of $\rho DC_{V,vib}$ slightly decreases with density. On the other hand, $\lambda_{MD}$ increases with density due to the increasing contribution from the intermolecular potential. Therefore, the vibrational contribution to the thermal conductivity decreases with density from 21.7% at 18.9 kg/m$^3$ to 17.9% at 95.1 kg/m$^3$ as shown in Figure 1. As the density or pressure is further increased, the vibrational contribution to the thermal conductivity will be even lower. In very high density fluids where the potential contribution to the thermal conductivity dominates, the vibrational contribution to the thermal conductivity becomes small or negligible.

To test validity of the proposed correction for the vibrational contribution to the thermal conductivity in high density fluid, the MD simulation should be extended to higher density range. However, the BUK intermolecular potential employed in this work

has been proved not suitable for high density $CO_2$ fluids. As an example, Bratschi *et al.* [30] showed that BUK potential predicts too large critical temperature and pressure compared to the experimental results. To test the validity of Equation (4) in high density fluids, therefore, a more appropriate intermolecular potential should be employed.

Nieto-Draghi *et al.* [1] calculated the thermal conductivity of $CO_2$ along the supercritical isotherm at 470 K using EPM2 potential. EPM2 model is a well know potential model for carbon dioxide which reproduces accurately the critical properties. Using the rigid-rotor assumption, Nieto-Draghi *et al.* calculated the thermal conductivity of $CO_2$ by MD simulations. An underestimation of 30% and 9% were found at 300 kg/m$^3$ and 800 kg/m$^3$, respectively. With the classical treatment of the vibrational motions in the simulation, they obtained an underestimation of 23% at 300 kg/m$^3$. Nieto-Draghi *et al.* discussed in their paper that "*an increase in the accuracy of the thermal conductivity might require a quantum treatment of the atomic vibration inside the molecule*". Since 470 K is much lower than the characteristic vibrational temperature of bending mode of $CO_2$, all vibrational modes should be constrained in the simulation based on the assumption made in this work. According to the analysis shown in this work, the deviations in their calculations can be corrected by $\rho DC_{V,vib}$. The vibrational quantum effects is taken into account by $C_{V,vib}$. We compare our corrected results with Draghi *et al.*'s results based on the rigid-rotor assumption and the experimental results in Table 4. The self-diffusion coefficient data are taken from the correlation provided by [31]. The vibrational heat capacity at 470 K is 14.62 J/mol·K [25]. It can be seen from Table 4 that the deviations between Nieto-Draghi *et al.*'s results and the experimental data can be corrected by the proposed vibrational correction very well. The deviation is reduced from

30% to 3.3% at 300 kg/m$^3$, and from 9% to 0.5% at 800 kg/m$^3$. From this calculation we can see the vibrational contribution to the thermal conductivity might be non-negligible even at a density close to the liquid density.

## 5. Conclusions

A simple correction term $\rho DC_{V,vib}$ is proposed to account for the vibrational contribution to the thermal conductivity. The proposed correction term is based on the assumption that, depending on the simulation temperature, the molecular vibrational mode with a relatively higher characteristic temperature can be considered constrained in the MD simulation. It is proved that the energy of constrained vibrations mainly contribute to the thermal conductivity through the self-diffusion process. Base on the proposed expression, the calculated thermal conductivities of $CO_2$ fluid at gaseous and supercritical states agree well with experimental data.

## Acknowledgement

This work was supported by Office of Naval Research through the Multidisciplinary University Research Initiative (MURI) program, Award No. N00014-05-1-0432.

## References

[1] C. Nieto-Draghi, T. de Bruin, J. Perez-Pellitero, J.B. Avalos and A.D. Mackie, J. Chem. Phys. **126**, 064509 (2007).

[2] X. Li, L. Zhao, T. Cheng, L. Liu and H. Sun, Fluid Phase Equilibr. **274**, 36 (2008).

[3] B. Eckl, J. Vrabec and H. Hasse, Fluid Phase Equilibr. **274**, 16 (2008).

[4] P. Ungerer, C. Nieto-Draghi, B. Rousseau, G. Ahunbay and V. Lachet, J. Mol. Liq. **134**, 71 (2007).

[5] G.A. Fernandez, J. Vrabec and H. Hasse, Mol. Simul. **31**, 787 (2005).

[6] D.K. Dysthe, A.H. Fuchs, and B. Rousseau, J. Chem. Phys. **110**, 4047 (1999).

[7] D.K. Dysthe, A.H. Fuchs, B. Rousseau and M. Durandeau, J. Chem. Phys. **110**, 4060 (1999).

[8] Z. Liang and H.L. Tsai, Mol. Phys. (in press).

[9] Z. Liang and H.L. Tsai, Fluid Phase Equilibr. (submitted).

[10] D. Frenkel and B. Smit, *Understanding Molecular Simulation* (Academic Press, San Diego, 2002).

[11] R. Bukowski, J. Sadlej, B. Jeziorski, P. Jankowski, K. Szalewicz, S.A. Kucharski, H.L. Williams, and B.M. Rice, J. Chem. Phys. **110**, 3785 (1999).

[12] S. Bock, E. Bich, E. Vogel, A. S. Dickinson, and V. Vesovic, J. Chem. Phys. **117**, 2151 (2002).

[13] S. Bock, E. Bich, E. Vogel, A. S. Dickinson, and V. Vesovic, J. Chem. Phys. **120**, 7987 (2004).

[14] M.S. Green, Phys. Rev. **119**, 829 (1960).

[15] R. Kubo, J. Phys. Soci. Japan **12**, 570 (1957).

[16] B.D. Todd, P.J. Daivis, and D.J. Evans, Phys. Rev. E **51**, 4362 (1995).

[17] G. Galliero and C. Boned, Phys. Rev. E **80**, 061202 (2009).

[18] S. Chapman and T.G. Cowling, *The Mathematical Theory of Non-Uniform gases* (Cambridge University Press, Cambridge, 1952), Chap. 13.

[19] D.A. McQuarrie, *Statistical Mechanics* (University Science Books, Sausalito, 2000).

[20] M.P. Allen and D.J. Tildesley, *Computer Simulation of Liquids* (Clarendon, Oxford, 2000).

[21] M. Neuman, J. Chem. Phys. **85**, 1567 (1986).

[22] K. Singer, A. Taylor, and J.V.L. Singer, Mol. Phys. **33**, 1757 (1977).

[23] H.J.C. Berendsen, J.P.M. Postma, W.F. Van Gunsteren, A. DiNola, and J.R. Haak, J. Chem. Phys. **81**, 3684 (1984).

[24] D. Fincham, N. Quirke, D.J. Tildesley, J. Chem. Phys. **84**, 4535 (1986).

[25] Eds. P.J. Linstrom and W.G. Mallard, National Institute of Standards and Technology, Gaithersburg MD, 20899, http://webbook.nist.gov (retrieved February 23, 2010).

[26] A. Boushehri, J. Bzowski, J. Kestin, and E.A. Mason, J. Phys. Chem. Ref. Data. **17**, 255 (1988).

[27] V. Vesovic, W.A. Wakeham, G.A. Olchowy, J.V. Sengers, J.T.R. Watson, J. Millat, J. Phys. Chem. Ref. Data **19**, 763 (1990).

[28] L.I. Stiel and G. Thodos, Can. J. Chem. Eng. **43**, 186 (1965).

[29] K. Meier, A. Laesecke and S. Kabelac, J. Chem. Phys. **121**, 9526 (2004).

[30] C. Bratschi, H. Huber and D.J. Searles, J. Chem. Phys. 126, 164105 (2007).

[31] T. Groβ, J. Buchhauser, and H.-D. Ludemann, J. Chem. Phys. 109, 4518 (1998).

Table 1. The time step size $\Delta t$, total simulation length $t_{total}$ and calculated density of fluid $\rho$ at each simulated state point. The statistical error of $\rho$ is less than 0.2%.

| P (atm) | T (K) | $\rho$ (kg/m$^3$) | $\Delta t$ (fs) | $t_{total}$ (μs) |
|---|---|---|---|---|
| 1 | 300 | 1.805 | 12.5 | 6.24 |
| 1 | 400 | 1.347 | 12.5 | 7.41 |
| 1 | 500 | 1.075 | 12.5 | 8.58 |
| 1 | 600 | 0.900 | 10.5 | 9.76 |
| 1 | 700 | 0.767 | 10.5 | 10.9 |
| 1 | 800 | 0.671 | 10.5 | 12.1 |
| 1 | 900 | 0.597 | 8.5 | 13.3 |
| 1 | 1000 | 0.537 | 8.5 | 14.4 |
| 10 | 300 | 18.85 | 8.5 | 1.56 |
| 20 | 300 | 40.10 | 8.5 | 0.78 |
| 30 | 300 | 64.57 | 8.5 | 0.51 |
| 40 | 300 | 95.09 | 8.5 | 0.39 |

Table 2. The simulated self-diffusion coefficient and thermal conductivity at 1 atm. The statistical error of the self-diffusion coefficient is less than 0.1%. The vibrational heat capacity is calculated by Equation (10) using the experimental data in [25]. The statistical error of the thermal conductivity $\lambda_{MD}$ is less than 1.0%. The deviations are determined by $|\lambda_{all,MD} - \lambda_{all,\exp.}|/\lambda_{all,\exp.} \times 100\%$.

| T (K) | $\rho D \quad mg/m \cdot s$ | | Dev (%) | $C_{V,vib}$ $J/mol \cdot K$ | Conductivity $mW/m \cdot K$ | | | Dev (%) |
|---|---|---|---|---|---|---|---|---|
| | MD | Exp. [26] | | | $\lambda_{MD}$ | $\lambda_{all,MD}$ | $\lambda_{all,\exp.}$ [27] | |
| 300 | 20.61 | 21.52 | 4.19 | 8.126 | 12.7 | 16.5 | 16.8 | 1.79 |
| 400 | 27.32 | 27.79 | 1.70 | 12.24 | 17.0 | 24.6 | 25.1 | 1.99 |
| 500 | 33.50 | 33.36 | 0.42 | 15.53 | 20.7 | 32.6 | 33.5 | 2.69 |
| 600 | 39.22 | 38.69 | 1.37 | 18.23 | 24.4 | 40.6 | 41.6 | 2.40 |
| 700 | 44.26 | 43.26 | 2.32 | 20.47 | 28.2 | 48.8 | 49.3 | 1.01 |
| 800 | 49.05 | 47.80 | 2.63 | 22.34 | 30.8 | 55.7 | 56.7 | 1.76 |
| 900 | 53.59 | 52.09 | 2.87 | 23.91 | 33.1 | 62.2 | 63.8 | 2.51 |
| 1000 | 57.83 | 56.11 | 3.08 | 25.22 | 37.6 | 70.7 | 70.6 | 0.14 |

Table 3. The simulated self-diffusion coefficient and thermal conductivity at 300 K. The statistical error of the self-diffusion coefficient is less than 0.1%. The statistical error of the thermal conductivity $\lambda_{MD}$ is less than 1.2%. The deviations are determined by $|\lambda_{all,MD} - \lambda_{all,\exp.}|/\lambda_{all,\exp.} \times 100\%$.

| P (atm) | $\rho D \quad mg/m \cdot s$ MD results | Dev (%) | Conductivity $mW/m \cdot K$ | | | Dev (%) |
|---|---|---|---|---|---|---|
| | | | $\lambda_{MD}$ | $\lambda_{all,MD}$ | $\lambda_{all,\exp.}$ [25] | |
| 10 | 20.28 | 1.46 | 13.5 | 17.2 | 17.3 | 0.58 |
| 20 | 20.17 | 1.99 | 14.2 | 17.9 | 18.0 | 0.56 |
| 30 | 19.93 | 3.16 | 15.0 | 18.7 | 19.0 | 1.58 |
| 40 | 19.85 | 3.55 | 16.8 | 20.5 | 20.7 | 0.97 |

Table 4. The correction term $\rho DC_{V,vib}$ of the calculated thermal conductivity of supercritical $CO_2$ in [1]. $\lambda_{\mathrm{ND}}$ denotes the thermal conductivity calculated by Nieto-Draghi *et al.* based on the rigid-rotor assumption. $\lambda_{all,\mathrm{exp.}}$ denotes the experimental data of the thermal conductivity shown in TABLE III of [1]. The self-diffusion coefficient is obtained from [31].

| $\rho$ $kg/m^3$ | $\lambda_{\mathrm{ND}}$ $mW/m\cdot K$ | $\lambda_{all,\mathrm{exp.}}$ $mW/m\cdot K$ | Dev. (%) | $D$ $m^2/s$ | $\rho DC_{V,vib}$ $mW/m\cdot K$ | $\lambda_{all,corrected}$ $mW/m\cdot K$ | Dev. (%) (corrected) |
|---|---|---|---|---|---|---|---|
| 300 | 30.0 | 42.6 | 30 | $113\times10^{-9}$ | 11.3 | 41.3 | 3.3 |
| 800 | 86.3 | 94.4 | 9 | $28.5\times10^{-9}$ | 7.56 | 93.9 | 0.5 |

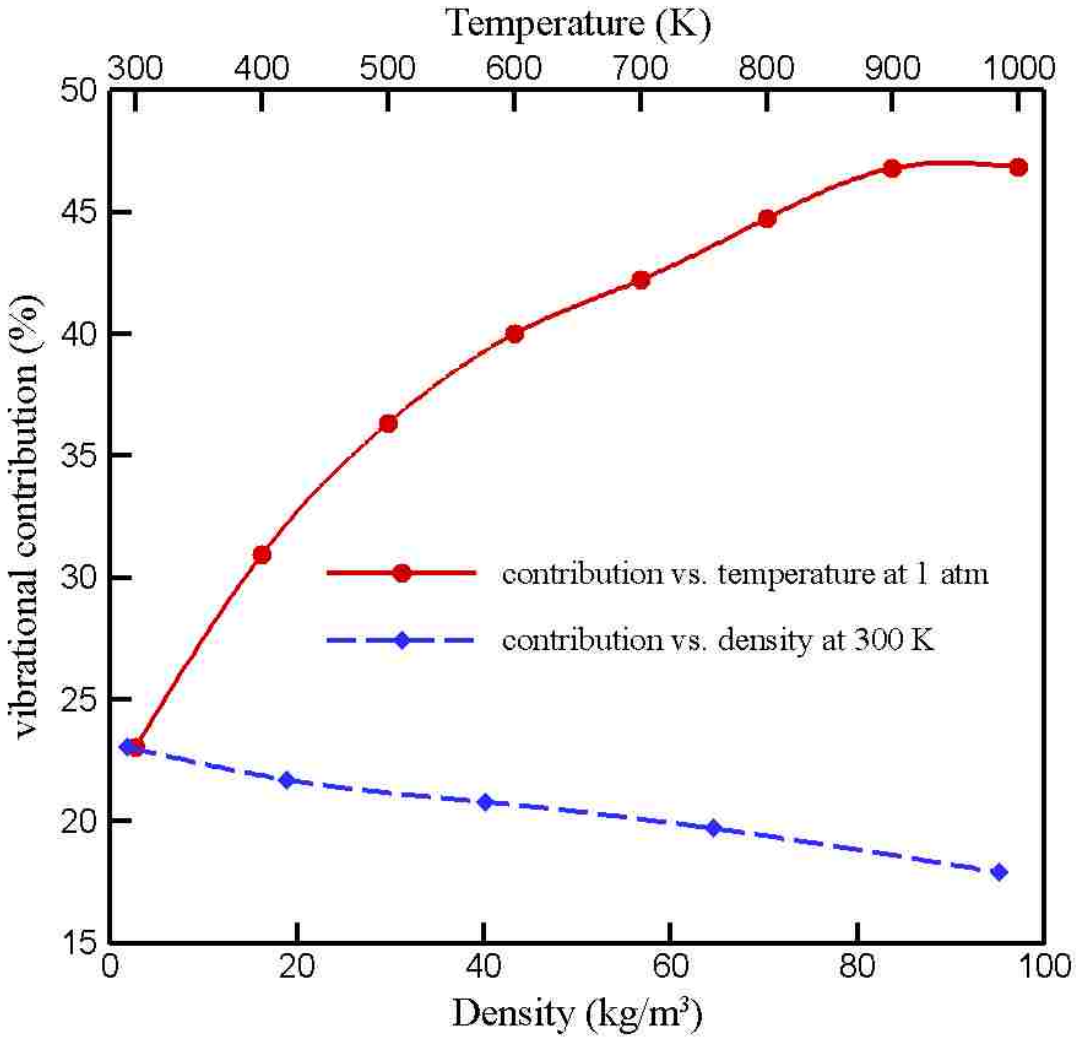


Figure 1. The vibrational contribution to the thermal conductivity as a function of temperature at 1 atm and as a function of density at 300 K.

# 5. Molecular dynamics simulations of self-diffusion coefficient and thermal conductivity of methane at low and moderate densities

Zhi Liang and Hai-Lung Tsai*

Department of Mechanical and Aerospace Engineering, Missouri University of Science and Technology, 400 W. 13th Street, Rolla, MO 65409, USA

**Abstract**

This article demonstrates a highly accurate molecular dynamics (MD) simulation of thermal conductivity of methane using an *ab initio* intermolecular potential. The quantum effects of the vibrational contribution to thermal conductivity are more efficiently accounted for in the present MD model by an analytical correction term as compared to by the Monte Carlo method. The average deviations between the calculated thermal conductivity and the experimental data are 0.92% for dilute methane and 1.29% for methane at moderate densities, as compared to approximately 20% or more in existing MD calculations. The results demonstrate the importance of considering vibrational contribution to the thermal conductivity which is mainly through the self-diffusion process.

*Keywords:* Methane; Molecular dynamics; Transport coefficients; Vibration

---

* Corresponding author. Tel.: +1 573 341 4945; fax: +1 573 341 4607.

*E-mail address:* tsai@mst.edu (H.L. Tsai).

## 1. Introduction

Methane is of specific importance in different fields ranging from its industrial application as a feed-gas for ultra-smooth diamond coating to its environmental impact as an important greenhouse gas. Moreover, it is the principal component of natural gas which is often described as the cleanest fossil fuel. Accurate knowledge of the transport properties of methane is therefore essential for the engineering design of chemical process and fluid transportation. Although the experimental data for transport properties of methane are available, they, especially the self-diffusion coefficient and thermal conductivity data, are of acceptable accuracy only around room temperature [1]. This work attempts to calculate the self-diffusion coefficient and thermal conductivity of methane in a wide range of temperature at dilute phase and in an intermediate dense phase by equilibrium MD simulations using an *ab initio* potential energy surface (PES) which was recently proposed by Hellmann *et al.* [2]. A quantum mechanical treatment of vibrational motions is employed in the MD model to improve the accuracy of the calculated thermal conductivity.

In addition to MD simulations, there also exist several other approaches for the calculation of transport properties from a known intermolecular potential. For example, the classical-trajectory (CT) method has been shown to be highly accurate in reproducing the transport and relaxation properties of simple molecular gases in a wide range of temperatures [1,3-5]. However, this method is restricted to the computation of transport properties in the dilute gas limit. For the calculation of transport properties at moderate and high densities, Rainwater-Friend [6,7] and modified Enskog theories [8,9] need to be used. The application of these theories must rely on the existence and accuracy of the

experimental transport property data because some scaling parameters used in these calculations are obtained by the best fit of the available experimental data [10,11]. On the other hand, MD simulations do not have such restrictions and are applicable at arbitrary densities and temperatures. If an accurate intermolecular PES is available and the simulation length is long enough, MD simulations have been demonstrated to be able to reproduce the thermophysical properties of a polyatomic fluid in a wide range of temperature and density with a high accuracy [12−14].

In MD simulations of methane fluids, the potential was often approximated by an isotropic Lennard-Jones (LJ) type function in which the two adjustable parameters were fitted to experimental data [15,16]. The spherical approximation of the methane molecule is an oversimplification for the calculation of transport properties, especially thermal conductivity. Using the approximation, it is not surprising that the deviations of the calculated thermal conductivity from the experimental data reached 20% in dense phase [15] and up to 55% in more dilute ones [16]. In order to calculate the thermal conductivity of methane accurately, therefore, an anisotropic PES should be employed to take into account exchange of energy between translational and internal modes of motion. In MD simulations, a classical treatment of translational and rotational motions is normally valid, which, however, may not be true for vibrational motions. The methane molecule has nine vibrational modes with the lowest vibrational frequency of 1306 $cm^{-1}$ [17]. The high vibrational frequency implies that the classical treatment of methane vibrations is not only inefficient, but also inappropriate due to the strong quantum effects at simulation temperatures. On the other hand, the negligence of vibrational motions in the MD simulation could cause a significant underestimate of thermal conductivity

[14,18]. Therefore, a quantum treatment of molecular vibrations is necessary in the MD model. Since the exchange of vibrational and other kinetic energy caused by collisions is rare, it is assumed in this work that there is no exchange of energy between vibrational and other modes of motion. Accordingly, the methane molecule is considered as a rigid rotor and the molecular structure is assumed to be unaffected by the vibrational state of the molecule and the interaction between molecules. Hence, the influence of molecular vibrations on the transport of mass is neglected in this work. The transport of energy by vibrational excited molecules, on the contrary, cannot be neglected and is accounted for by a correction term [14] based on the assumption that the vibrational energy mainly contributes to the thermal conductivity through self-diffusion processes. Therefore, the calculation of the self-diffusion coefficient is correlated with that of the thermal conductivity in this work. The calculation method is more efficient than the previously proposed Monte Carlo method [12,13] which involves the average of autocorrelation functions corresponding to thousands of initial vibrational energy distributions. The accuracy of the calculation method is examined by comparing the simulation results with experimental data whenever possible.

## 2. Intermolecular potential

As methane is the simplest alkane and suitable for very accurate *ab initio* calculations, it has attracted many theoretical studies on the interaction potential for methane pair in the past decades. The two most recent *ab initio* PES for the methane dimer are proposed by Hellmann *et al.* [2] and Chao *et al.* [19]. Both these groups calculated the PES by the counterpoise-corrected supermolecular approach at the

CCSD(T) level of theory with the basis sets of aug-cc-pVTZ and aug-cc-pVQZ qualities. The calculated PES's were both extrapolated to the complete basis set. The major difference between the two PES's is that Hellmann *et al.* introduced an isotropic correction term to include the effects of zero-point vibrations so that a more accurate PES is obtained. Compared with Chao *et al.*'s potential, the global minimum of Hellmann *et al.*'s potential is deeper by about 50 K. Hellmann *et al.* used a nine-site potential function to fit the *ab initio* potential data. The potential function was validated against the experimental second pressure virial coefficient data. Chao *et al.* used a four-site Lennard-Jones (LJ) potential function to fit the calculated potential data. Although the expression of Chao *et al.*'s potential is much simpler, the fitting errors are relatively large. In MD simulations, we use the PES proposed by Hellmann *et al.*

Hellmann *et al.*'s potential assumes the methane molecule as a rigid rotor with the C-H bonds fixed at the experimental zero-point vibrationally averaged value of 1.099 Å. The bond angles of $CH_4$ were established to give a regular tetrahedron and each molecule contains 9 sites. Hence, each pair interaction contains 81 site-site contributions. The partial charges were assigned to the denoted C and H sites to reproduce the octupole moment of the methane monomer obtained from *ab initio* calculations. The total potential which includes a correction for zero-point vibrational effects is given by Eq. (1).

$$U_{ij} = \sum_{a\in i}\sum_{b\in j}\left[ A_{ab}\exp(-\alpha_{ab}r_{ab}) + \frac{q_a q_b}{r_{ab}} - f_6(\beta_{ab}r_{ab})\frac{C_{6ab}}{r_{ab}^6} - f_8(\beta_{ab}r_{ab})\frac{C_{8ab}}{r_{ab}^8}\right] - f_6(\beta_{corr}r_{ab})\frac{\Delta C_6}{r_{ij}^6} - f_8(\beta_{corr}r_{ab})\frac{\Delta C_{8,iso}}{r_{ij}^8}, \quad (1)$$

where $f_n(x) = 1 - e^{-x}\sum_{k=0}^{n}\frac{x^k}{k!}$ . (2)

Here, sites *a* belong to molecule *i*, sites *b* belong to molecule *j*, $r_{ab}$ is the distance between *a* and *b*, and $r_{ij}$ is the distance between centers of mass of two molecules. Parameters $A_{ab}$, $\alpha_{ab}$, $\beta_{ab}$, $q_a$, $C_n^{ab}$, $\beta_{corr}$, $\Delta C_6$ and $\Delta C_{8,iso}$ are given in Ref. [2]. Figure 1 depicts the anisotropy of Hellmann *et al.*'s potential. Since the methane molecule is modeled as a rigid rotor, the dipole moment of methane is exactly zero at each time step in the simulation. Therefore, it is not necessary to use the reaction field method [20] to account for the long-range electrostatic interactions. In fact, the first nonvanishing electrostatic interaction for a methane dimer is the octupole-octupole interaction, which decays as $r^{-7}$ at a large intermolecular separation. In the application, the cut-off radius, within which all pair interactions are calculated, is chosen to be 14 Å.

**3. Theory**

The influence of vibrational motions is neglected in the calculation of self-diffusion coefficient. Hence, the self-diffusion coefficient is calculated directly from the Green-Kubo (GK) formulas [21,22]. The accurate determination of self-diffusion coefficient is important in this work because it will be used in calculating the vibrational contribution to the thermal conductivity. The self-diffusion coefficient $D$ is given by [23]

$$D = \tfrac{1}{3}\int_0^\infty dt \left\langle \vec{v}_i(t)\cdot\vec{v}_i(0)\right\rangle, \tag{3}$$

where $\vec{v}_i$ is the translational velocity of molecule *i*, *t* is the time, and $\langle\cdots\rangle$ denotes the ensemble average.

Due to the strong quantum effects, vibrational motions are not directly taken into account in classical MD simulations. As a result, the vibrational energy is not included in

the GK formula. The thermal conductivity $\lambda_{T,0}$ which does not include the vibrational contribution is calculated by [24]

$$\lambda_{T,0} = \frac{V}{k_B T^2} \int_0^\infty dt \left\langle J_\alpha \;\; t \;\; J_\alpha \;\; 0 \right\rangle . \tag{4}$$

Here, $J_\alpha$ is a component of the energy current which does not take into account the quantized vibrational energies, $V$ is the volume of the system, $k_B$ is the Boltzmann constant and $T$ is the average temperature of the system. Using the rigid-rotor assumption, the expression for the energy current $J_\alpha$ which contains the contributions from translational energy, rotational energy and molecular interactions is given by [25]

$$\begin{aligned} J_\alpha = & \frac{1}{V} \sum_i v_{i\alpha} \left( \tfrac{1}{2} m \vec{v}_i^{\,2} + \tfrac{1}{2} \vec{\omega}_i \mathbf{I}_i \vec{\omega}_i + \tfrac{1}{2} \sum_{j \neq i} U_{ij} \right) \\ & + \frac{1}{V} \sum_i \sum_{j>i} r_{ij_\alpha} \;\; \tfrac{1}{2} \;\; \vec{v}_i + \vec{v}_j \;\; \cdot \vec{f}_{ij} + \tfrac{1}{2} \;\; \vec{\omega}_i \cdot \vec{\Gamma}_{ij} - \vec{\omega}_j \cdot \vec{\Gamma}_{ji} \end{aligned} , \tag{5}$$

where $\vec{\omega}_i$ and $\mathbf{I}_i$ are, respectively, the angular velocity and the matrix of moments of inertia for molecule *i*, $m$ represents the mass of the methane molecule. $r_{ij}$ and $f_{ij}$ denote, respectively, the intermolecular distance and force. $U_{ij}$ and $\vec{\Gamma}_{ij}$ are, respectively, the intermolecular potential energy between molecule *i* and molecule *j* and the torque acting on molecule *i* due to the interaction between molecule *i* and molecule *j*.

The energy current varies with time due to the interaction between molecules. Since collisions resulting in the exchange of vibrational and other kinetic energy are rare, the quantized vibrational energy is considered as frozen in the molecule and only contributes to the thermal conductivity by diffusion. Hence, the vibrational contribution to thermal

conductivity is calculated separately in this work. The thermal conductivity $\lambda_T$ which includes the vibrational contribution is given by [14]

$$\lambda_T = \lambda_{T,0} + \rho D C_{V,vib}, \tag{6}$$

where $\rho$ is the density of the system and $C_{V,vib}$ is the isochoric vibrational heat capacity. The quantum effects of the molecular vibrations are included by $C_{V,vib}$ which can be normally calculated using the quantum harmonic approximation [24]. It is notable that Eq. (6) is similar to the modified Eucken formula [11] which is used for the estimation of thermal conductivity of dilute gas

$$\lambda_T = \frac{15k_B}{4m}\eta + \rho D C_{V,\mathrm{int}}. \tag{7}$$

In Eq. (7), the first term on the right side represents the translational contribution to thermal conductivity, and the second term represents the contribution from the internal modes of motion, $C_{V,\mathrm{int}}$ is the contribution to the isochoric heat capacity from internal modes of motion. In this work, $C_{V,\mathrm{int}} = C_{V,vib} + 1.5R$ where $R$ is the gas constant. The major difference between the modified Eucken formula and Eq. (6) is that the modified Eucken formula assumes that there is no exchange of energy between the translational and internal modes of motion, whereas energy exchange between translational and rotational motion is taken into account in Eq. (6) by MD simulations. In the case of dilute methane gas, the self-diffusion coefficient $D$ is available through MD calculations and very accurate experimental shear viscosity $\eta$ data exist. Therefore, the accuracy of the modified Eucken formula, i.e. Eq. (7), and Eq. (6) for the calculation of thermal conductivity of dilute methane gas can be both examined by comparing the calculated

results with the experimental thermal conductivity data. As the fluid density increases, it is unlikely to neglect exchange of energy between the translational and rotational energies. Hence, the modified Eucken formula, Eq. (7), is not applicable to dense fluids. In this case, the thermal conductivity is calculated by Eq. (6) and compared with experimental data to examine if the decoupling between vibrations and other degrees of freedom is also valid for a moderately dense methane fluid.

## 4. Simulation details and results

### 4.1. Simulation details

Two sets of simulations of the self-diffusion coefficient and thermal conductivity of methane are carried out in the microcanonical ensemble. In the first set of simulations, the pressure of methane gas is fixed at 1 atm and the temperature varies from 200 K to 900 K. The density of the methane is determined from the ideal gas law. In the second set of simulations, the temperature is fixed at 200 K or 300 K and the density varies from 0 to 5 mol/L. For a given temperature and density, the number of molecules included in a cubic simulation box is 1024 for densities lower than 1 mol/L and 512 for higher densities. The coordinates of the center of mass and the orientations of the molecules are both initialized randomly inside the simulation box with periodic boundary conditions. The minimum distance between any two molecules is set to be greater than 6 Å to avoid unrealistic large potentials and forces. The translational and angular velocities are both initialized by the Maxwell-Boltzmann relation at the given temperature. The equations of molecular translational and rotational motions are integrated by the Verlet leap-frog algorithm and the quaternion algorithm [23], respectively. Berendsen *et al*.'s algorithm

[26] is applied to equilibrate the system to the desired temperature with a time constant of 2.0 ps. Using these settings, the system can be well equilibrated within 50 ps at all simulated state points. After the system is equilibrated and reaches the desired total energy corresponding to the given temperature and density, the thermostat is turned off and the transport properties are calculated in the constant-NVE ensemble. A step size of 2.5 fs is chosen for dilute gases of which the temperature is lower than 600 K. For moderately dense fluids and dilute gases with higher temperatures, the step size is chosen as 2 fs. The time step size is chosen such that the total energy of the system is always kept constant within 2 parts in $10^4$.

In order to obtain the thermal conductivity with a low statistical error (~1%) from the MD simulation, it is necessary to carry out a very long simulation length. For dilute gases at 1 atm, the total simulation length is increased from 3 μs at 200 K to 6 μs at 900 K. For moderately dense fluids, the total simulation length is decreased from 240 ns at 1 mol/L to 40 ns at 5 mol/L. With such long simulation lengths, the statistical error of the calculated self-diffusion coefficient can be reduced to less than 0.1% by additional averaging all the molecules in the system. Since the *ab initio* potential employed in this work is a nine-site potential model with a complex analytical expression for each site-site interaction, the total computational cost is very high. To save the computational time, the long simulation is divided into hundreds of shorter parallel runs which are independently initialized and equilibrated at the given temperature and density. The statistical error is estimated by Fincham's block averaging method [27].

4.2. Simulation results of dilute gases

The calculated self-diffusion coefficients comparing with the values extrapolated to the dilute gas limit [1] from the density-dependent experimental data measured by Dawson *et al.* [28] and Oosting and Trappeniers [29] are shown in Table 1. The uncertainties of the experimental data were estimated to be ±6% [28] and ±2% [29]. Due to the difficulties of the measurements, the experimental self-diffusion coefficient data at temperatures higher than 350 K are scarce or nonexistent. Comparing with the available experimental data at 200 K and 300 K, the deviations of MD simulation results are generally within the experimental uncertainties. However, the deviation between the simulated self-diffusion coefficient and Oosting and Trappeniers' data [29] at 200 K is greater than the experimental uncertainty. We compared our MD simulation results with those calculated from CT method [1] in which the same intermolecular PES was used and the methane molecule was also treated as a rigid rotor. As is shown in Table 1, very good agreement is found at all simulation temperatures. The CT method has been proved to be very accurate in reproducing transport properties of dilute gases [4,5,30,31]. Therefore, the deviations found in Table 1 should not be attributed to the MD simulation method or the GK formula used in the calculation of self-diffusion coefficient. A better prediction of the self-diffusion coefficient may require a more accurate intermolecular potential.

In Table 1, the MD simulation results of the thermal conductivity of dilute methane gases are compared with the experimental data [32,33], results from CT method [3] and modified Eucken formula. For temperatures lower than 600 K, the experimental results are obtained from the correlation provided by NIST [32] with the uncertainty estimated to be ±2.5%. At higher temperatures, the experimental data are from Assael *et*

*al.* [33] with the uncertainty estimated to be ±4%. In Table 1, $\lambda_{T,0}$ is obtained directly from the integral of the time correlation function of energy current which does not include the vibrational energy. The statistical errors are less than 1%. It is evident that $\lambda_{T,0}$ significantly underestimates the thermal conductivity except at a very low temperature. The vibrational contribution $\rho D C_{V,vib}$ is then included to obtain $\lambda_T$ according to Eq. (6). In the calculation, the vibrational heat capacity $C_{V,vib}$ shown in Table 1 is calculated by Eq. (8).

$$C_{V,vib} = C_{V,\rho=0} - 3R \tag{8}$$

where $C_{V,\rho=0}$ represents the isochoric heat capacity at zero density. Since experimental data of $C_{V,\rho=0}$ at each simulation temperature are all available [32] and the uncertainty is within ±1%, $C_{V,vib}$ calculated from Eq. (8) is supposed to be more accurate than that calculated from quantum harmonic approximation. It can be seen from Table 1 that the calculated thermal conductivity $\lambda_T$ which includes the vibrational contribution agrees well with the experimental data. The ratio of the vibrational contribution to the total thermal conductivity increases from 0.8% at 200 K to 50% at 900 K. Hence, the vibrational contribution to the thermal conductivity of the dilute methane gas is non-negligible even at a temperature much lower than the lowest characteristic vibrational temperature (~ 1870 K) of methane.

To compare the accuracy of different calculation methods, the thermal conductivities calculated from CT method and the modified Eucken formula are also shown in Table 1. The shear viscosity used in the modified Eucken formula is obtained directly from the accurate experimental data [32,34]. The uncertainty of the experimental shear viscosity is

estimated to be ±0.2% around room temperature and ±1% at low and high temperatures. The thermal conductivity calculated from CT method is provided by Hellmann *et al.* [3]. For the aforementioned three calculation methods, the deviations between the calculated thermal conductivity and the experimental data [32,33] at each simulation temperature are shown in Fig. 2. It can be seen that both the MD calculation employed in the work and the CT method employed by Hellmann *et al.* predict the thermal conductivity within the experimental uncertainty. Using the following Eq. (9), the averaged absolute deviations (AAD) of the results from MD method and CT method are calculated to be 0.92% and 0.94%, respectively.

$$\mathrm{AAD} = \frac{1}{N_{data}} \sum_{i=1}^{N_{data}} \left| \frac{\text{calculated result at state point } i}{\text{experimental data at state point } i} - 1 \right| \times 100\% \tag{9}$$

where $N_{data}$ means the number of data points. Therefore, the MD method is as accurate as CT method in calculating the thermal conductivity. The good agreement with experimental data indicates the assumption that the vibrations mainly contribute to thermal conductivity through self-diffusion processes is valid in a dilute gas.

As shown in Fig. 2, the modified Eucken formula is not able to predict the thermal conductivity within the experimental uncertainty if the temperature is lower than 500 K. At relatively low temperatures, the vibrational contribution to the thermal conductivity is small. The large deviations are, therefore, mainly caused by neglecting the exchange of energy between translational and rotational motions. The MD calculation with an anisotropic intermolecular potential takes into account this kind of energy exchange, hence gives much better results. Nevertheless, the modified Eucken formula predicts reasonable thermal conductivities if the temperature is higher than 600 K. The results

indicate that the exchange of energy between translational and internal modes of motion might become negligible for dilute gases at high temperatures so that both rotational and vibrational motions contribute to the thermal conductivity mainly through self-diffusion processes.

## 4.3 Simulation results at moderate densities

The MD simulation results of self-diffusion coefficients of moderately dense methane at 200 K and 300 K are shown in Fig. 3. The experimental data are obtained from Dawson [35] who measured the density dependence of the self-diffusion coefficient of methane from 154 K to 354 K. The uncertainty was estimated to be ±4.5% and is depicted by dashed lines in Fig. 3. The statistical error of the calculated self-diffusion coefficient is about 0.1% which is less than the size of symbols in Fig. 3. At 300 K, the deviations between the calculated and experimental results are within the experimental uncertainty. The AAD between the MD results and experimental data is 1.21%. At 200 K, however, the calculated results only agree with the experimental data at densities lower than 3 mol/L. At higher densities, the deviations reached 4.55% and 5.25% which are higher than the experimental uncertainty. The vibrational energies of methane are rarely excited at 200 K. Hence, the disagreement should not be attributed to the decoupling between the vibrations and other degrees of freedom in the MD model. The relatively large deviations at higher densities may come from the neglect of three-body effects in the pair potential employed in the calculation. To obtain better results at high densities, therefore, non-additive terms which account for three-body effects must be included in addition.

Figure 4 depicts the calculated thermal conductivity and the experimental data [32] as a function of density at 200 K and 300 K. The uncertainty of the experimental data provided by NIST [32] was estimated to be ±2% and is depicted by dashed lines in Fig. 4. The statistical error of the calculated thermal conductivity is about 0.9% which is smaller than the size of symbol shown in Fig. 4. Without the vibrational correction term, the MD results underestimate the thermal conductivity at both temperatures. The AADs between the calculated thermal conductivity without the vibrational correction term and the experimental data at 200 K and 300 K are 1.54% and 7.36%, respectively. It is evident, especially at 300 K, that the accuracy of the calculation results is greatly improved when the vibrational correction term $\rho DC_{V,vib}$ is included. With the correction term, the AADs at 200 K and 300 K are 1.05% and 1.53%, respectively. The calculated thermal conductivity at both temperatures has generally a good agreement with the experimental data. Although the MD results underestimate the self-diffusion coefficient of methane at relatively high densities at 200 K, the underestimation has little effects on the calculated thermal conductivity because the vibrational contribution to the thermal conductivity at 200 K is negligible. Nevertheless, it is found at both temperatures that the calculated thermal conductivity always slightly underestimates the experimental data at moderate densities even when the vibrational contribution is included. The small deviations might come from the neglect of the exchange of energy between vibrations and other modes of motions. As is discussed in the self-diffusion results, however, the vibrational energy of methane at 200 K is negligible. It is more possible that the underestimations are caused by the neglect of three-body effects in the pair potential. Therefore, in order to extend the calculation to more dense methane fluids or test the accuracy of the MD calculation

method in calculating self-diffusion coefficient and thermal conductivity of methane at high densities, Hellmann *et al.*'s potential should be employed with a correction term to account for three-body effects. The determination of an accurate potential that includes the three-body effects needs further investigations.

## 5. Conclusions

MD simulations of the self-diffusion coefficient and thermal conductivity of methane are performed in a wide range of temperature at dilute phase and in an intermediate dense phase. At the simulated state points, the experimental data of the two transport properties of interest are of relatively low accuracy or nonexistent. By comparing the MD simulation results with the available experimental data, it is found that the decoupling between vibrations and other degrees of freedom of methane is appropriate in a dilute or intermediate dense phase. On the other hand, the exchange of energy between translational and rotational motions cannot be neglected even in a dilute gas. The vibrational energies are proved to contribute to the thermal conductivity mainly through self-diffusion processes. The correction term $\rho D C_{V,vib}$ is able to nicely account for the vibrational contribution which is shown to be significant in the total thermal conductivity of methane at both low and intermediate densities. In order to obtain better results or extend the MD simulation to methane fluids at higher densities, the *ab initio* pair potential employed in this work needs some improvement to incorporate the three-body effects.

*List of symbols*

| | |
|---|---|
| $a$ | interaction site index |
| AAD | averaged absolute deviations |
| $b$ | interaction site index |
| $C_{V,vib}$ | vibrational heat capacity |
| $C_{V,\text{int}}$ | the contribution to the isochoric heat capacity from internal modes of motion |
| $C_{V,\rho=0}$ | the isochoric heat capacity at zero density |
| $D$ | self-diffusion coefficient |
| I | the matrix of moments of inertia |
| $J_\alpha$ | a component of the energy current |
| $k_B$ | Boltzmann constant |
| $m$ | the mass of molecule |
| $N_{data}$ | the number of data points |
| $q_a$ | partial charge on interaction site $a$ |
| $q_b$ | partial charge on interaction site $b$ |
| $r_{ab}$ | distance between interaction site $a$ and $b$ |
| $r_{ij_\alpha}$ | a component of the distance vector from the molecule $j$ to $i$ |
| $R$ | gas constant |
| $t$ | time |
| $T$ | temperature |
| $U_{ij}$ | intermolecular potential |
| $\vec{v}_i$ | translational velocity of molecule $i$ |
| $v_{i\alpha}$ | a component of translational velocity of molecule $i$ |
| $V$ | volume |

*Greek letters*

| | |
|---|---|
| $\vec{\Gamma}_{ij}$ | torque acting on molecule $i$ due to the interaction between molecule $i$ and molecule $j$ |
| $\eta$ | shear viscosity |
| $\lambda_{T,0}$ | thermal conductivity that does not include the vibrational contribution |
| $\lambda_T$ | thermal conductivity that includes the vibrational contribution |
| $\rho$ | density |
| $\vec{\omega}_i$ | angular velocity of molecule |

**Acknowledgements**

This work was supported by Office of Naval Research through the Multidisciplinary University Research Initiative (MURI) program, Award No. N00014-05-1-0432.

**References**

[1] R. Hellmann, E. Bich, E. Vogel, A.S. Dickinson, V. Vesovic, J. Chem. Phys. 129 (2008) 064302.

[2] R. Hellmann, E. Bich, E. Vogel, J. Chem. Phys. 128 (2008) 214303.

[3] R. Hellmann, E. Bich, E. Vogel, A.S. Dickinson, V. Vesovic, J. Chem. Phys. 130 (2008) 124309.

[4] S. Bock, E. Bich, E. Vogel, A.S. Dickinson, V. Vesovic, J. Chem. Phys. 117 (2002) 2151-2160.

[5] S. Bock, E. Bich, E. Vogel, A.S. Dickinson, V. Vesovic, J. Chem. Phys. 120 (2004) 7987-7997.

[6] D.G. Friend, J.C. Rainwater, Chem. Phys. Lett. 107 (1984) 590-594.

[7] J.C. Rainwater, D.G. Friend, Phys. Rev. A 36 (1987) 4062-4066.

[8] H.J.M. Hanley, R.D. McCarty, E.G.D. Cohen, Physica 60 (1972) 322-356.

[9] B. Najafi, R. Araghi, J.C. Rainwater, S. Alavi, R.F. Snider, Physica A 275 (2000) 48-69.

[10] H. Behnejad, A. Pedram, Chem. Phys. 325 (2006) 351-358.

[11] J. Millat, J.H. Dymond, C.A. Nieto de Castro, Transport Properties of Fluids, Cambridge University Press, New York, 1996 (Chapter 5, 4).

[12] Z. Liang, H.L. Tsai, Mol. Phys. (In press, DOI: 10.1080/00268970902776740).

[13] Z. Liang, H.L. Tsai, Fluid Phase Equilibr. (DOI: 10.1016/j.fluid.2010.03.007).

[14] Z. Liang, H.L. Tsai, Mol. Phys. (accepted).

[15] G.A. Fernandez, J. Vrabec, H. Hasse, Fluid Phase Equilibr. 221 (2004) 157-163.

[16] M. Bugel, G. Galliero, Chem. Phys. 352 (2008) 249-257.

[17] T. Shimanouchi, Natl. Stand. Ref. Data Ser. Natl. Bur. Stand. (U.S.) 39 (1972).

[18] C. Nieto-Draghi, T. de Bruin, J. Perez-Pellitero, J.B. Avalos, A.D. Mackie, J. Chem. Phys. 126 (2007) 064509.

[19] S.W. Chao, A. H. Li, S.D. Chao, J. Comput. Chem. 30 (2009) 1839-1849.

[20] M. Neuman, J. Chem. Phys. 85 (1986) 1567-1580.

[21] M.S. Green, Phys. Rev. 119 (1960) 829-830.

[22] R. Kubo, J. Phys. Soci. Japan 12 (1957) 570-586.

[23] M.P. Allen, D.J. Tildesley, Computer Simulation of Liquids, Clarendon, Oxford, 2000 (Chapter 2, 3).

[24] D.A. McQuarrie, Statistical Mechanics, University Science Books, Sausalito, 2000 (Chapter 21, 8).

[25] D.J. Evans, W.B. Streett, Mol. Phys. 36 (1978) 161-176.

[26] H.J.C. Berendsen, J.P.M. Postma, W.F. Van Gunsteren, A. DiNola, J.R. Haak, J. Chem. Phys. 81 (1984) 3684-3690.

[27] D. Fincham, N. Quirke, D.J. Tildesley, J. Chem. Phys. 84 (1986) 4535-4546.

[28] R. Dawson, F. Khoury, R. Kobayashi, AIchE J. 16 (1970) 725-729.

[29] P.H. Oosting, N.J. Trappeniers, Physica 51 (1971) 418-431.

[30] E.L. Heck, A.S. Dickinson, Mol. Phys. 81 (1994) 1325-1352.

[31] E.L. Heck, A.S. Dickinson, V. Vesovic, Mol. Phys. 83 (1994) 907-932.

[32] P.J. Linstrom, W.G. Mallard, National Institute of Standards and Technology, Gaithersburg MD, 20899, http://webbook.nist.gov, (retrieved January 10, 2010).

[33] M.J. Assael, J. Millat, V. Vesovic, W.A. Wakeham, J. Phys. Chem. Ref. Data 19 (1990) 1137-1147.

[34] R.D. Trengove, W.A. Wakeham, J. Phys. Chem. Ref. Data 16 (1987) 175-187.

[35] R. Dawson, Self-diffusion in Methane, Ph. D. thesis, Rice University, 1966, (page 104).

Table 1. Thermophysical properties of methane at 1 atm. The statistical error of self-diffusion coefficient is less than 0.1%. The statistical error of thermal conductivity is less than 1%.

| T (K) | $\rho D \quad mg/m\cdot s$ | | | $\eta$ $\mu Pa\cdot s$ | $C_{V,vib}$ $J/mol\cdot K$ | $\lambda_T \quad mW/m\cdot K$ | | | | |
|---|---|---|---|---|---|---|---|---|---|---|
| | MD | Exp. | CT | Exp. [32,34] | Exp. [32] | MD $\lambda_{T,0}$ | MD $\lambda_T$ | Exp. [32,33] | CT | Modified Eucken |
| 200 | 10.50 | 10.48 [28], 10.16 [29] | 10.53 | 7.81 | 0.257 | 21.62 | 21.79 | 21.94 | 21.75 | 23.50 |
| 300 | 15.25 | 14.99 [28], 15.29 [29] | 15.25 | 11.25 | 2.521 | 32.35 | 34.75 | 34.55 | 34.36 | 36.14 |
| 400 | 19.37 | - | 19.36 | 14.27 | 7.351 | 41.16 | 50.03 | 50.13 | 50.04 | 51.70 |
| 500 | 23.07 | - | 23.04 | 16.98 | 13.25 | 49.83 | 68.90 | 68.56 | 68.45 | 70.04 |
| 600 | 26.45 | - | 26.42 | 19.43 | 19.24 | 56.38 | 88.13 | 88.92 | 88.62 | 90.11 |
| 700 | 29.58 | - | 29.56 | 21.63 | 25.35 | 67.12 | 113.9 | 112.1 | 109.9 | 112.1 |
| 800 | 32.61 | - | 32.52 | 23.71 | 30.83 | 73.74 | 136.5 | 134.3 | 131.8 | 134.6 |
| 900 | 35.45 | - | 35.35 | 25.71 | 35.89 | 79.55 | 158.9 | 156.6 | 154.1 | 157.5 |

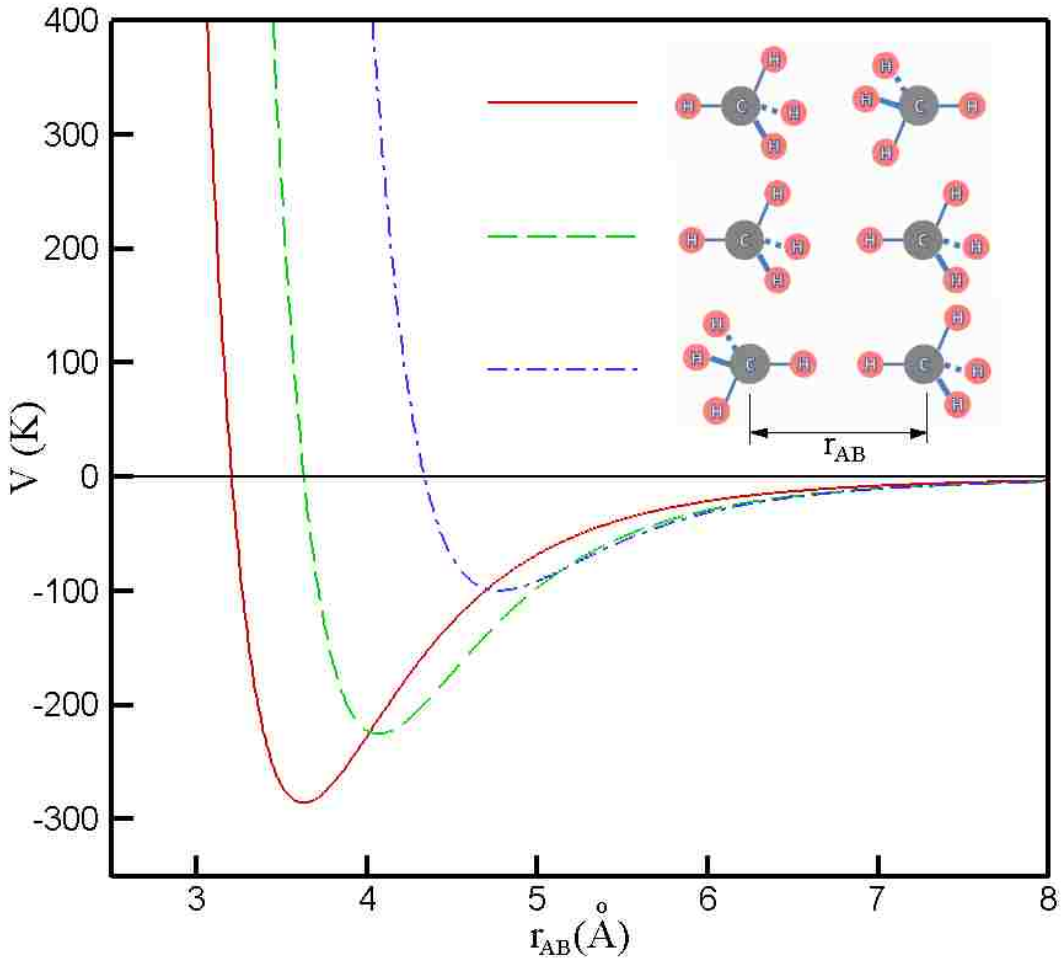


Fig. 1. Hellmann *et al.*'s potential as a function of the center of mass separation for different angular orientations.

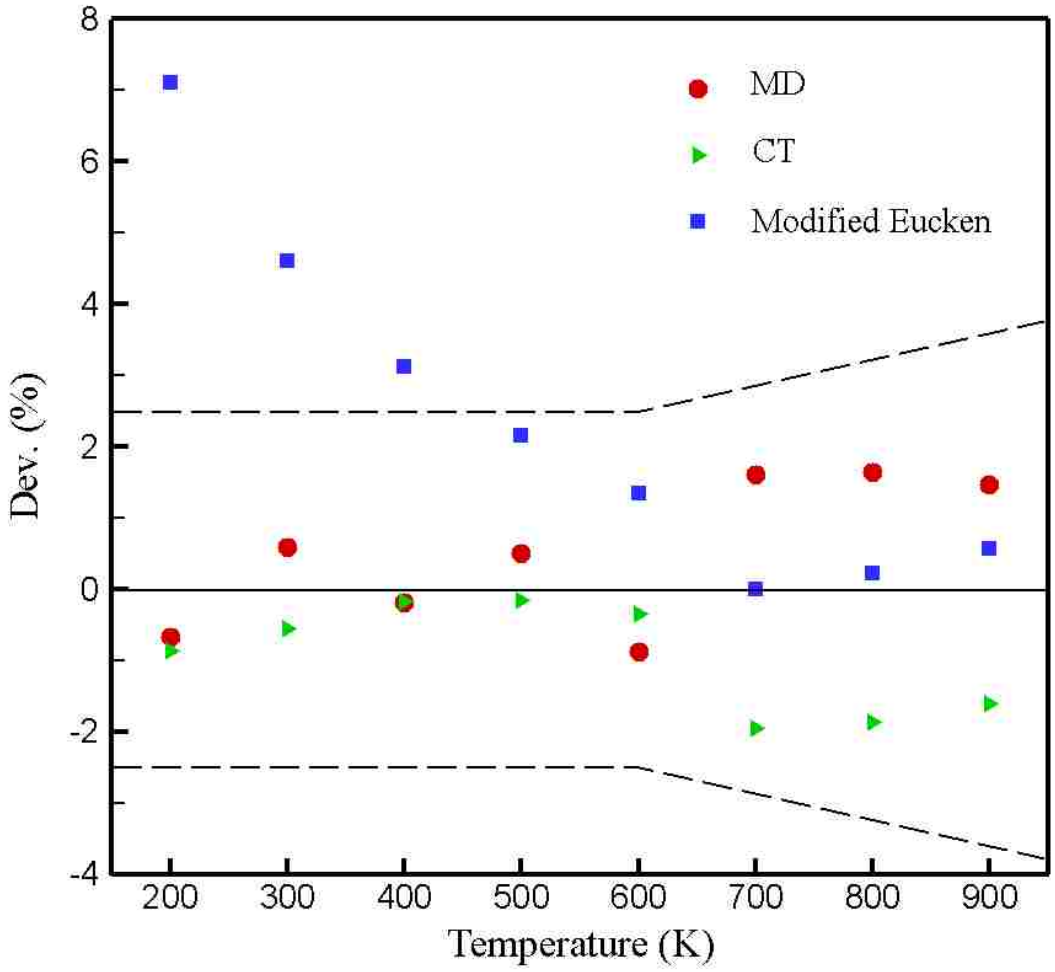


Fig. 2. The deviations between the calculated thermal conductivity and experimental data of dilute methane gases. The dashed lines show the uncertainties of the experimental data. Dev.% = $\lambda_{T,cal.}/\lambda_{T,\exp.} - 1 \times 100\%$

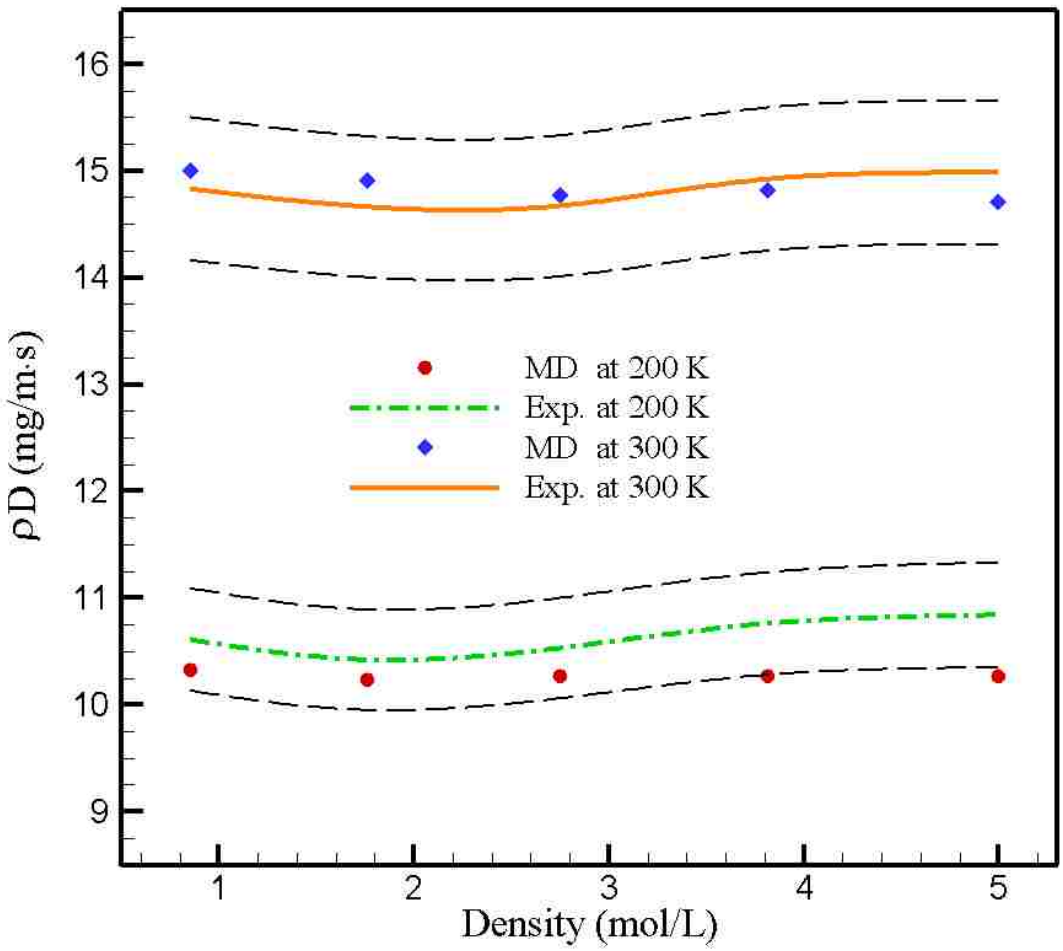


Fig. 3. The product $\rho D$ as a function of density at 200 K or 300 K. The dashed lines show the uncertainties of the experimental data. The statistical errors are smaller than the size of the symbols.

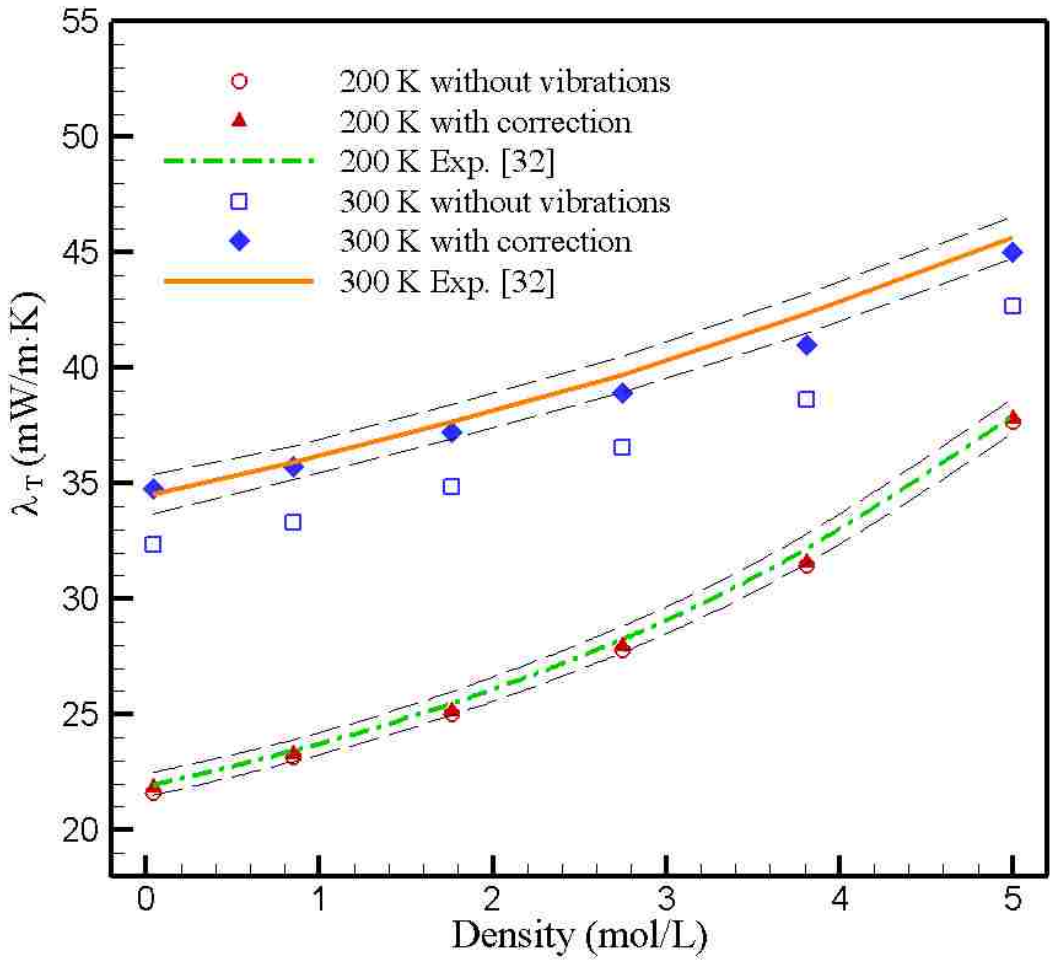


Fig. 4. The thermal conductivity as a function of density at 200 K or 300 K. The dashed lines show the uncertainties of the experimental data. The statistical errors are smaller than the size of the symbols.

# SECTION

# 2. CONCLUSIONS

It is shown in this dissertation that the DFT method is able to predict an excellent $CO_2$ geometry and fairly good vibrational energy eigen values and transition dipole moments. The high efficiency of the *ab initio* method developed in this work makes it applicable to larger and more complicated molecules. Based on the *ab initio* calculation results of the single-molecule properties and the pair potential, the thermophysical properties of $CO_2$ at low and intermediate densities can be accurately reproduced without using any experimental data. For fluids at high densities where the three-body effects become non-negligible, however, the parameters in the pair potential needs to be adjusted to fit the experimental pure substance vapor-liquid equilibrium data since an accurate determination of an effective polyatomic pair potential which includes the three-body effects is so far computational prohibitive. It is found that the molecular vibrations can be considered constrained in the molecule if the simulation temperature is lower than the characteristic temperature of the vibrational mode. The influence of the vibrations to the transport of mass and momentum in a polyatomic fluid is negligible, whereas the vibrational contribution to the thermal conductivity of a polyatomic fluid is important. The vibrations are found to contribute to the thermal conductivity mainly through self-diffusion processes. The deviations between the calculated thermophysical properties and the experimental data at all simulated state points are generally within the experimental uncertainty. It is shown the calculation methods can be extended to calculate

thermophysical properties of other polyatomic fluids such as methane of which the experimental data is of acceptable accuracy only around the room temperature.

# BIBLIOGRAPHY


[1] Z. Wang, M. Gong, Y. Zhang, E. Feng, and Z. Cui, Chem. Phys. Lett. **454**, 7 (2008).

[2] C. Leonard, M. Diehr, P. Rosmus, and W.C. Maguire, JQSRT. **109**, 535 (2008).

[3] Z.G. Huang, E. C. Yang, and D.Q. Xie Chin. Chem. Lett., **article in press**, (2008).

[4] T. Stoecklin and A. Voronin, Chem. Phys. **331**, 385 (2007).

[5] K.A. Peterson and G.C. McBane, J. Chem. Phys. **123**, 084314 (2005).

[6] U. Lourderaj, N. Sathyamurthy, Chem. Phys. **308**, 277 (2005).

[7] R. Tarroni, Mol. Phys. **102**, 2167 (2004).

[8] J. Noga and R.J. Bartlett, J. Chem. Phys. **86**, 7041(1987).

[9] P.E. Bl¨ochl, Phys. Rev. B **50**, 17953 (1994).

[10] T. Pang, "An introduction to computational physics," (2006).

[11] M.S. Green, J. Chem. Phys. 19, 1036 (1951).

[12] M.S. Green, Phys. Rev. 119, 829 (1960).

[13] R. Kubo, J. Phys. Soc. Jpn. 12, 570 (1957).

[14] B.J. Alder, D.M. Gass, and T.E. Wainwright, J. Chem. Phys. 53, 3813 (1970).

[15] D. Levesque, L. Verlet, and J. Kürkijarvi, Phys. Rev. A 7, 1690 (1973).

[16] M. Schoen and C. Hoheisel, Mol. Phys. 56, 653 (1985).

[17] H. Stassen and W.A. Steele, J. Chem. Phys. 102, 932 (1995).

[18] K. Meier, A. Laesecke, and S. Kabelac, J. Chem. Phys. 121, 3671 (2004).

[19] K. Meier, A. Laesecke, and S. Kabelac, J. Chem. Phys. 121, 9526 (2004).

[20] K. Meier, A. Laesecke, and S. Kabelac, J. Chem. Phys. 122, 014513 (2004).

[21] K. Meier, “Computer Simulation and Interpretation of the Transport Coefficients of the Lennard-Jones Model Fluid”, Ph. D. dissertation, University of the Federal Armed Forces Hamburg, (2002).

[22] R. Hellmann, E. Bich, E. Vogel, A.S. Dickinson, V. Vesovic, J. Chem. Phys. 129, 064302 (2008).

[23] R. Hellmann, E. Bich, E. Vogel, A.S. Dickinson, V. Vesovic, J. Chem. Phys. 130, 124309 (2008).

[24] S. Bock, E. Bich, E. Vogel, A. S. Dickinson, V. Vesovic, J. Chem. Phys. 117, 2151 (2002).

[25] S. Bock, E. Bich, E. Vogel, A. S. Dickinson, V. Vesovic, J. Chem. Phys. 120, 7987 (2004).

[26] D.G. Friend, J.C. Rainwater, Chem. Phys. Lett. 107, 590 (1984).

[27] J.C. Rainwater, D.G. Friend, Phys. Rev. A 36, 4062 (1987).

[28] H.J.M. Hanley, R.D. McCarty, E.G.D. Cohen, Physica 60, 332 (1972).

[29] B. Najafi, R. Araghi, J.C. Rainwater, S. Alavi, R.F. Snider, Physica A 275, 48 (2000).

[30] D. Evans, Phys. Rev. A 34, 1449 (1986) .

[31] D.M. Heyes, Phys. Rev. B 37, 5677 (1988).

[32] F. Müller-Plathe, J. Chem. Phys. 106, 6082 (1997).

[33] C. Nieto-Draghi, T. de Bruin, J. Perez-Pellitero, J. B. Avalos and A.D. Mackie 126, 064509 (2007).

[34] X. Li, L. Zhao, T. Cheng, L. Liu and H. Sun, Fluid Phase Equilibr. **274**, 36 (2008).

[35] P. Ungerer, C. Nieto-Draghi, B. Rousseau, G. Ahunbay and V. Lachet, J. Mol. Liq. **134**, 71 (2007).

[36] D.K. Dysthe, A.H. Fuchs, and B. Rousseau, J. Chem. Phys. **110**, 4047 (1999).

[37] D.K. Dysthe, A.H. Fuchs, B. Rousseau and M. Durandeau, J. Chem. Phys. **110**, 4060 (1999).

[38] B. Eckl, J. Vrabec and H. Hasse, Fluid Phase Equilibr. **274**, 16 (2008).

[39] G.A. Fernandez, J. Vrabec and H. Hasse, Mol. Simul. **31**, 787 (2005).

# VITA

Zhi Liang was born on July 07, 1979 in Nantong, Jiangsu, China. He received his secondary education in Nantong, graduating from Nantong High School in July of 1997. In June 2001, he received his B.S. in Material Science and Engineering from Shanghai Jiaotong University, Shanghai, China. In March 2004, he received his M.S. in Material Processing Engineering from Shanghai Jiaotong University, Shanghai, China. In August 2010, he received his Ph. D. in Mechanical Engineering from Missouri University of Science and Technology, Rolla, Missouri, USA.

Zhi Liang won the 2nd place of the Hewlett-Packard Best Paper Award (Heat Transfer Division) at the 2008 International Mechanical Engineering Congress & Exposition held in November in Boston, Massachusetts, for the paper titled "Ab Initio Calculations of Vibrational Energy Levels and Transition Dipole Moments of $CO_2$ molecules."

Zhi Liang won the 1st place award for the poster titled "Thin Film Coating at Room Temperature and in Open Atmosphere by Using Multiple Lasers" at the third annual Intelligent Systems Center poster presentation on November 5, 2007 at University of Missouri-Rolla.

Zhi Liang won the 2nd place award for the paper "Thin Film Coating at Room Temperature and in Open Atmosphere by Using Multiple Lasers," at the Intelligent Systems Center Research Symposium on April 25, 2007 at University of Missouri Rolla.

Zhi Liang won the 2nd place award for the paper "A Study of Laser-Gas Interactions by Ab Initio Method," at the Intelligent Systems Center Research Symposium on April 22, 2008 at Missouri University of Science and Technology.